David Taylor Research Center
Bethesda, MD 20084–5000

DTRC–91/007 July 1991

Ship Hydromechanics Department
Research and Development Report

At–Sea Hydrodynamic Evaluation of Bare Double–Armored Tow Cables

by
Richard K. Knutson
Kedric C. Eisenberg

DTRC–91/007 At–Sea Hydrodynamic Evaluation of Bare Double–Armored Tow Cables

MAJOR DTRC TECHNICAL COMPONENTS

CODE 011 DIRECTOR OF TECHNOLOGY, PLANS AND ASSESSMENT

12 SHIP SYSTEMS INTEGRATION DEPARTMENT

14 SHIP ELECTROMAGNETIC SIGNATURES DEPARTMENT

15 SHIP HYDROMECHANICS DEPARTMENT

16 AVIATION DEPARTMENT

17 SHIP STRUCTURES AND PROTECTION DEPARTMENT

18 COMPUTATION, MATHEMATICS & LOGISTICS DEPARTMENT

19 SHIP ACOUSTICS DEPARTMENT

27 PROPULSION AND AUXILIARY SYSTEMS DEPARTMENT

28 SHIP MATERIALS ENGINEERING DEPARTMENT

DTRC ISSUES THREE TYPES OF REPORTS:

1. **DTRC reports, a formal series,** contain information of permanent technical value. They carry a consecutive numerical identification regardless of their classification or the originating department.

2. **Departmental reports, a semiformal series,** contain information of a preliminary, temporary, or proprietary nature or of limited interest or significance. They carry a departmental alphanumerical identification.

3. **Technical memoranda, an informal series,** contain technical documentation of limited use and interest. They are primarily working papers intended for internal use. They carry an identifying number which indicates their type and the numerical code of the originating department. Any distribution outside DTRC must be approved by the head of the originating department on a case-by-case basis.

REPORT DOCUMENTATION PAGE

1a. REPORT SECURITY CLASSIFICATION: UNCLASSIFIED	1b. RESTRICTIVE MARKINGS
2a. SECURITY CLASSIFICATION AUTHORITY	3. DISTRIBUTION/AVAILABILITY OF REPORT: Approved for public release; distribution is unlimited.
2b. DECLASSIFICATION/DOWNGRADING SCHEDULE	
4. PERFORMING ORGANIZATION REPORT NUMBER(S): DTRC-91/007	5. MONITORING ORGANIZATION REPORT NUMBER(S)
6a. NAME OF PERFORMING ORGANIZATION: David Taylor Research Center; 6b. OFFICE SYMBOL (If applicable): Code 1541	7a. NAME OF MONITORING ORGANIZATION
6c. ADDRESS (City, State, and ZIP Code): Bethesda, Maryland 20084-5000	7b. ADDRESS (City, State, and ZIP Code)
8a. NAME OF FUNDING/SPONSORING ORGANIZATION: Naval Coastal Systems Center; 8b. OFFICE SYMBOL (If applicable)	9. PROCUREMENT INSTRUMENT IDENTIFICATION NUMBER
8c. ADDRESS (City, State, and ZIP Code): Panama City, Florida 32407	10. SOURCE OF FUNDING NUMBERS: PROGRAM ELEMENT NO. 0602315N; PROJECT NO.; TASK NO. WX-90020 WX-00013; WORK UNIT ACCESSION NO.

11. TITLE (Include Security Classification): At-Sea Hydrodynamic Evaluation of Bare Double-Armored Tow Cables

12. PERSONAL AUTHOR(S): Knutson, Richard K., and Kedric C. Eisenberg

13a. TYPE OF REPORT	13b. TIME COVERED	14. DATE OF REPORT (YEAR, MONTH, DAY)	15. PAGE COUNT
R&D	FROM _____ TO _____	1991 July	107

16. SUPPLEMENTARY NOTATION

17. COSATI CODES			18. SUBJECT TERMS (Continue on reverse if necessary and identify by block number)
FIELD	GROUP	SUB-GROUP	Tow Cables, Double-Armored Cable, Towed Systems, Electro-Mechanical Tow Cable, Cable Drag, Bare Cable

19. ABSTRACT (Continue on reverse if necessary and identify by block number)

Two double-armored, bare cables were evaluated at-sea to determine the normal drag coefficient and normal loading function. A special device was attached at various positions along the cable to measure the in-plane cable inclination angles. This data collection method allowed a direct determination of the normal hydrodynamic loading using the differential equation that relates the inclination angle to the normal force. The resulting normal loading function differs from the classical sine squared functional relationship usually assumed for bare cables. A normal drag coefficient C_T of 1.70, independent of the Reynolds number, was determied for the two cables.

20. DISTRIBUTION/AVAILABILITY OF ABSTRACT	21. ABSTRACT SECURITY CLASSIFICATION
☐ UNCLASSIFIED/UNLIMITED ☒ SAME AS RPT ☐ DTIC USERS	UNCLASSIFIED

22a. NAME OF RESPONSIBLE INDIVIDUAL	22b. TELEPHONE (Include Area Code)	22c. OFFICE SYMBOL
David Pickett	301-227-1546	Code 1541

DD FORM 1473, JUN 86 *Previous editions are obsolete.*

CONTENTS

CONTENTS (Continued)

FIGURES

FIGURES (Continued)

FIGURES (continued)

FIGURES (Continued)

TABLES

TABLES (Continued)

NOTATION

C_n	Cable normal force coefficient based on frontal area
C_r	Cable normal drag coefficient based on frontal area
C_{td}	Cable tangential drag coefficient based on frontal area
C_s	Cable side force coefficient based on frontal area
d	Cable diameter
F	Cable hydrodynamic force per unit length normal to the cable axis in the plane defined by the cable and the free-stream direction
F_s	Cable hydrodynamic side force per unit length at the orientation of the cable that produces the maximum value
f	Pode frictional parameter
f_n, f_t, f_s	Normal, tangential, and side force loading functions
G	Cable hydrodynamic force per unit length tangential to the cable axis
H	Cable hydrodynamic force per unit length normal to the plane defined by the cable and the free-stream direction
R	Cable drag per unit length when the cable is normal to the free-stream direction
R_e	Reynolds number based on cable diameter
s	Cable length
T	Cable tension
UN_r	Uncertainty of the variable r
V	Free-stream velocity
W	Cable weight per unit length in a fluid
X	Axis of space-fixed coordinate system positive in the direction of tow
Y	Axis of space-fixed coordinate system positive to the right

NOTATION (Continued)

Z	Axis of spaced-fixed coordinate system positive in the direction of gravity
X_1, Y_2, Z_3	Intermediate coordinate system defined by a rotation of angle β about the X-axis
x, y, z	Distances along the X, Y, and Z directions
β	Cable kite angle measured from the Z-axis to the tangent of the cable axis projected onto the Y-Z plane
μ	Eames friction ratio
ρ	Fluid density
ϕ	Cable angle measured from the free-stream direction to the tangent of the cable axis

ABSTRACT

Two double-armored, bare cables were evaluated at sea to determine the normal drag coefficient and normal loading function. A special device was attached at various positions along the cable to measure the in-plane cable inclination angles. This data collection method allowed a direct determination of the normal hydrodynamic loading using the differential equation that relates the inclination angle to the normal force. The resulting normal loading function differs from the classical sine squared functional relationship usually assumed for bare cables. A normal drag coefficient C_r of 1.70, independent of the Reynolds number, was determined for the two cables.

ADMINISTRATIVE INFORMATION

The work described in this report was performed under Naval Coastal Systems Center Work Orders N6133189WX90020 and N6133190WX00013, Program Element 0602315N, David Taylor Research Center Work Unit 1541-309.

INTRODUCTION

Submerged cables are used in a large variety of marine systems. Applications include acoustic arrays, mine countermeasures, submarine communications, and environmental mapping. Water flow, induced either by ocean currents or by towing, has a profound effect on the cable posture. Thus, detailed knowledge of the hydrodynamic forces acting on the cable is required to accurately predict system performance. Some systems incorporate streamlined fairing around the cable to reduce hydrodynamic drag, but bare, un-faired cables remain the dominate type used in Navy systems today.

The differential equations that relate cable forces to the static cable configuration are known, and several computer programs have been developed to numerically determine cable configuration. The difficulty is the determination of the cable forces. No satisfactory analytical methods are available to calculate drag; therefore, empirical methods are required.

Bare cables, exposed to water flow, create vortex shedding which induces cable vibration. The vibration causes unsteady, fluctuating forces which increase the average hydrodynamic force, especially in the direction normal to the cable axis. Because long cables vibrate in a different manner than short ones, wind tunnels and towing tanks have never been totally suitable for the determination of bare cable drag. Thus, the usual practice is to perform evaluations at sea to determine hydrodynamic loading.

Two types of at-sea evaluations have been performed in the past. These include body-dominated tows in which the forces produced by a body at the lower end of the cable are substantially larger than the forces produced by the cable itself, and cable-dominated tows, in which the cable forces predominate. An example of a body-dominated tow is reported by Gibbons and Walton.[1] The results of an extensive series of experiments with cable-dominated tows are reported by Diggs.[2] Both types of tows have advantages and disadvantages when attempting to define cable hydrodynamic forces. In either case, the usual procedure is to measure tension and cable inclination angle at the ship and depth at the bottom of the cable. Then a regression analysis is performed using a numerical cable program. In this type of analysis, various force coefficients are assumed until a reasonable match between predicted and measured performance is obtained. One problem that occurs with this procedure is that the cable inclination angles measured at the ship are usually quite small even for body-dominated tows and short cable lengths. Although angles are frequently steep near the towed body, the angles change rapidly along the cable and become shallow over short distances. Therefore, a force/angle dependency is difficult to establish.

Since the cable force/angle dependency cannot be dete. ed directly using the at-sea evaluation procedures described above, an angle dependent function must be chosen a priori. The usual practice is to assume that the component of force normal to the

cable varies as the sine squared of the inclination angle. This form of normal loading is valid for circular, nonvibrating cylinders but has never been verified for long, vibrating cables.

The net result is that the force relationships developed by the various experiments seldom agree with one another. In particular, the results obtained with body-dominated tows tend to overpredict both tension and depth obtained during cable-dominated, critical angle tows. One attempt to minimize these discrepancies was reported by Folb and Nelligan.[3] They assumed that the normal drag coefficient determined by the body-dominated tow performed by Gibbons and Walton[1] was correct, but that the force/inclination-angle relationship needed to be adjusted at the shallower angles to more closely agree with the results obtained during cable-dominated tows. Thus, they developed a new normal-force/angle relationship that does not vary as sine squared. Using this procedure, Folb and Nelligan were able to better predict static towing performance over a wider range of conditions.

A more direct approach would be to measure the cable inclination over a large range of angles. Then the normal-force loading could be obtained directly from the differential equations that define the towing configuration. This method would allow both the normal force coefficient and the normal-force/angle dependency to be determined simultaneously without making any assumptions regarding the form of the functions. This procedure was adopted for the at-sea evaluation and analysis described in this report. To make the necessary measurements, a special device was developed that could be attached at any desired position along the cable to measure inclination angle in the plane of the cable at that position. Although side loading is known to occur on stranded bare cables, no attempt was made to determine this effect.

This report describes the bare cables that were evaluated; discusses the at-sea evaluation including descriptions of the equipment, instrumentation, and procedures; presents the results in tabular and graphical form; describes the method used to reduce the data to hydrodynamic drag coefficients; and compares predicted performance to measured performance using the newly developed coefficients. An error analysis also is performed to establish experimental uncertainties.

EXPERIMENT CABLES

Two double-armored, electro-mechanical cables were provided for evaluation. One cable, herein designated the small cable, has an average diameter of 0.376 in. (9.55 mm). The other cable, designated the large cable, has a diameter of 0.778 in. (19.76 mm). Both cables have geometrically similar exterior features. The small cable has 20 helically-wrapped exterior strands each of which is 0.047 in. (1.19 mm) in diameter; the large cable has 24 exterior strands each of which is 0.085 in. (2.16 mm) in diameter. Physical characteristics of the small and the large cables are listed in Tables 1 and 2, respectively.

The diameters, air weights, and in-water weights of both cables were carefully determined in the laboratory using 10.00-ft (3.05-m) long sections of each. The cable lengths were measured to an estimated accuracy of ±0.05 in. (±1.3 mm). Diameters were measured at various locations while the cables were under tension loads varying between zero and 1200 lb (5.3 kN). The diameter measurements were made to an accuracy of ±0.001 in. (±0.03 mm). The diameters reported are the averages over a tension range from 200 to 1200 lb (0.9 to 5.3 kN), although the diameters of both cables varied no more than 0.001 in. (0.03 mm). Change in length under tension also was determined. Length change of the small cable was 0.5% at 1200 lb (5.3 kN); length change of the large cable was 0.1% at 1200 lb (5.3 kN). The length change is negligible.

Table 1. Small cable physical characteristics.

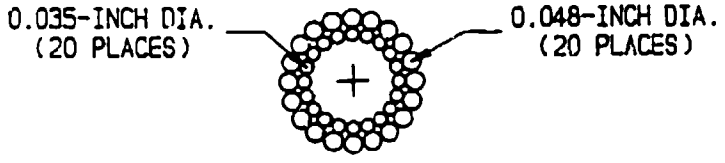

Diameter, in. (mm)	0.376 (9.55)
Air weight per unit length, lb/ft (N/m)	0.234 (3.41)
Fresh-water wt per unit length, lb/ft (N/m)	0.192 (2.80)
Sea-water wt per unit length, lb/ft (N/m)	0.190 (2.77)
Construction	Double Armor
Lay direction of exterior strands	Left Hand
Lay angle of exterior strands, deg	20
Number of exterior strands	20
Diameter of exterior strands, in. (mm)	0.048 (1.21)
Number of interior strands	20
Diameter of interior strands, in. (mm)	0.035 (0.89)

Table 2. Large cable physical characteristics.

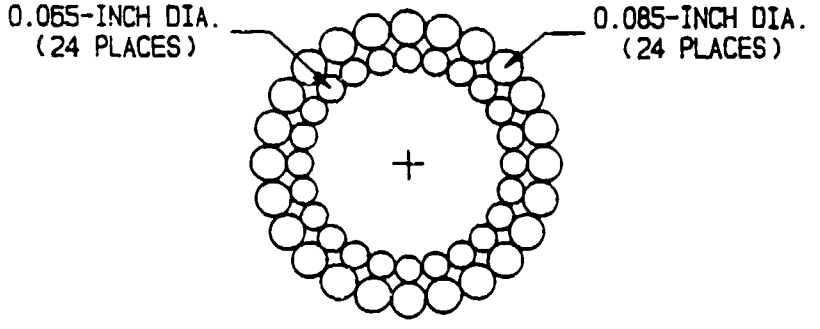

Diameter, in. (mm)	0.778 (19.76)
Air weight per unit length, lb/ft (N/m)	0.920 (13.42)
Fresh-water wt per unit length, lb/ft (N/m)	0.731 (10.67)
Sea-water wt per unit length, lb/ft (N/m)	0.726 (10.59)
Construction	Double Armor
Lay direction of exterior strands	Left Hand
Lay angle of exterior strands, deg	20
Number of exterior strands	24
Diameter of exterior strands, in. (mm)	0.085 (2.15)
Number of interior strands	24
Diameter of interior strands, in. (mm)	0.065 (1.65)

Air weights and fresh-water weights of the 10-ft (3.05-m) sections of cable were determined to an accuracy of ±0.0004 lb/ft (±0.006 N/m). To determine fresh-water weight, the cables were submerged for at least 60 hr prior to weighing to allow any trapped air bubbles time to escape. Weight in standard sea water was calculated using the air weight and fresh-water weight. With an assumed uncertainty in fresh-water density of ±0.002 $lb \cdot s^2/ft^4$ and an uncertainty in sea-water density of ±0.005 $lb \cdot s^2/ft^4$, the accuracy of the sea-water weight determination is ±0.0005 lb/ft (±0.008 N/m).

EXPERIMENTAL EVALUATION

In addition to the at-sea evaluation, several experiments were conducted in the towing basins to characterize and to calibrate various equipment. The results of the calibration experiments are discussed in Appendixes A, B, and C.

The at-sea evaluation of the two bare cables was conducted in May 1989 aboard R/V ATHENA II operating out of Andros Island in the Bahamas. The actual area of operation is designated the Tongue of the Ocean (TOTO). This location was chosen because underwater currents are known to be minimal in the area. An illustration of the general towing configuration is shown in Fig. 1. A block diagram of the instrumentation arrangement is shown in Fig. 2. Details of the support equipment, instrumentation, and procedures used during the evaluation are described below.

EQUIPMENT

The at-sea evaluation of the cables required the following support equipment to collect, store, and analyze data.

DTRC Research Depressor

The DTRC research depressor, shown in Fig. 3, was used during the evaluation to provide a depression force at the lower end of the experiment cables.

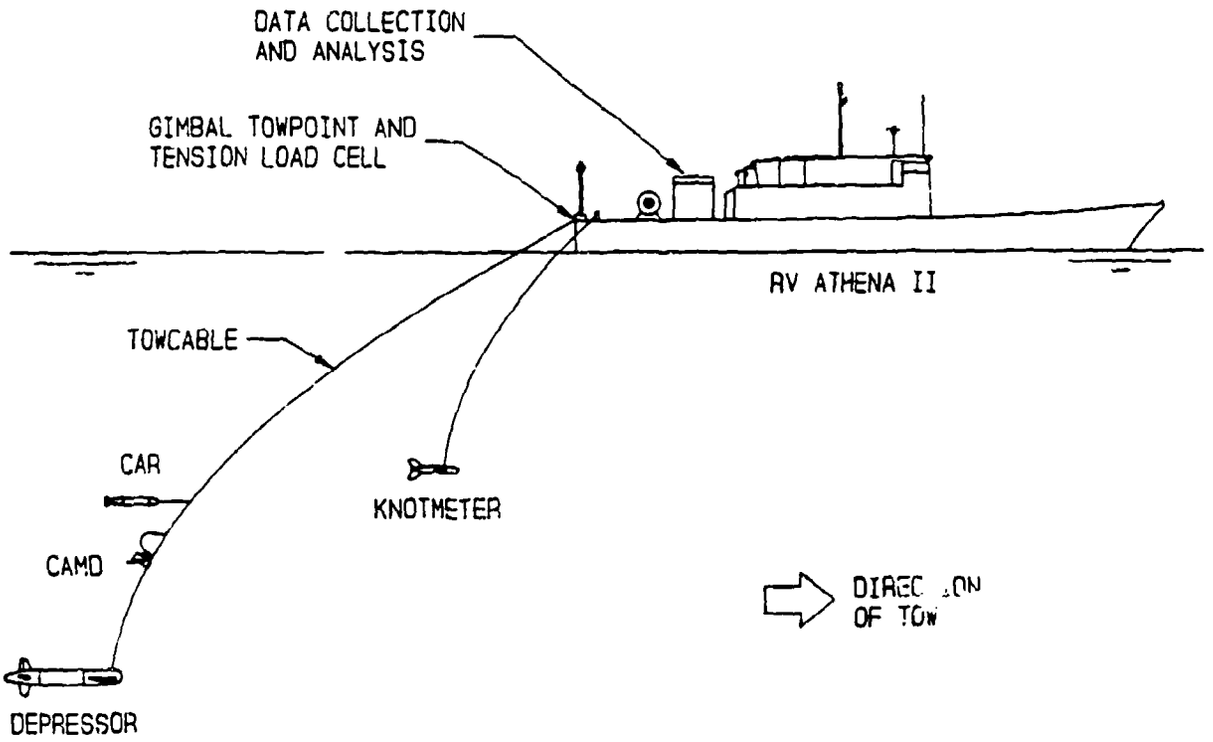

Fig. 1. Towing configuration.

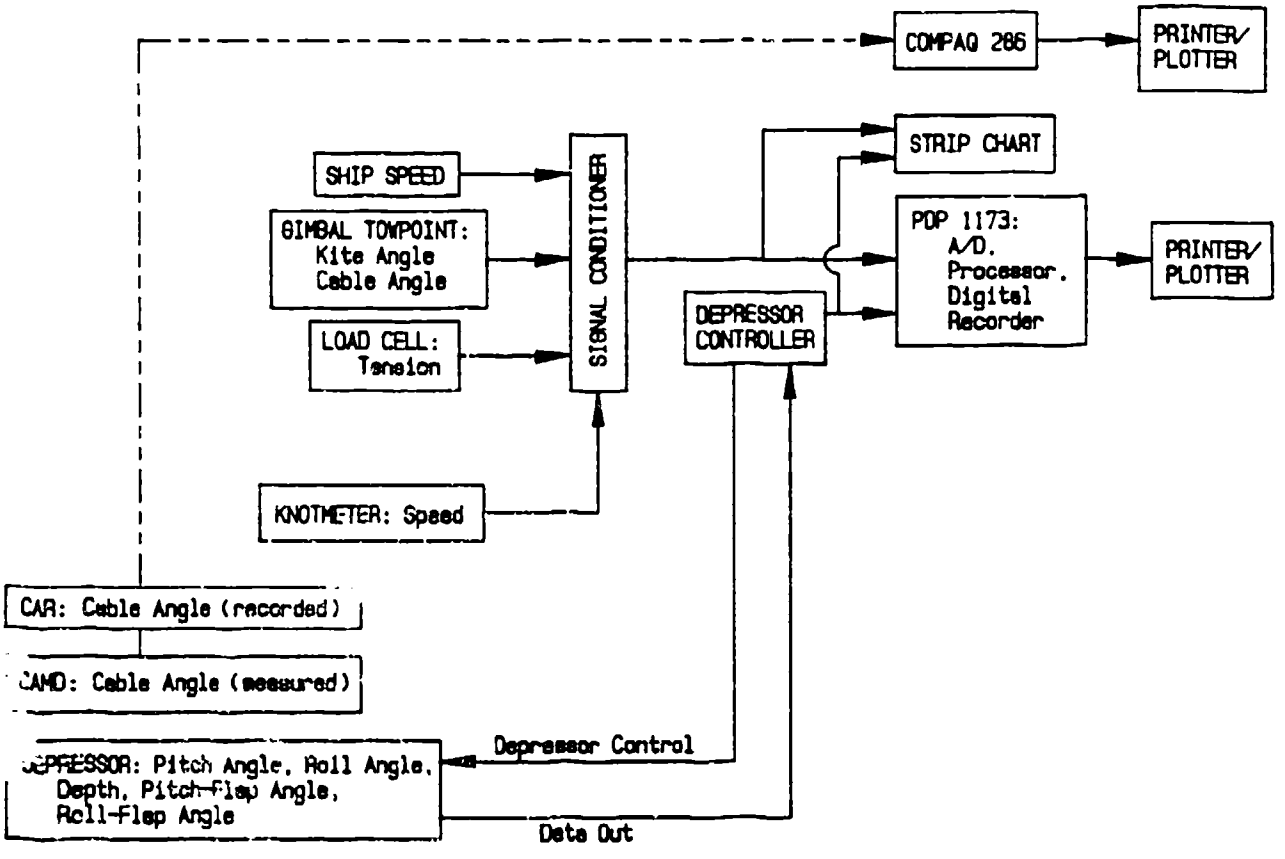

Fig. 2. Instrumentation diagram.

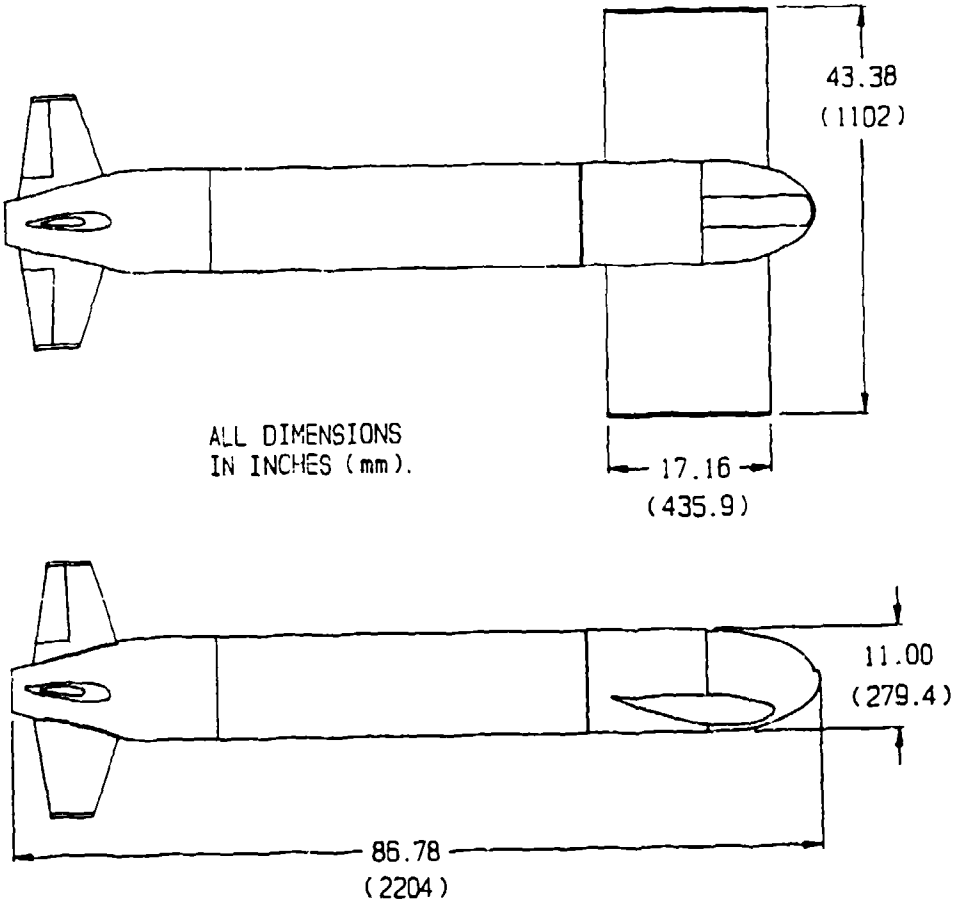

Fig. 3. DTRC research depressor.

The depressor incorporates a wing to produce most of the depression force, a cylindrical fuselage to house control and sensor electronics, and aft lifting surfaces to provide hydrodynamic stabilization. The wing and stabilizers are composite construction with epoxy impregnated fiberglass skins and syntactic foam cores. The fuselage nose is a fiberglass shell. The fuselage mid-body and tail section, which form a pressure housing, are constructed of anodized 6061-T6 aluminum. Control flaps located on the horizontal and vertical stabilizers provide depressor pitch and roll control. The flaps are remotely adjusted through a control console on the ship and can be operated either in a manual or an automatic mode. Physical characteristics of the research depressor are listed in Table 3.

A vertical axis gyro provides measurement of depressor pitch and roll angles. A pressure gage provides depressor depth. The towpoint of the depressor is attached to the bottom of the cable through a strain-gaged clevis pin. The clevis pin is intended to provide measurements of longitudinal and normal force produced by the depressor relative to the fuselage longitudinal axis. These forces determine the cable tension and cable angle at the depressor towstaff. However during calibration experiments prior to the at-sea evaluation, the clevis pin force measurement system was determined to be insufficiently accurate for purposes of the evaluation. Thus, the clevis pin was not used to determine force. Instead, a basin experiment was performed to determine the force characteristics of the depressor.

The results of the basin towing experiment are discussed in Appendix A. Since the depressor trim conditions are not the same in fresh water and sea water, the forces measured in the basin were not used directly. Rather, depressor forces in fresh water were predicted using analytical techniques and validated with the basin data. The predictions were then converted to standard sea conditions. The predicted depressor forces were thus used to reduce the at-sea cable data.

Table 3. DTRC research depressor physical characteristics.

Complete Depressor	
Length, in. (m)	86.78 (2.204)
Width, in. (m)	43.38 (1.102)
Height, in. (mm)	27.00 (685.8)
Towpoint Location (TP)	
aft of nose, in. (mm)	8.75 (222.2)
above fuselage axis, in. (mm)	1.94 (49.3)
Displacement including entrained water	
Fresh water, lb (kN)	319.0 (1.419)
Standard sea water, lb (kN)	327.9 (1.458)
Weight including entrained water	
Fresh water, lb (kN)	359.5 (1.599)
Sea water, lb (kN)	360.8 (1.605)
Center of Buoyancy (CB)	
Distance Aft of towpoint, in. (mm)	30.05 (763.3)
Distance below towpoint, in. (mm)	2.38 (60.5)
Center of mass in fresh water (CG)	
Distance Aft of towpoint, in. (mm)	27.43 (696.7)
Distance below towpoint, in. (mm)	3.22 (81.8)
Center of mass in sea water (CG)	
Distance Aft of towpoint, in. (mm)	27.35 (694.7)
Distance below towpoint, in. (mm)	3.22 (81.8)
Fuselage	
Length, in. (m)	86.78 (2.204)
Diameter, in. (mm)	11.00 (279.4)
Wing	
Section shape	NACA 63_3-618
Span, in. (m)	43.38 (1.102)
Chord, in. (mm)	17.16 (435.9)
Incidence angle, deg (rad)	-6.00 (-0.105)
Vertical Stabilizer	
Section shape	NACA 0021
Span, in. (mm)	27.00 (685.8)
Root chord, in. (mm)	9.13 (231.9)
Tip chord, in. (mm)	4.38 (111.3)
Horizontal Stabilizer	
Section shape	NACA 0021
Span, in. (mm)	27.00 (685.8)
Root chord, in. (mm)	9.13 (231.9)
Tip chord, in. (mm)	4.36 (111.3)
Incidence angle, deg (rad)	-6.00 (-0.105)

Cable Angle Measuring Device (CAMD)

The cable angle measuring device (CAMD), shown in Fig. 4, provided cable-angle measurement in the plane of the cable at selected positions along the length of the cable. The angle measured by this device is the inclination angle relative to the free-stream flow vector in the plane defined by the cable segment and the free-stream flow. This angle is generally called cable angle ϕ.

The CAMD consists of a rectangular main section with a circular nose and triangular after body. The circular nose separates from the main section for the purpose of attachment to the cable. The main section is a pressure housing that contains a rotary potentiometer for measurement of cable inclination angle. The faired after body is attached to the pressure housing to reduce flow interference and to minimize drag. The potentiometer is actuated by a flat-plate, horizontal vane attached to a shaft protruding from the pressure housing. The horizontal vane aligns with local free-stream flow. The shaft turns a set of 4:1 reducing gears located inside the pressure housing which rotates the shaft of the potentiometer. The gears provide a 4-deg rotation of the potentiometer for every one-deg rotation of the shaft. The design of the CAMD allows for a ± 30-deg rotation of the vane. For shallower cable angles, precision machined wedges are inserted between the main body and the nose section of the device. The wedges provided have 30- and 55-deg included angles. The wedge angles are machined to an accuracy of ±0.01 deg.

The nose section, the pressure housing, and the vane support arms are constructed of anodized 6061-T6 aluminum. The faired after body is made of syntactic foam. The vane is made of expanded polyvinyl chloride sheet. The vane assembly, composed of the support arms and vane, is near neutrally buoyant in sea-water.

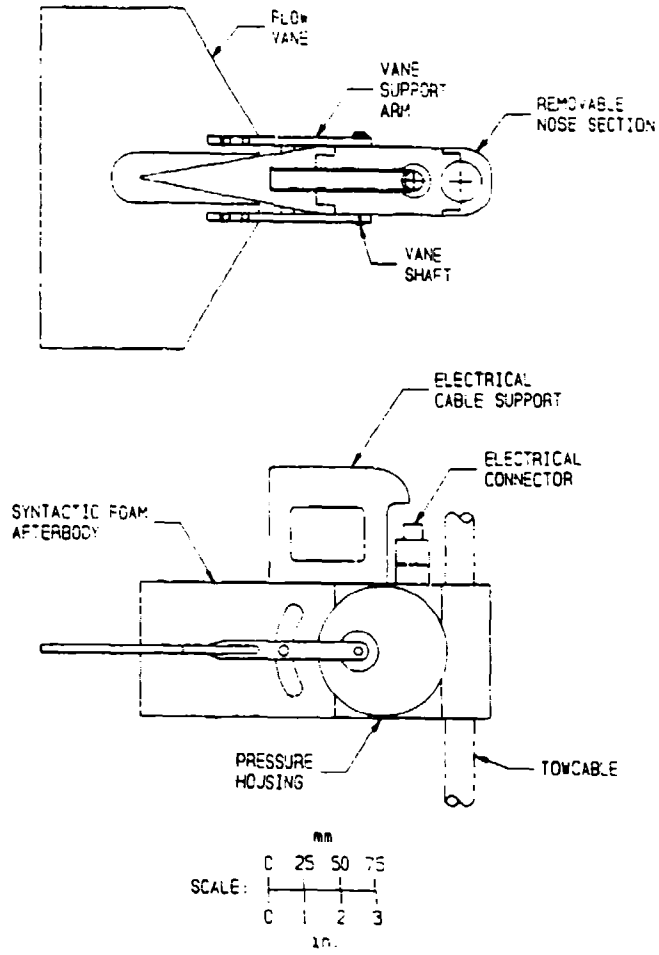

Fig. 4. Cable angle measuring device.

The CAMD attaches to the cable in a manner that allows it to freely rotate to align with the flow. This is accomplished by bushings that are secured to the cable. The bushings restrain longitudinal movement but not rotation.

Experiments were conducted in the towing basin to calibrate the CAMD and to determine the influence of the experiment cables on measured inclination angle. During these experiments, the CAMD was attached to actual samples of both the small and the large cables. Inclination angles were measured with the CAMD and compared to angles

measured with a pendulum potentiometer over the speed and the angle ranges measured at sea. The results of the basin calibration experiment are presented in Appendix B. An estimate of the effect of CAMD drag on cable inclination angle also is included in Appendix B.

Cable Angle Recorder (CAR)

The cable angle recorder (CAR) recorded and stored the angle information measured by the CAMD.

CAR is an electronically instrumented, torpedo shaped, low drag, nose-towed body as shown in Fig. 5. Six 500-mahour AA NICAD batteries provide the main power source; an 850-mahour 1/2 AA lithium battery provides memory and clock backup.

CAR was initially developed as a speed/depth recorder[4] designed to measure and record depth, speed, and time of day. The data are stored on a RAM chip and downloaded upon retrieval. The depth/speed recorder had previously been evaluated in the DTRC model basin for accuracy and hydrodynamic performance.[5] For purposes of the present evaluation, the recorder was modified to receive and store the electronic signal from the CAMD through an electrical cable connection. To accomplish the modification, the depth measurement function was disabled.

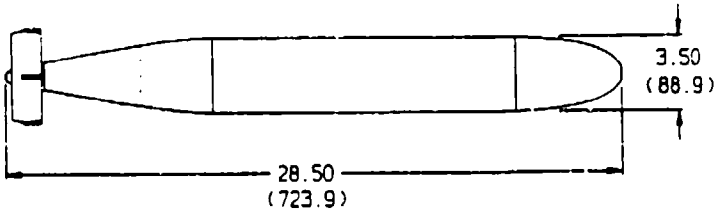

ALL DIMENSIONS IN INCHES (mm)

Fig. 5. Cable angle recorder.

Gimbal Towpoint

The gimbal towpoint provided the cable attachment point at the ship. The gimbal allows omnidirectional motion of the tow cable while providing measurements of the cable angles in the horizontal and vertical planes. A VRN 7501 series potentiometer provides measurement of horizontal angle; a Humphries CP17 series pendulum potentiometer provides measurement of vertical angle. During the evaluation, the cable was attached to the towpoint through a load cell that was used to measure cable tension at the ship.

The horizontal cable angle measurement potentiometer did not function properly during the at-sea evaluation. However, since no attempt was made to determine cable side loading, this angle was not deemed important.

DTMB Mark 2 Knotmeter

The DTMB Mark 2 knotmeter provided measurement of tow speed. The knotmeter is a cable-towed body with associated cable and processing instrumentation. The knotmeter is constructed of fiberglass reinforced epoxy and weighs approximately 10 lb (44 N) in seawater. The knotmeter incorporates a wing to provide downforce.

A magnetic pickup located in the fuselage senses the rotation of an impeller located at the aft end of the fuselage and sends a signal up the towcable for display on a digital indicator. The Mark 2 knotmeter is designed to operate in a speed range from 3 to 15 knots. Under steady towing conditions, the knotmeter is capable of a speed accuracy of ±0.01 knot. However in a seaway with ship motions, the accuracy is degraded somewhat. For example, a peak-to-peak motion of 3 ft (0.9 m) at a frequency of 0.2 Hz introduces an additional speed error of 0.02 knot at 4 knots decreasing to nearly zero at 6 knots. More information on the knotmeter is presented by Springston.[6]

The knotmeter towcable provided for the evaluation measures 0.31 in. (8 mm) in diameter. The lower 50 ft (15 m) of length is faired with a trailing type fairing to minimize drag and to maximize towing depth.

The knotmeter was calibrated in the towing basin prior to the at-sea evaluation. The calibration results are presented in Appendix C.

Data Collection Equipment

Various computers and strip-chart recorders were provided for collection and processing of the measurements made by the support equipment described above. Data collection and processing included the following devices:

1. PDP 1173 - This is the main computer used for data collection and analysis and is compatible with the DTRC depressor. The PDP 1173 is a minicomputer with a 30-megabyte hard disc, a 10-megabyte removable cartridge, and an 8-in. floppy disc drive. It also uses a 16-byte high speed A/D converter and an RT 11 operating system. The computer and operating system are manufactured by Digital Equipment Corporation.

2. COMPAC 286 - The COMPAC 286 is a portable computer with a 20-megabyte hard disc and 1.2-megabyte floppy disc. The primary function of the COMPAC was to receive data from CAR and analyze the results. This computer also is compatible with the PDP 1173 and can be used as a back-up terminal.

3. GOULD STRIP CHART RECORDER - The Brush 481 recorder, manufactured by Gould, is a general purpose analog recorder featuring eight 40-mm analog channels, two event markers, twelve pushbutton-controlled chart speeds, and eight isolated preamplifiers. Frequency response is flat from d-c to 40 Hz full scale. Analog data from the depressor and gimbal towpoint were recorded on the strip charts as backup to the PDP 1173.

INSTRUMENTATION

Instrumentation located at the depressor consisted of transducers to measure depth, roll angle, pitch angle, and control-flap deflection angles. Instrumentation located at the ship consisted of a load cell to measure cable tension and a gimbaled towpoint to measure cable angle. Instrumentation located on the towcable consisted of the cable angle measuring device (CAMD) and the cable angle recorder (CAR). Other instrumentation included the DTMB Mark 2 knotmeter.

The types, ranges, and accuracies of the various sensors used during the evaluation are listed in Table 4. The table reflects specifications provided by the manufacturer as well as calibrations that were performed in the laboratory and in the towing basins. All measurement transducers were calibrated prior to the at-sea evaluation.

Table 4. Measurement transducer characteristics.

Measurement	Instrument	Range	Accuracy
Depressor Depth	Pressure Transducer	675 ft (206 m)	±2.1 ft (±0.64 m)
Depressor Roll Angle	Vertical Axis Gyro	±90 deg	±1.0 deg
Depressor Pitch Angle	Vertical Axis Gyro	±60 deg	±1.0 deg
Depressor Flap Angles	Rotary Potentiometer	±170 deg	±0.2 deg
Tension at Ship	Tension Load Cell	2000 lb 8.90 kN	±10.0 lb ±44.5 N
Cable angle at Ship	Pendulous Potentiometer	±45 deg	±1.0 deg
CAMD Cable Angle	Rotary Potentiometer	±45 deg with gears	±0.5 deg
Tow Speed	Knotmeter	15 kn	±0.02 kn

The CAMD accuracy value listed in Table 4 is the measurement accuracy provided by the vane potentiometer. The potentiometer with the reduction gears has an accuracy of ±0.5 deg. However, the basin experiment discussed in Appendix B indicates a reduced accuracy, probably due to the influence of the cables on the local flow angle. The results from the basin experiment indicate measurement accuracies of ±1.5 deg for the small cable and ±1.7 deg for the large cable. Also, as discussed in Appendix B, the CAMD drag itself introduces a small bias error in the measurement of cable angle. The bias error produced by CAMD drag is estimated to be -0.4 deg near the depressor decreasing to about -0.1 deg at a cable length 300 ft (90 m) from the depressor.

The stated knotmeter accuracy of ±0.02 knot reflects the basin calibration experiment discussed in Appendix C. The accuracy does not reflect the uncertainties induced by ship motion at sea. Environmental effects on measured speed uncertainty are discussed in a later section of this report.

PROCEDURES

The initial evaluation plan indicated towing speeds up to at least 13 knots which is approximately the maximum ship speed under diesel power. However, early data runs demonstrated that the CAMD electrical cabling would not survive the higher speeds due to severe vibrations. Therefore, maximum speed was reduced. During the remainder of the evaluation, data runs were made at nominal speeds of 3, 6, and 8 knots.

To minimize the effect of ocean current gradients, data were collected on reciprocal headings at all towing speeds. Data runs were made on north and south headings. Typically, measurements were made at increasing speed increments in one direction, and then after making a turn, measurements were made at decreasing speed

increments in the opposite direction. During runs, data were collected for 5-min intervals before changing speed for the next run. Data collection was initiated after reaching steady-state conditions as indicated by knotmeter readings and depressor behavior.

Various towcable lengths were evaluated. With the small size cable, the towcable lengths, measured from the depressor to the ship, were 200, 400, 600, and 800 ft (61.0, 121.9, 182.9, and 243.8 m). With the large cable, towcable lengths of 300, 500, and 700 ft (91.4, 152.4, and 213.4 m) were used. The cable lengths are estimated to be accurate to within ±1.0 ft (±0.3 m). The lengths were predetermined and carefully measured in the laboratory prior to the evaluation. The specified cable lengths were chosen

1. to assure that the CAMD was always below the wake of the ship,
2. to provide various lengths necessary for determination of tangential hydrodynamic loading, and
3. to provide a cable inclination range from near vertical at the depressor to near critical angle at the ship.

To minimize the effect of CAMD drag on measured cable angle, a single CAMD was attached to the cable during a data run. Also, the CAR (angle recorder) was attached to the cable above the CAMD so that its drag would not affect the angle being measured. The method of attachment of the CAMD and CAR to the towcable is illustrated in Fig. 6. The CAMD was attached to the towcable at predetermined locations starting at 3 ft from the depressor and progressing up the cable at increments estimated to correspond to 5-deg cable angle changes. The placement accuracy of the CAMD relative to the depressor is estimated to be ±1.0 in. (25 mm). After each set of data runs, the CAMD was recovered, and the data were downloaded to a disk and checked. The CAMD was then placed at a new position on the cable.

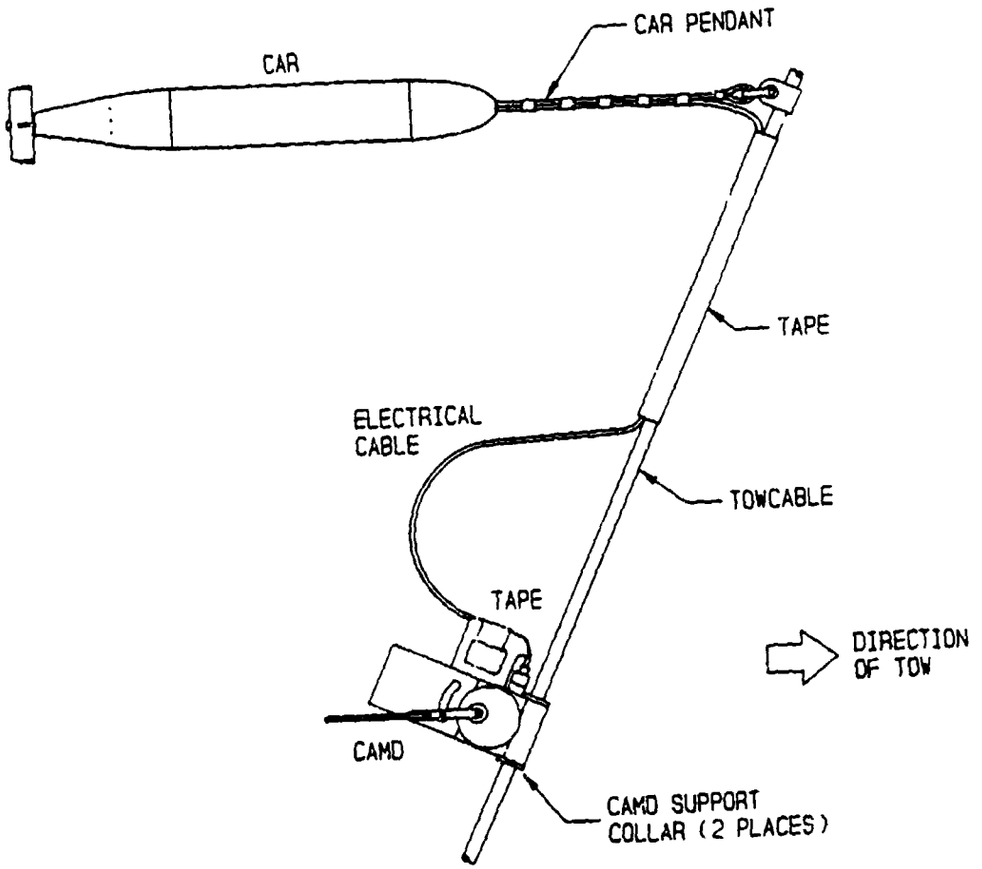

Fig. 6. Attachment of the cable angle measuring device and the cable angle recorder to the towcable.

Some CAMD placement locations were repeated at different cable lengths. This was done to examine the effect of cable length on cable hydrodynamic drag.

The knotmeter was towed from a boom that extended approximately 10 ft (3 m) off the starboard side of the ship. Sufficient knotmeter cable was deployed to provide an estimated depth between 75 ft (23 m) and 60 ft (18 m) through the speed range. The knotmeter was deployed during all data collection runs.

The depressor pitch flaps were maintained at the maximum deflection angle of 19.9 deg while in the manual pitch mode to provide maximum depressor downforce. This configuration produced a moderate loading on the small cable relative to cable diameter and a fairly light loading on the large cable. Near zero depressor roll angle was maintained throughout the evaluation using the automatic mode of roll control. The depressor was adjusted to 0.0±1.0 deg roll prior to each run. This adjustment was accomplished using the roll-flap trim offset control.

DATA

The towing configurations that were evaluated are listed in Table 5. Corrected data collected during all valid data runs are listed in Appendix D. The data are arranged by cable size and include CAMD position relative to the depressor, cable length, knotmeter speed, ship heading, depressor depth, and cable tension and angle measured at the ship.

The sea conditions were estimated to vary between state 1 and state 2 throughout the evaluation. Ship motions had minimal effect on data accuracy. For example, even under the worst conditions, standard deviation of knotmeter speed was typically no greater than 10%, standard deviation of depressor depth was less than 1%, and standard deviation of ship tension was less than 15% of the measured mean values. Standard deviation of CAMD measurements was typically less than 0.3 deg but always remained

within 1.0 deg. Also depressor motions were minimal. Standard deviations of both pitch and roll were less than 1.0 deg during runs, and the depressor maintained zero average roll to within ±1.0 deg.

Table 5. Towing configurations.

Small Cable (0.376-in. dia)		Large Cable (0.778-in. dia)	
CAMD Position from Depressor, ft (m)	Total Cable Length, ft (m)	CAMD Position from Depressor, ft (m)	Total Cable Length, ft (m)
3.00 (0.91)	200 (61.0)	3.00 (0.91)	300 (91.4)
3.00 (0.91)	800 (243.8)	3.00 (0.91)	300 (91.4)
8.00 (2.43)	200 (61.0)	6.00 (1.83)	500 (152.4)
15.00 (4.57)	200 (61.0)	9.00 (2.74)	500 (152.4)
22.00 (6.71)	200 (61.0)	18.00 (5.49)	700 (213.4)
22.00 (6.71)	400 (121.9)	30.00 (9.14)	700 (213.4)
30.00 (9.14)	400 (121.9)	46.00 (14.02)	700 (213.4)
48.00 (14.63)	400 (121.9)	60.00 (18.29)	700 (213.4)
75.00 (22.86)	400 (121.9)	80.00 (24.38)	700 (213.4)
75.00 (22.86)	600 (182.9)	110.00 (33.53)	700 (213.4)
115.00 (35.05)	600 (182.9)	180.00 (54.86)	700 (213.4)
145.00 (35.05)	600 (182.9)	400.00 (121.92)	700 (213.4)
195.00 (59.44)	800 (243.8)		
300.00 (91.44)	800 (243.8)		

To obtain the cable hydrodynamic drag loading from the data, tension at the depressor, tension at the ship, cable angle along the cable measured by the CAMD, and depth at the bottom of the cable must all be referenced to common speeds. This can be accomplished by curve fitting these data as functions of tow speed. The values desired are the fitted values at the chosen reference speeds. For the purposes of this analysis, speeds of 4, 6, and 8 knots were chosen as the reference speeds for both experiment cables. These speeds are within the range of the data at all the configurations evaluated, and therefore, no extrapolation outside the measured range is required.

Measured depressor pitch angle for several of the runs with both sizes of experiment cables is compared to predicted pitch angle (see Appendix A) in Fig. 7 to assure accurate prediction of depressor performance. Predicted pitch angle is within the accuracy and scatter of the measurements throughout the experiment speed range.

Cable tension and angle at the depressor predicted from the analysis of Appendix A are listed in Table 6 for the reference speeds of 4, 6, and 8 knots. The tension predictions are estimated to be accurate to within ±10 lb (±44 N). The angle predictions are estimated to be accurate to within ±1.0 deg. These accuracies are based on the basin experiment only. The uncertainties induced by environmental effects and measured speed error are included in the error analysis discussed later in this report.

Table 6. Predicted at-sea tension and cable angle at the depressor at 4, 6, and 8 knots.

Speed, kn	Tension, lb (kN)	Cable Angle ϕ, deg
4.00	185 (0.823)	82.6
6.00	363 (1.614)	81.8
8.00	612 (2.722)	81.4

Towcable tension measured at the ship as a function of speed for the various lengths of the small and the large cables is shown in Figs. 8 and 9, respectively. A second order polynomial equation was used to fit each set of data. This form of equation was chosen as the most physically suitable. The coefficients of the fitted equations are listed in the figures. The curve-fit equations are used to determine the tensions at the reference speeds of 4, 6, and 8 knots for the various cable lengths.

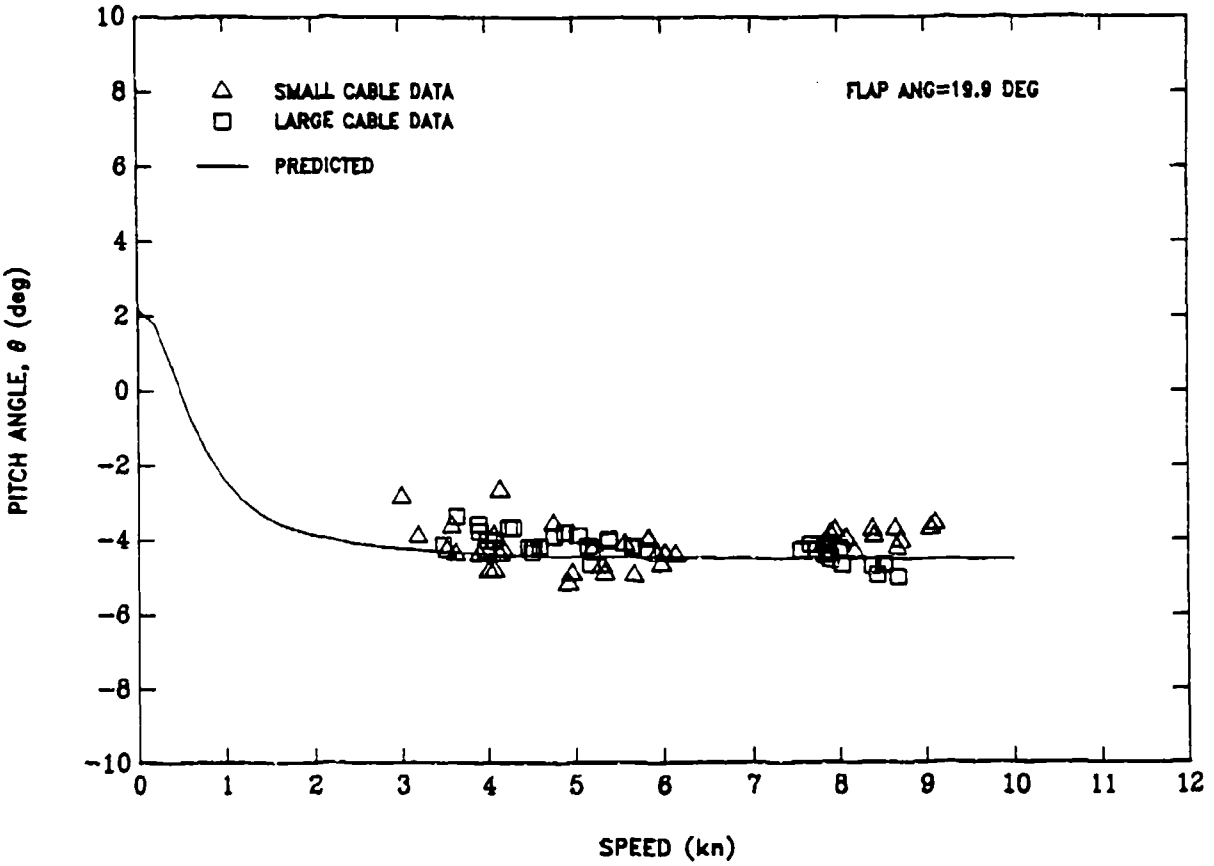

Fig. 7. Predicted depressor pitch angle compared to at-sea data.

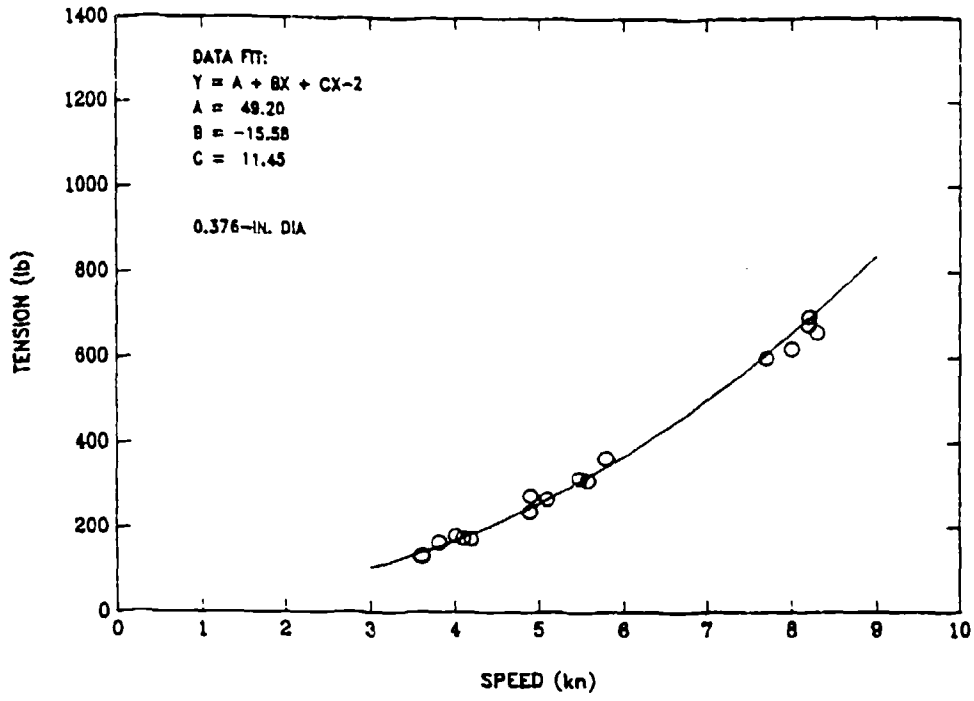

Fig. 8a. 200 ft.

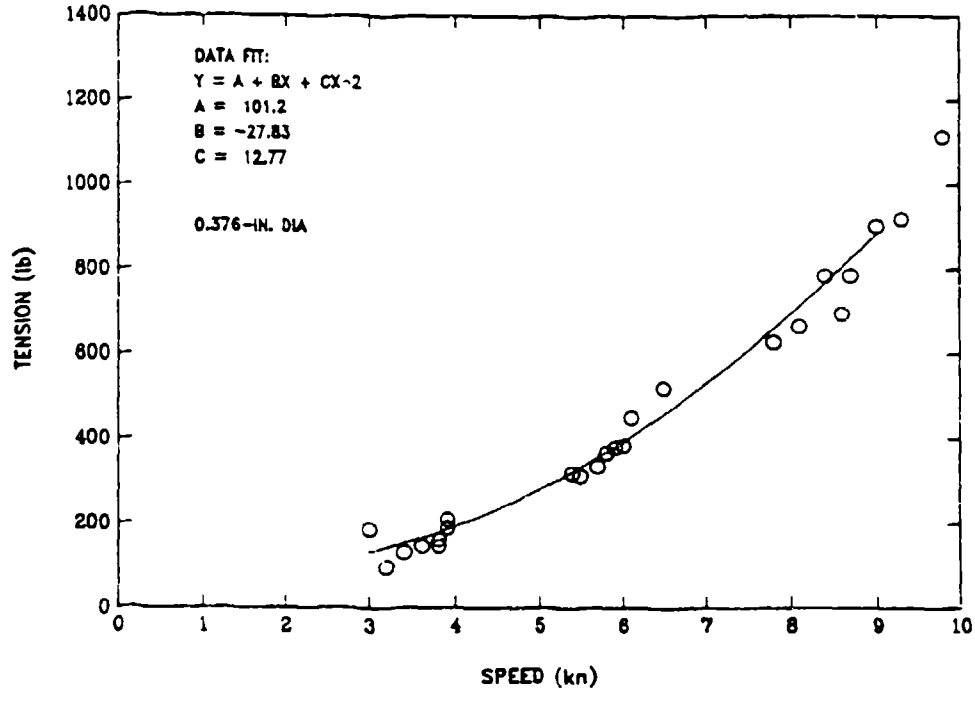

Fig. 8b. 400 ft.

Fig. 8. Tension at the ship as a function of speed for various lengths of the small cable.

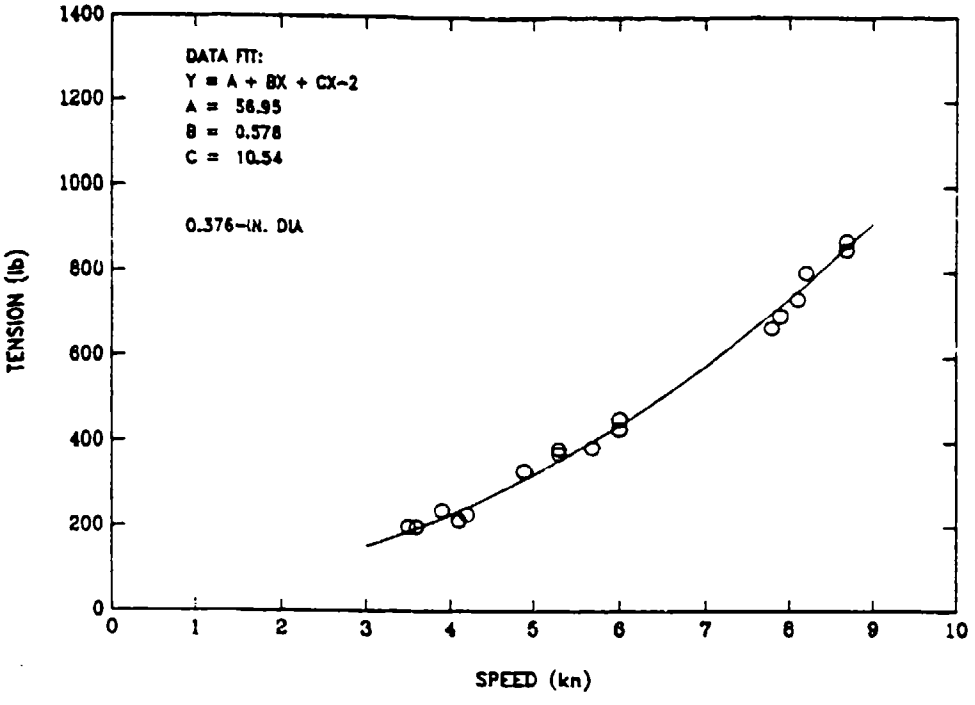

Fig. 8c. 600 ft.

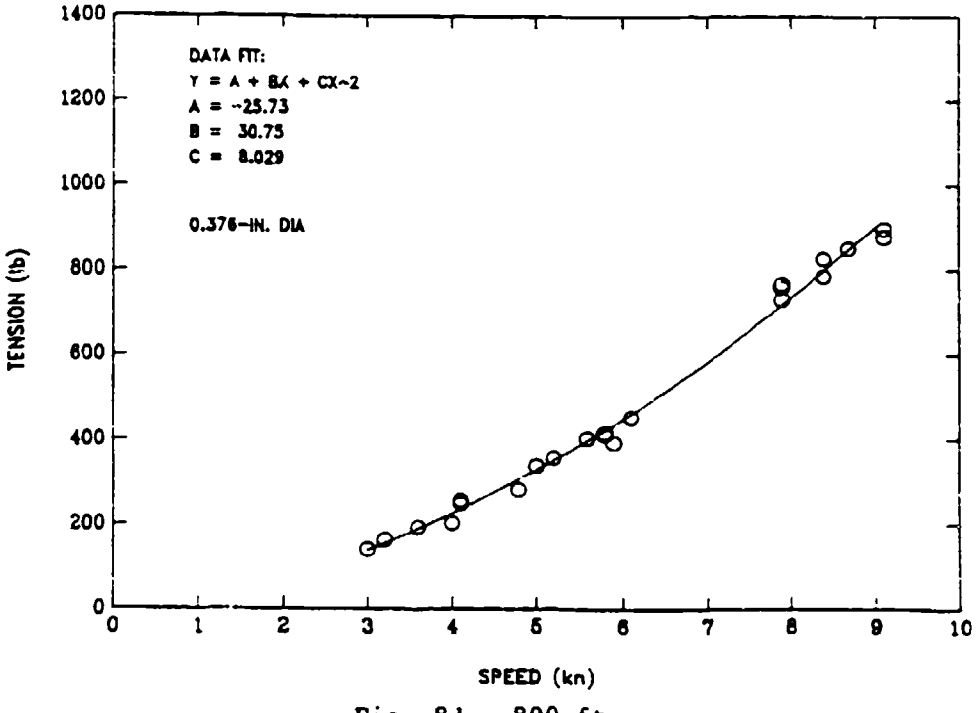

Fig. 8d. 800 ft.

Fig. 8. (Continued)

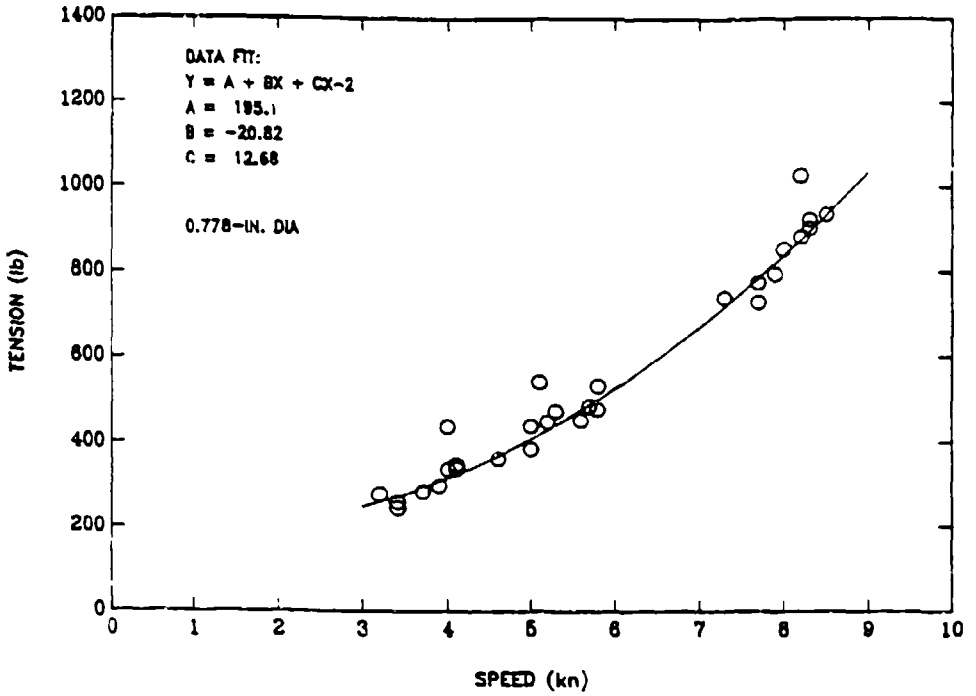

Fig. 9a. 300 ft.

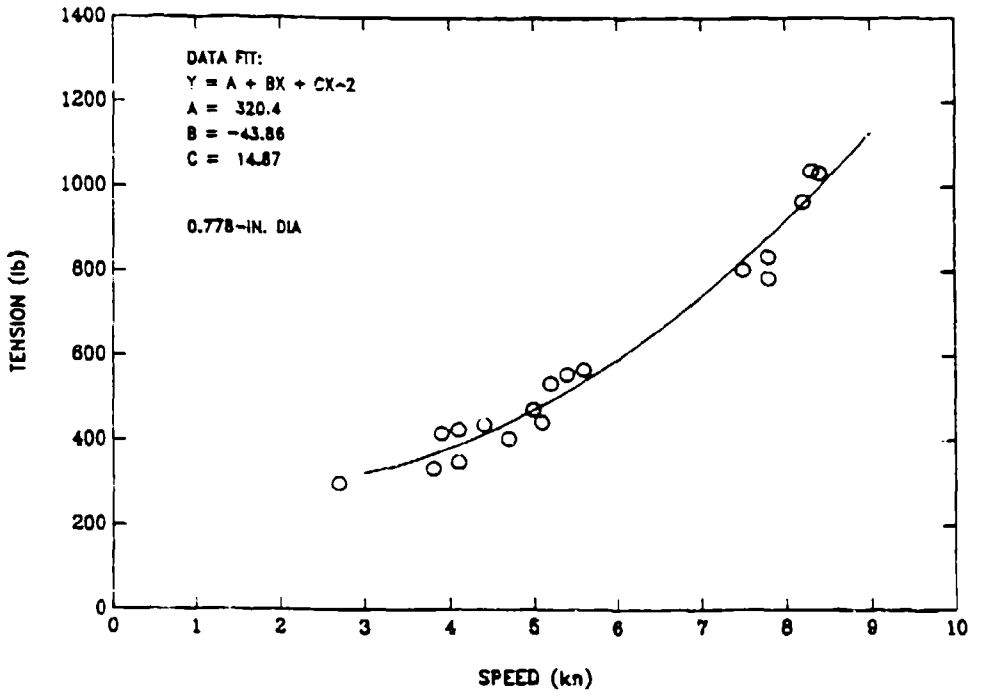

Fig. 9b. 500 ft.

Fig. 9. Tension at the ship as a function of speed for various lengths of the large cable.

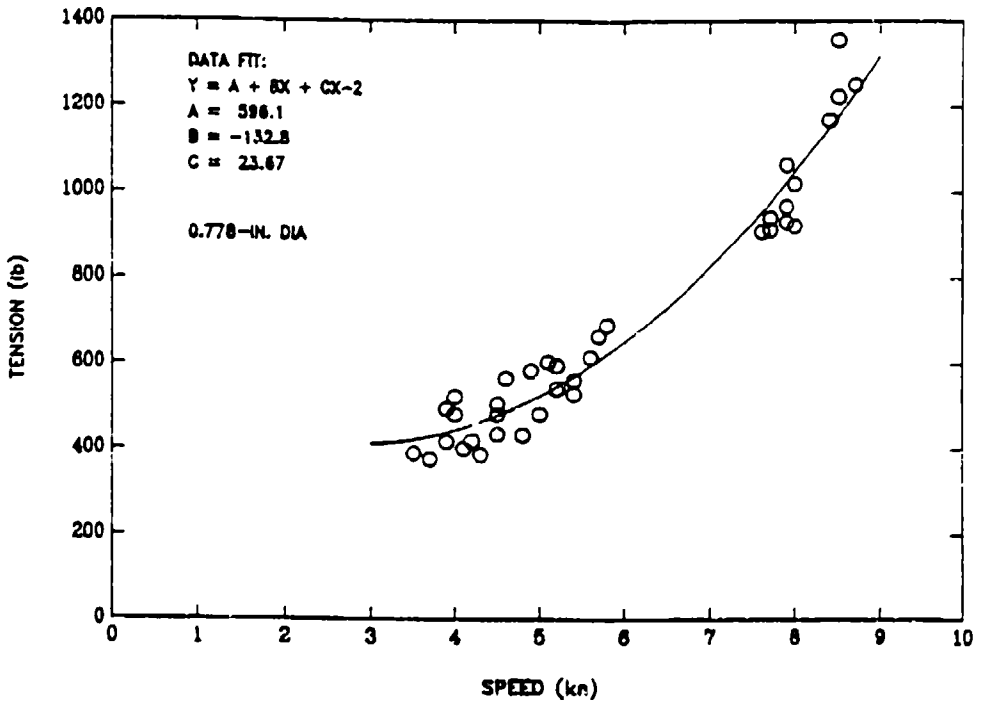

Fig. 9c. 700 ft.

Fig. 9. (Continued)

Measured depressor depths as a function of speed for the various lengths of the small and the large cables are shown in Figs. 10 and 11, respectively. The form of the equation used to fit the data is

$$Y = A + B/X$$

where Y represents depth, X represents speed, and A and B are the equation constants. This form of equation was chosen as the best overall fit of available curve fitting equations. The coefficients of the equations are listed in the figures.

Cable angle as a function of speed measured at various positions along the small and the large cables are shown in Figs. 12 and 13, respectively. The form of equation used to fit the angle data is the same as that used to fit depressor depth. The coefficients of the equations are listed in Table 7.

CABLE HYDRODYNAMIC DRAG

The cable tension, angle, and depth values determined at the reference speeds are used to calculate cable hydrodynamic drag loading coefficients from the differential equations that relate cable forces to cable configuration. The cable coordinate and force system utilized for the present analysis is based on Knutson.[7] This representation is reviewed in the next subsection. Reduction of the data to tangential and normal drag coefficients is presented in the subsections that follow. Cable hydrodynamic side loading, although present on bare stranded cables, was not determined.

CABLE COORDINATE AND FORCE SYSTEM

The differential equations that describe the three-dimensional static configuration of a cable in a uniform stream are derived from the equilibrium of external forces acting on an element of the cable. A free-body diagram showing a

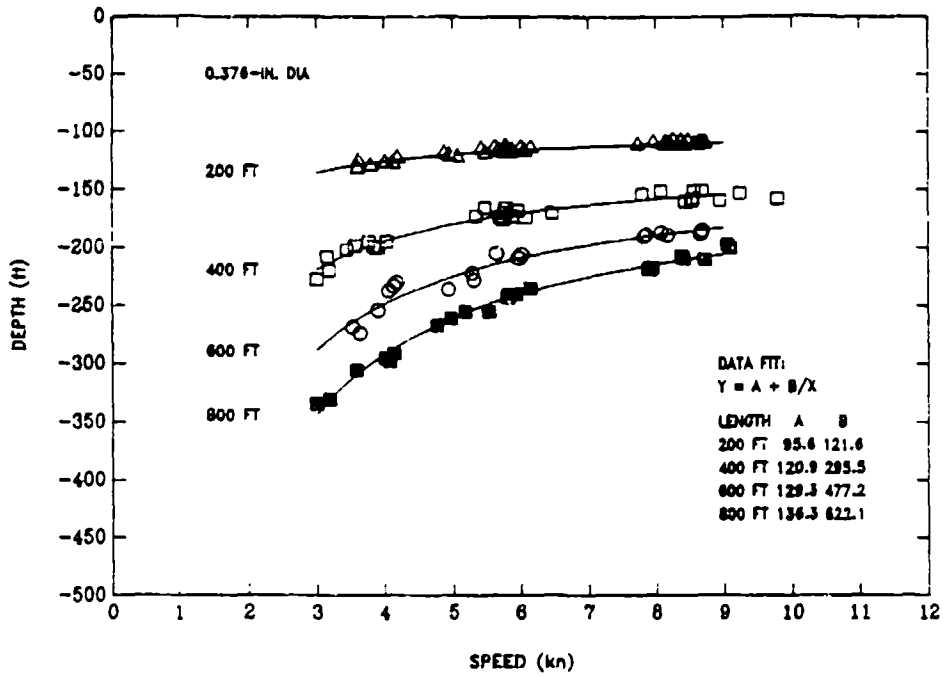

Fig. 10. Depressor depth as a function of speed for various lengths of the small cable.

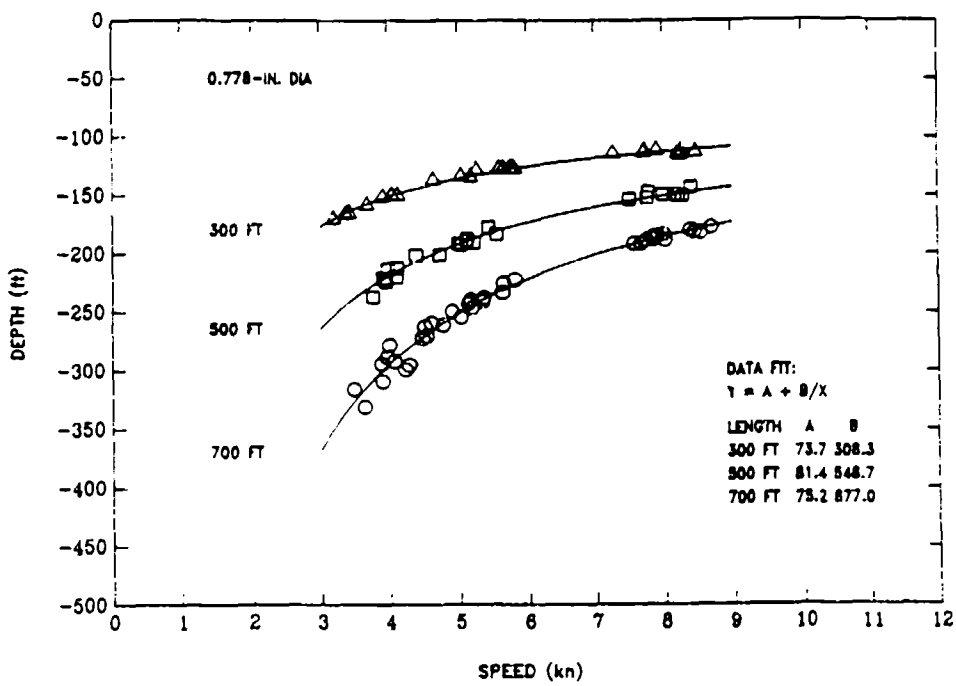

Fig. 11. Depressor depth as a function of speed for various lengths of the large cable.

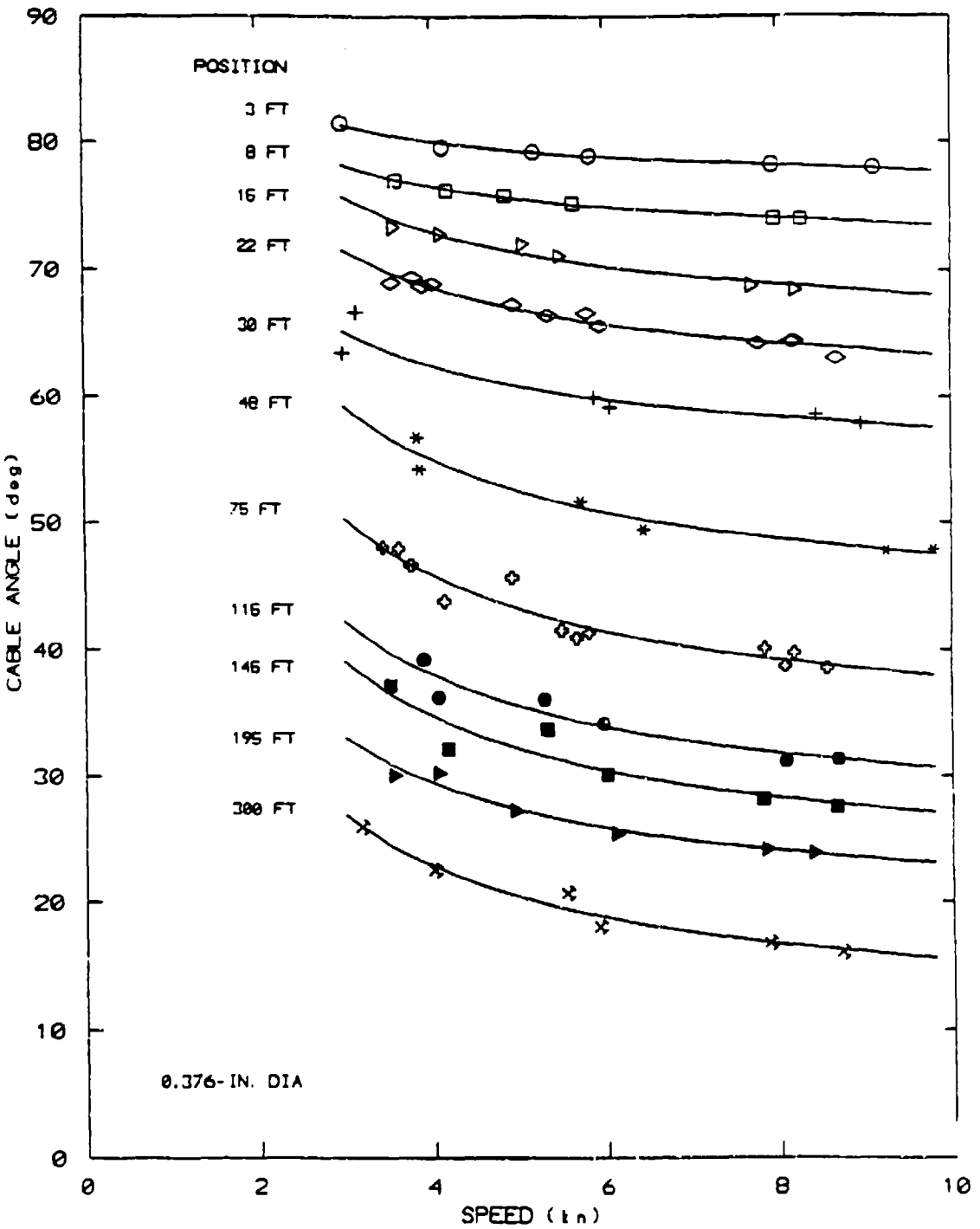

Fig. 12. Cable angle as a function of speed at various positions along the small cable.

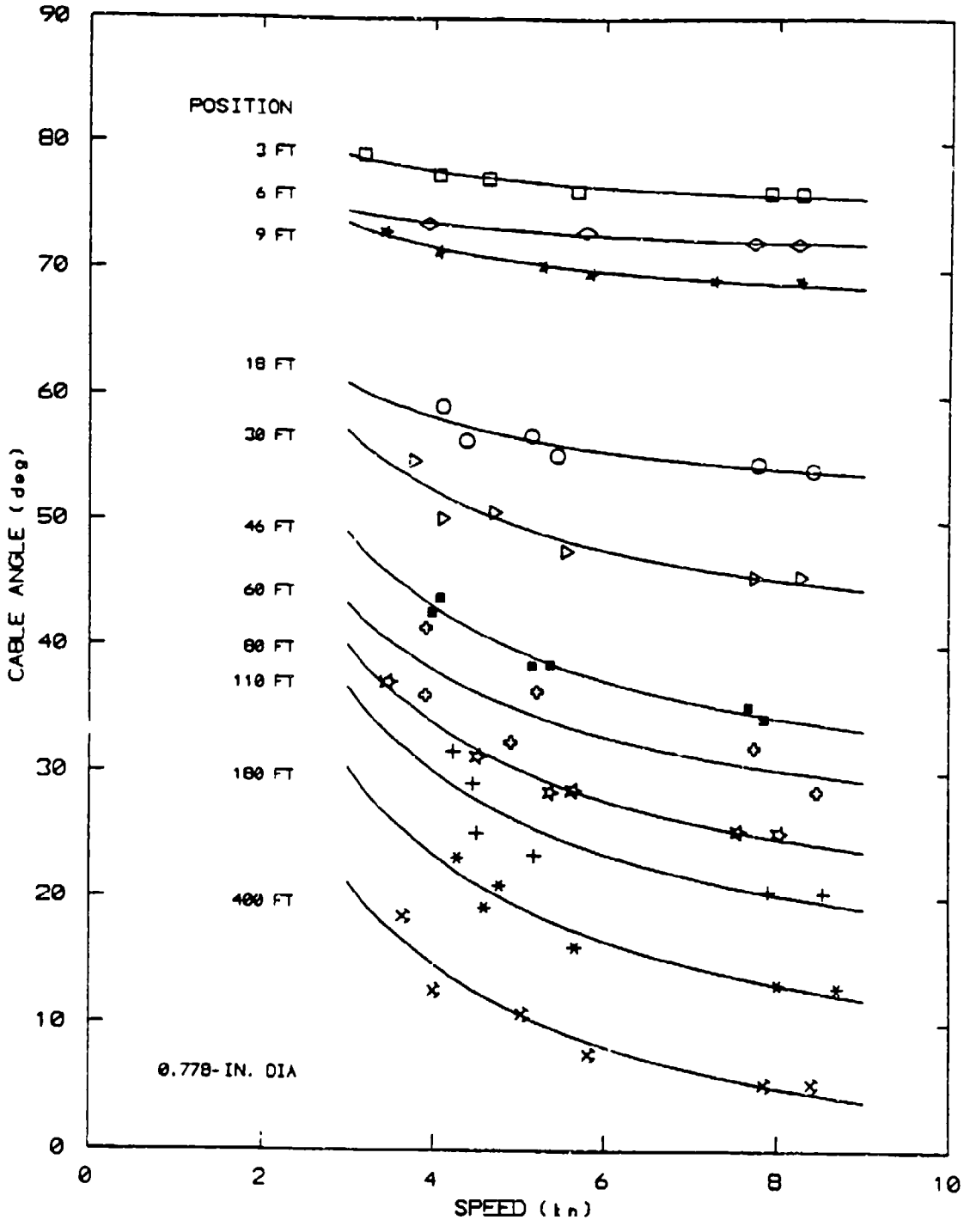

Fig. 13. Cable angle as a function of speed at various positions along the large cable.

Table 7. Coefficients of curve-fit equations used to determine cable angle at various positions along the cable as a function of speed.

Equation: $Y = A + B/X^*$			
Small Cable (0.376-in dia)			
Data point	CAMD position from Depressor, ft (m)	A	B
1	3.00 (0.91)	76.22	15.17
2	8.00 (2.43)	71.48	20.10
3	15.00 (4.57)	64.63	33.32
4	22.00 (6.71)	59.84	35.09
5	30.00 (9.14)	54.26	32.74
6	48.00 (14.63)	42.35	50.63
7	75.00 (22.86)	32.58	53.26
8	115.00 (35.05)	25.61	49.96
9	145.00 (44.20)	21.79	52.09
10	195.00 (59.44)	18.63	43.56
11	300.00 (91.44)	10.60	49.12
Large Cable (0.778-in dia)			
Data point	CAMD Position from Depressor, ft (m)	A	B
1	3.00 (0.91)	73.79	15.54
2	6.00 (1.83)	70.58	11.75
3	9.00 (2.74)	65.93	22.85
4	18.00 (5.49)	50.05	32.71
5	30.00 (9.14)	38.09	57.34
6	46.00 (14.02)	25.43	70.92
7	60.00 (18.29)	22.27	63.37
8	80.00 (24.38)	15.54	73.53
9	110.00 (33.53)	10.25	79.43
10	180.00 (54.86)	2.63	83.21
11	400.00 (121.92)	-4.86	78.15
* Y = Cable angle in deg; X = Speed in knots			

segment of cable of elemental length ds acted upon by hydrodynamic, hydrostatic, gravitational, and tension forces is illustrated in Fig. 14. The coordinate system (X,Y,Z) shown is a right-hand, orthogonal system fixed in space with the X-axis positive in the direction of tow (or negative in the free-stream direction) and the Z-axis positive in the direction of gravity. The equations are conveniently derived for an orthogonal coordinate system fixed to the cable. The hydrodynamic force is resolved into components Fds, Gds, and Hds where

F is the force component per unit length normal to the cable in the plane defined by the cable element and the free-stream direction,

G is the force component per unit length tangential to the cable, and

H is the (side) force component per unit length normal to the plane defined by the cable element and the free-stream direction.

The cable fixed coordinate system defined by the directions of F, G, and H may be obtained by first rotating the spatial system through an angle β about the X-axis and then rotating the resulting intermediate (X',Y',Z') coordinate system through an angle ϕ about the Y'-axis. In towed systems nomenclature, the angles β and ϕ are referred to as the kite angle and the cable (or towline) angle, respectively. Since the orientation of the cable changes in space, the angles β and ϕ are functions of cable scope. The forces per unit length in the normal, tangential, and lateral (side) directions are, respectively,

$$-T(d\phi/ds) + F + W\cos\beta\cos\phi = 0 \quad (1)$$

$$(dT/ds) + G - W\cos\beta\sin\phi = 0 \quad (2)$$

$$-T\sin\phi(d\beta/ds) + H - W\sin\beta = 0 \quad (3)$$

where

T is cable tension,

s is cable length, and

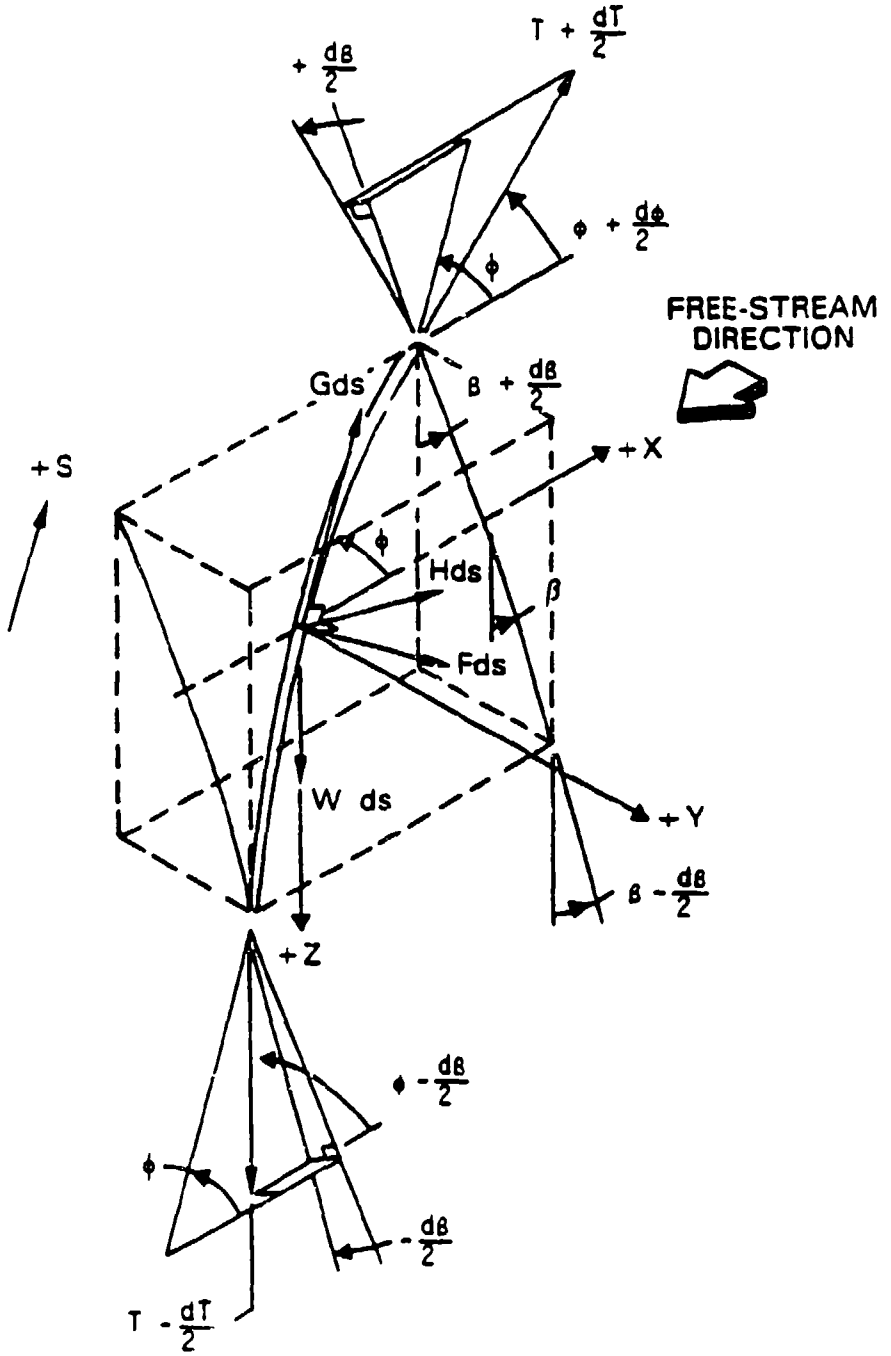

Fig. 14. Forces acting on a segment of cable of length ds.

W is cable weight per unit length in the fluid.

The equations that relate cable displacement to cable length are

$$dx = ds \cos\phi \tag{4}$$

$$dy = -ds \sin\phi \sin\beta \tag{5}$$

$$dz = -ds \sin\phi \cos\beta \tag{7}$$

where x, y, and z are displacements along the X, Y, and Z directions, respectively.

The hydrodynamic force components F and G result from fluid drag forces; the hydrodynamic force component H is the result of fluid side or lift forces. The drag force components F and G lie in the plane defined by a cable element and the free-stream flow direction. The side force component H has a direction normal to the cable plane. Generally, the drag components are assumed to be a product of a drag per unit length that is a function only of Reynolds number and a loading function that is a function only of cable angle ϕ. Similarly, the lift component is expressed conveniently as the product of a side force per unit length that is a function only of Reynolds number and a loading function that is a function only of cable angle ϕ. Under this convention, the hydrodynamic force components per unit length have the following form:

$$F(Re,\phi) = -R(Re) * f_n(\phi) \tag{8}$$

$$G(Re,\phi) = -R(Re) * f_t(\phi) \tag{9}$$

$$H(Re,\phi) = F_s(Re) * f_s(\phi) \tag{10}$$

where

R is cable drag per unit length when the cable is normal to the free-stream direction ($R = \frac{1}{2}\rho C_r V^2 d$),

F_s is cable hydrodynamic side force per unit length at the orientation of the cable that produces the largest value ($F_s = \frac{1}{2}\rho C_s V^2 d$),

Re is Reynolds number usually based on cable diameter,

ρ is fluid density,

C_r is cable normal drag coefficient based on frontal area,

C_s is cable side force coefficient based on frontal area,

d is cable diameter or thickness,

V is free-stream velocity,

f_n is cable normal hydrodynamic loading function,

f_t is cable tangential hydrodynamic loading function, and

f_s is cable hydrodynamic side force loading function.

The hydrodynamic loading functions $f_{n,t,s}$ are commonly expressed using the first five terms of a trigonometric series as follows:

$$f_{n,t,s} = A_0 + A_1 \cos\phi + B_1 \sin\phi + A_2 \cos(2\phi) + B_2 \sin(2\phi). \quad (11)$$

Bare electro-mechanical cables and wire ropes with helically wrapped outer strands have lateral shape asymmetries which can induce a significant hydrodynamic side (lift) force. The side force will, in turn, produce cable kiting. Although kiting was certainly produced on the experiment cables during the at-sea evaluation, a sensitivity analysis performed prior to the evaluation indicated that the expected kite angles would have negligible effect on the determination of the hydrodynamic drag force components. Therefore, kite angle β was not measured during the evaluation and is neglected in the analysis. The kiting may, however, have a measurable effect on towing depth especially for longer towline lengths. This effect is discussed further in the section of this report that compares predicted depth to measured depth.

TANGENTIAL HYDRODYNAMIC FORCE

The tangential hydrodynamic force is determined by rearrangement of Eq. 2 and substitution of Eq. 7. The result is

$$G = -(dT/ds) - W(dz/ds) \tag{12a}$$

or, in finite difference form, Eq. 12a becomes,

$$G = -(\Delta T/\Delta s) - W(\Delta z/\Delta s). \tag{12b}$$

The rate of change of tension T with respect to cable length s at the reference speeds of 4, 6, and 8 knots can be determined from the curve-fit equations of tension as a function of speed shown in Figs. 8 and 9. The tension values thus determined at the reference speeds are fitted as functions of cable length with curve-fit equations as shown in Figs. 15 and 16 for the small and the large cables, respectively. The linear equations shown in the figures provide satisfactory fits. The desired $\Delta T/\Delta s$ relationships are the values of the slopes of the various equations. The slope is the coefficient B indicated in the figures.

The rate of change of depth with respect to cable length $\Delta z/\Delta s$ at the reference speeds, also required to solve Eq. 12b, can be obtained from the curve-fit equations of depressor depth as a function of speed shown in Figs. 10 and 11. Since the functional relationships of depth variation with respect to cable length are not linear, no attempt was made to fit these data with curve-fit equations. Rather, the change in depth between successive cable lengths is used directly, which produces $\Delta z/\Delta s$ values related to an average cable length. Also an average cable angle at the ship corresponding to the average cable length is determined from the values of $\Delta z/\Delta s$ using Eq. 7.

With the required values of $\Delta T/\Delta s$ and $\Delta z/\Delta s$ thus determined and with the known in-water weight, Eq. 12b is solved for the tangential hydrodynamic force per unit length G. This force is assumed to be a function of angle as well as Reynolds number as indicated by Eq. 9. However, in all cases the average cable angles for which tension data are available are relatively shallow. These angles vary between 22 and 7 deg. Therefore, no angle dependency can be determined, and the values for various angles at

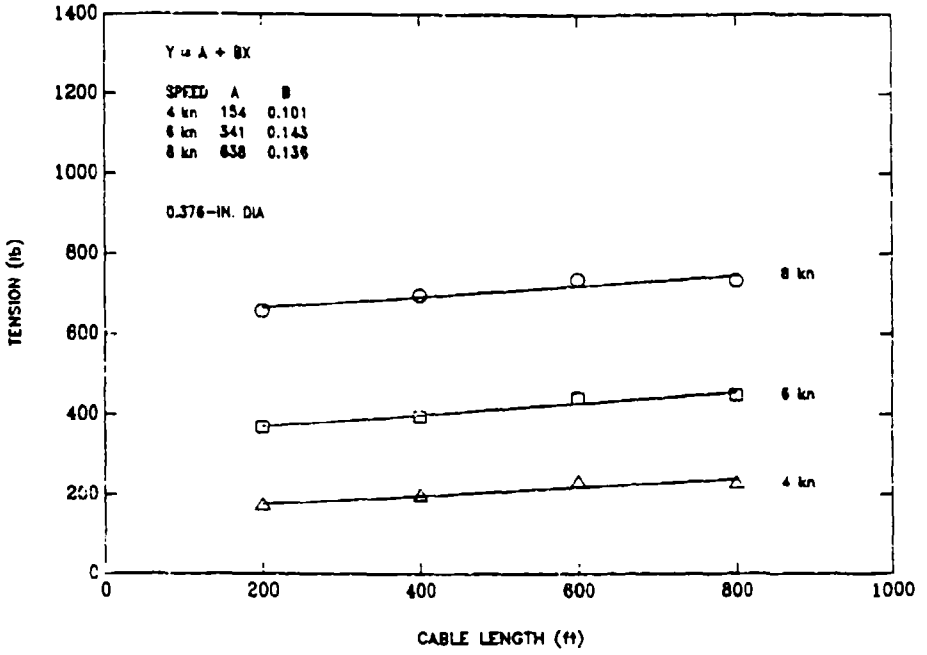

Fig. 15. Tension at the ship as a function of cable length for the small cable at 4, 6, and 8 knots.

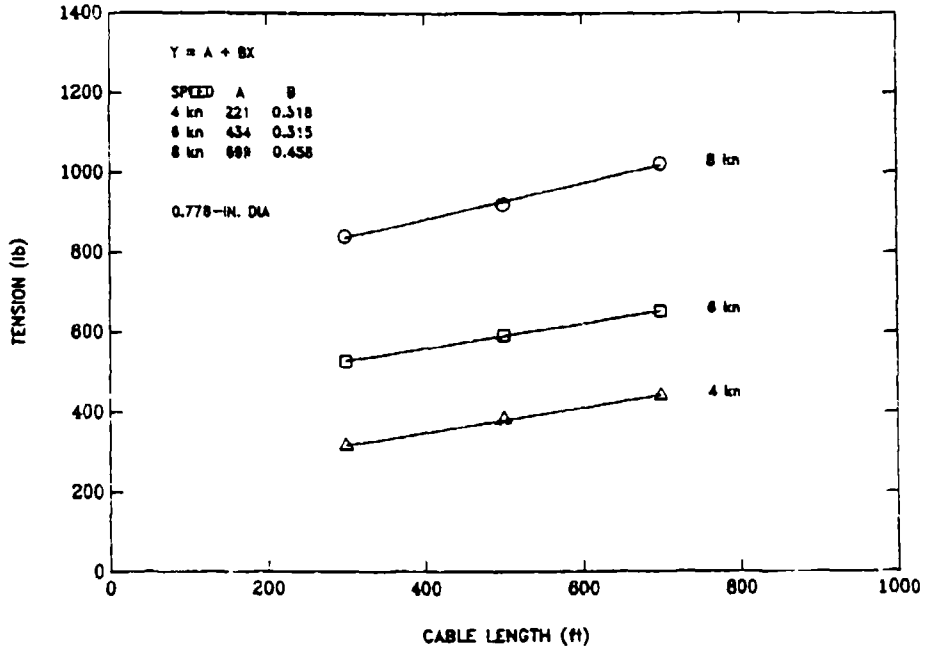

Fig. 16. Tension at the ship as a function of cable length for the large cable at 4, 6, and 8 knots.

a given speed are averaged to form a single value. The tangential drag coefficient C_{td} based on frontal area, determined by nondimensionalizing G, is plotted as a function of Reynolds number (based on cable diameter) for both the small and the large cables in Fig. 17. Although drag coefficient variations are apparent in the figure, these probably are due more to data scatter then to a Reynolds number dependency. The values appear to be similar for the two cables, and therefore an average tangential drag coefficient $C_{td} = 0.0249$ also is shown in Fig. 17 for comparison. The tangential drag coefficient C_{td} as used in this analysis is determined by the following relationship:

$$C_{td} = -G/(\tfrac{1}{2}\rho V^2 d) \tag{13}$$

where V is free-stream velocity and d is cable diameter.

This form of the tangential drag coefficient can be related to the Pode[8] friction factor f by dividing by the normal drag coefficient C_r defined previously. C_{td} can also be related to the Eames[9] friction ratio μ by dividing by C_r if it is tacitly assumed that the present values determined for the tangential hydrodynamic force are sufficiently close to zero cable angle. The relationships between Pode and Eames friction factors and the tangential loading function are, according to Pode,[8]

$$f_t = f \tag{14}$$

and according to Eames,[9]

$$f_t = \mu \cos\phi. \tag{15}$$

Eames assumes a tangential loading function that varies as a function of cable angle ϕ. Pode assumes that the angle dependency is negligible. In practice, the two forms of loading usually provide similar results since the tangential hydrodynamic loading is relatively small for bare cables.

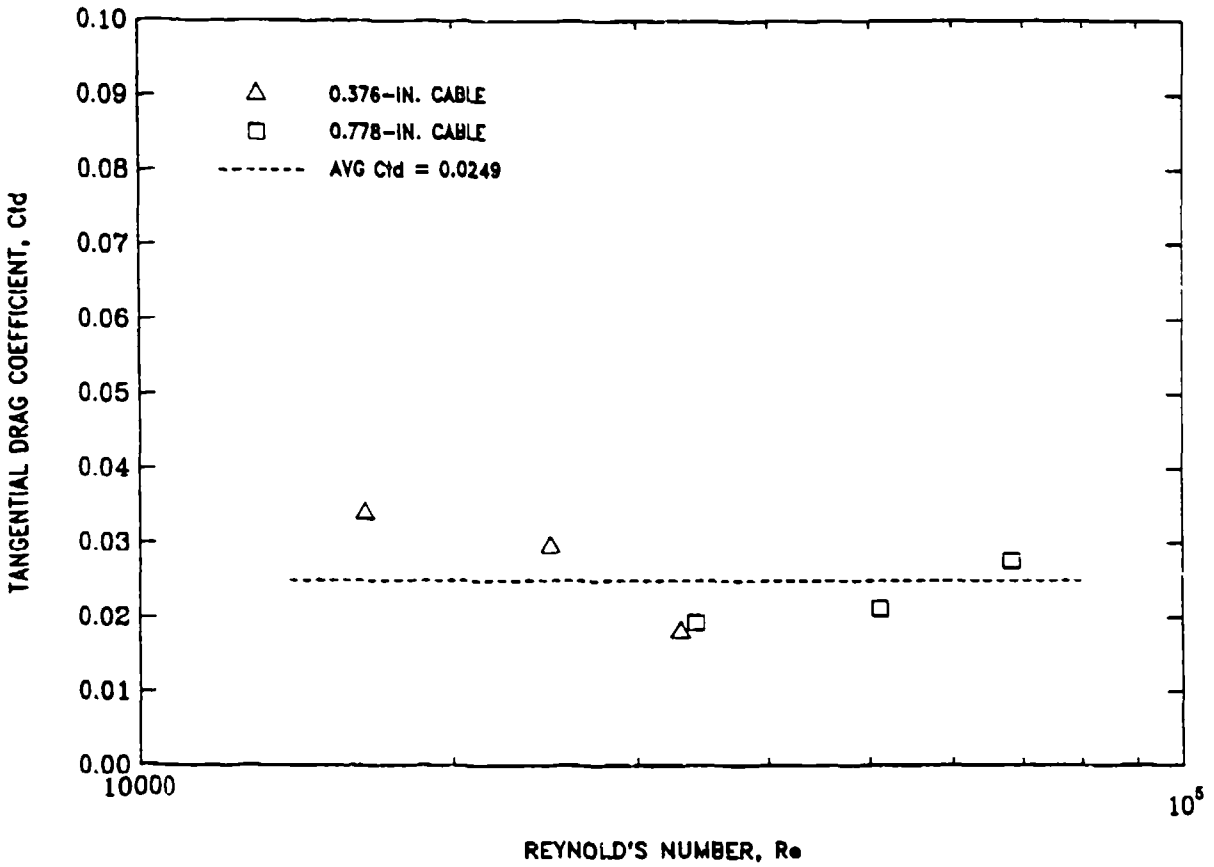

Fig. 17. Tangential drag coefficient as a function of Reynolds number.

NORMAL HYDRODYNAMIC FORCE

The hydrodynamic drag force component normal to the cable axis is determined from the evaluation data by rearrangement of Eq. 1. The result, neglecting kite angle β, is

$$F = T(d\phi/ds) \cdot W \cos\phi. \quad (16)$$

The angles required to determine the rate of change of cable angle ϕ with respect to cable length s at the reference speeds of 4, 6, and 8 knots can be obtained from the curve-fit equations of angle as a function of speed listed in Table 7. Data scatter is such that suitable slopes of angle ϕ with respect to length s cannot be determined by taking the differences between successive data points. Rather, the data are fitted with equations to obtain the slopes. Two equation forms are necessary to satisfactorily fit the full range of angles as a function of cable length. Thus in all cases, a third-order polynomial is used to fit data points 1 through 8 (defined in Table 7) and an exponential form is used to fit data points 6 through 11. The following form of equation provided the best overall fit of points 6 through 11:

$$Y = Ae^{(\ln X \cdot B)^2 /C}$$

where Y represents cable angle ϕ and X represents the distance along the cable from the depressor.

The fitted equations are compared to the data at the three reference speeds for the small and the large cables in Figs. 18 and 19, respectively. The coefficients of the curve-fit equations that relate cable angle to cable position are listed in Table 8. Of interest are the cable angle values predicted at zero cable length (which corresponds to the cable angle at the depressor). These predicted values are compared to the values determined for the depressor (see Appendix A) in Fig. 20. Excellent agreement is obtained.

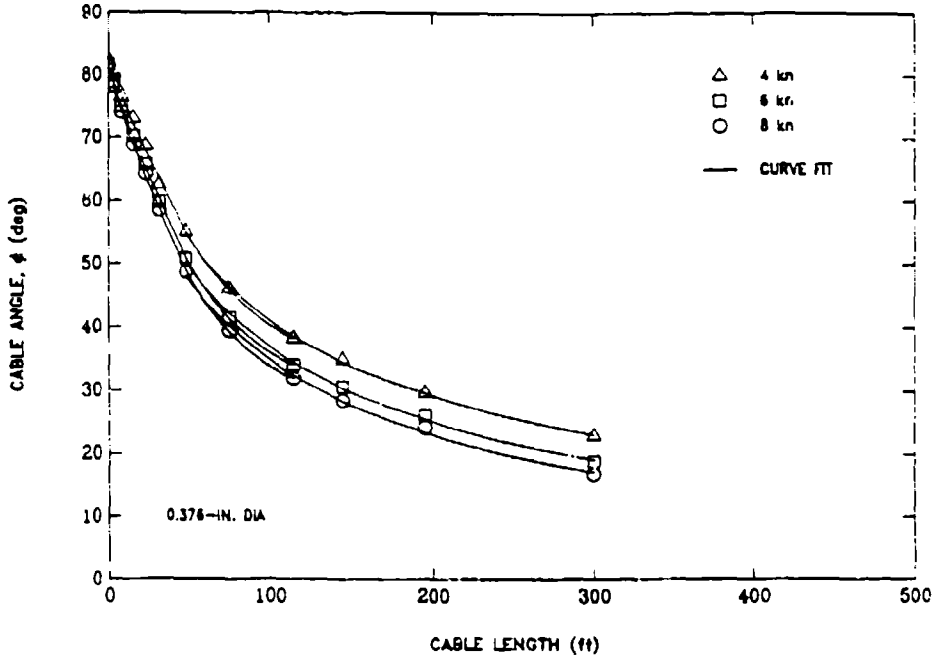

Fig. 18. Cable angle as a function of cable length from the depressor for the small cable at 4, 6, and 8 knots.

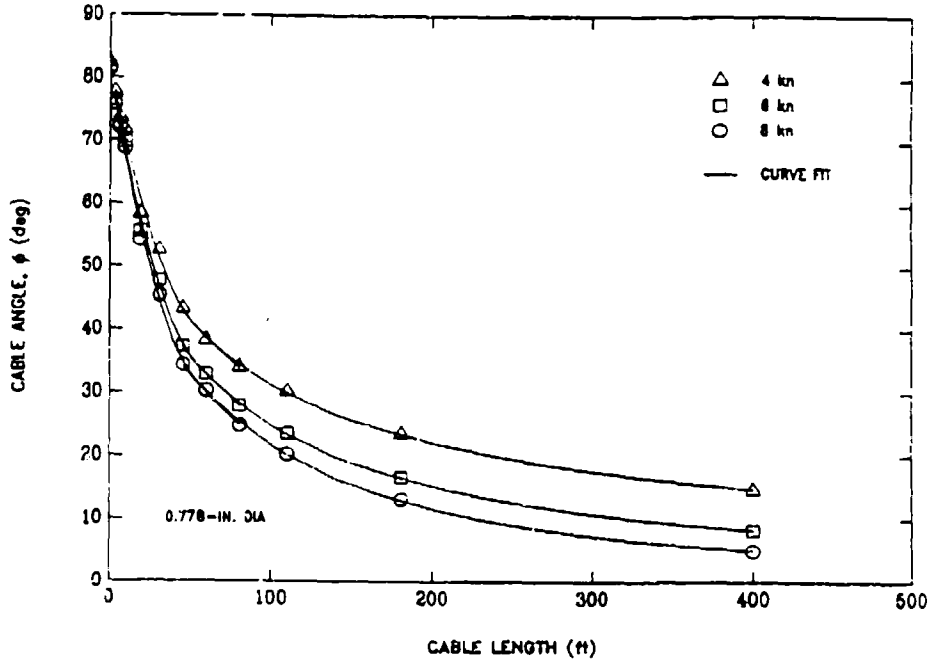

Fig. 19. Cable angle as a function of cable length from the depressor for the large cable at 4, 6, and 8 knots.

Table 8. Coefficients of curve-fit equations used to determine cable angle as a function of cable length from the depressor at 4, 6, and 8 knots.

Small Cable (0.376-in dia)							
	$Y = A+BX+CX^2+DX^3$ Data points 1-8				$Y = Ae^{(\ln X-B)2/C}$ Data points 6-11		
Speed, kn	A	B	C	D	A	B	C
4.0	82.45	-0.7408	3.835E-3	-6.469E-6	82.26	1.488	-13.94
6.0	81.39	-0.8375	4.670E-3	-8.458E-6	69.33	2.052	-10.31
8.0	80.85	-0.8857	5.083E-3	-9.417E-6	63.28	2.323	- 8.70
Large Cable (0.778-in. dia)							
	$Y = A+BX+CX^2+DX^3$ Data points 1-8				$Y = Ae^{(\ln X-B)2/C}$ Data points 6-11		
Speed, kn	A	B	C	D	A	B	C
4.0	82.19	-1.5020	1.807E-2	-8.568E-5	71.04	0.969	-16.02
6.0	81.96	-1.7100	2.061E-2	-9.635E-5	52.25	2.194	- 7.77
8.0	81.85	-1.8130	2.188E-2	-1.016E-4	41.00	2.919	- 4.46
Y = Cable angle in deg; X = Cable length from depressor in ft							

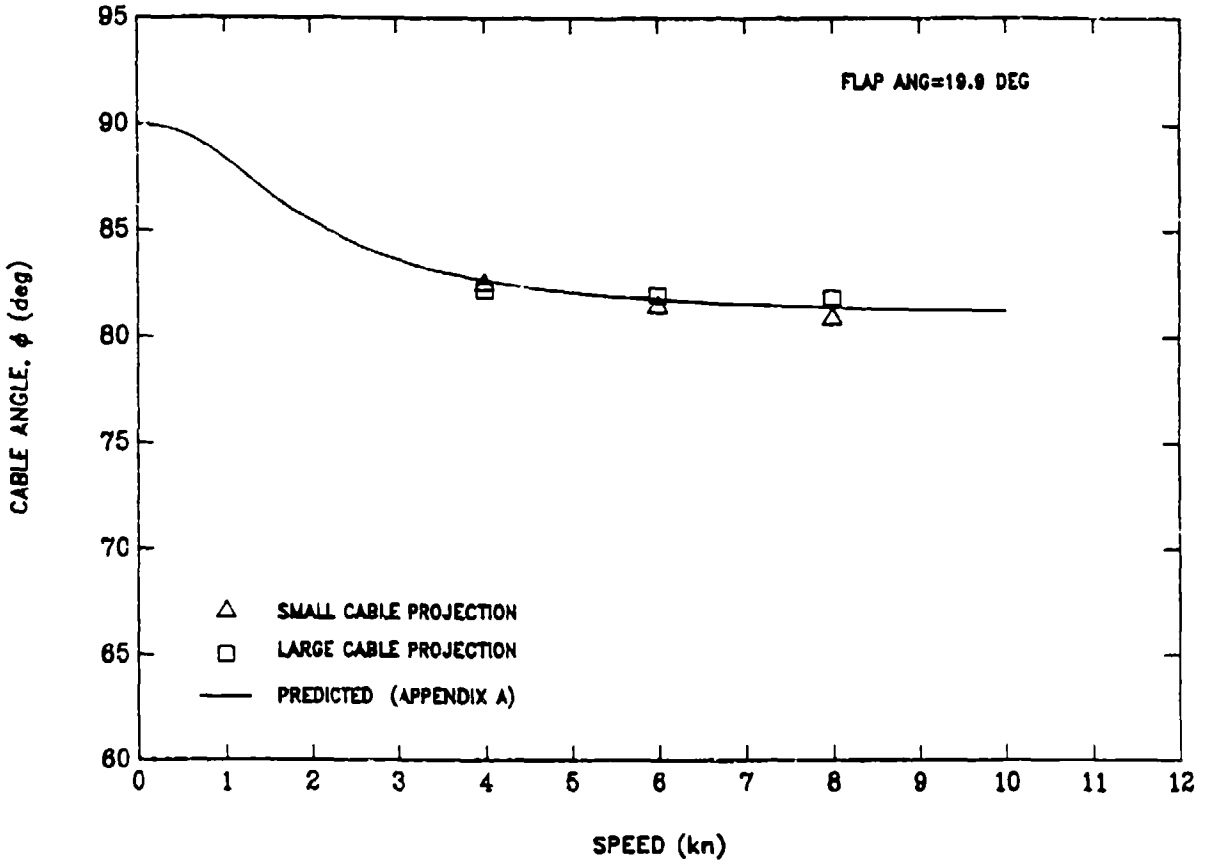

Fig. 20. Predicted cable angle at the depressor as a function of speed.

The rate of change of cable angle with respect to cable length $d\phi/ds$ is determined by differentiating the curve-fit equations discussed above. For this analysis, the polynomial fit is used for points 1 through 6 and the exponential fit is used for points 8 through 11. The value for point 7 is obtained by averaging the values for the two fits. The $d\phi/ds$ values plotted as functions of cable length for the small and large cables are shown in Figs. 21 and 22, respectively.

To solve Eq. 16, tension must also be known at points along the cable. Since tension was not measured at the cable length positions of interest, tension values must be calculated. This calculation is done by numerically integrating Eq. 2 and solving for tension T. The result in finite difference form is

$$T = To + \sum (-G_i + W \sin \phi_i)\Delta s_i \qquad (17)$$

where

To is cable tension at the depressor,

G_i is cable tangential loading of the ith cable segment,

W is in-water cable weight per unit length,

ϕ_i is average cable angle of the ith cable segment, and

s_i is length of the ith cable segment.

For calculation of tension, the Eames[9] form of tangential loading as indicated by Eq. 15 was assumed.

The normal hydrodynamic force per unit length F calculated from Eq. 16 is plotted in coefficient form for each cable angle and reference speed for both cables in Fig. 23 as a function of cable angle ϕ. The relationship between normal force per unit length F and the normal force coefficient C_n based on frontal area is

$$C_n = -F/(\tfrac{1}{2}\rho V^2 d) \qquad (18)$$

where V is free-stream velocity and d is cable diameter. In Fig. 23, the data points represent the values calculated from Eqs. 16 and 18. The curve in the figure is a

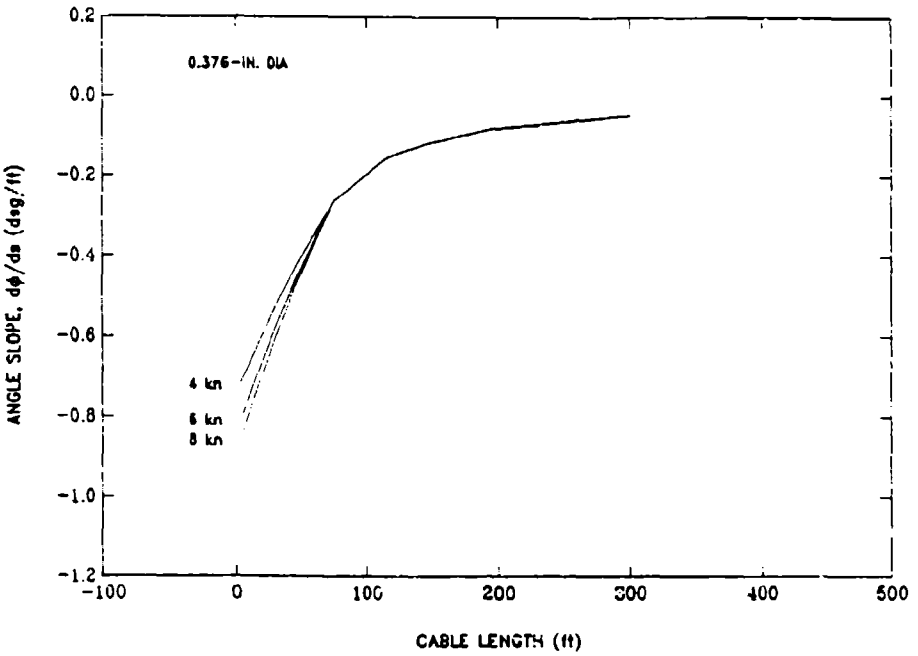

Fig. 21. Rate of change of cable angle with respect to cable length for the small cable at 4, 6, and 8 knots.

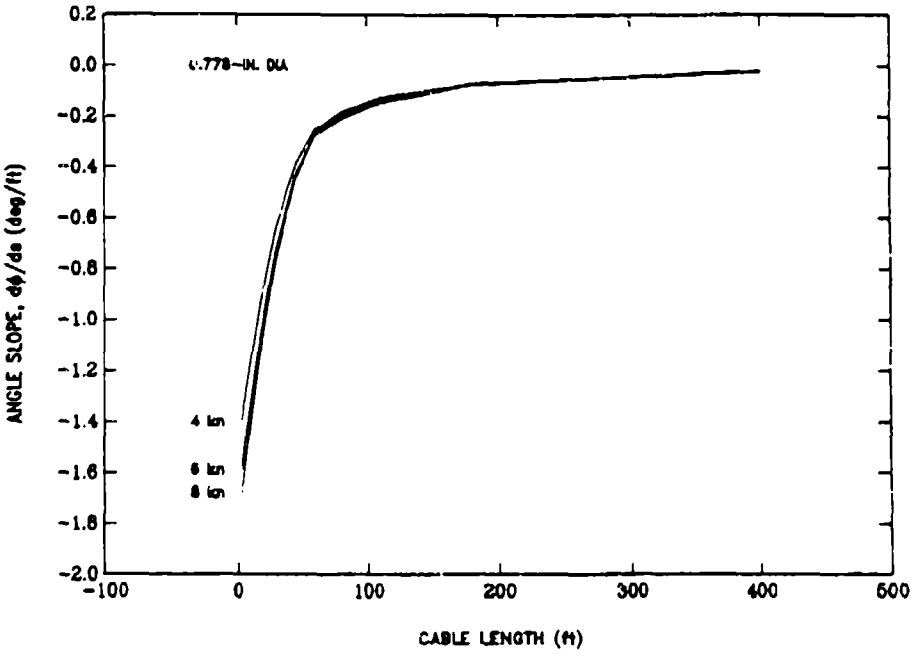

Fig. 22. Rate of change of cable angle with respect to cable length for the large cable at 4, 6, and 8 knots.

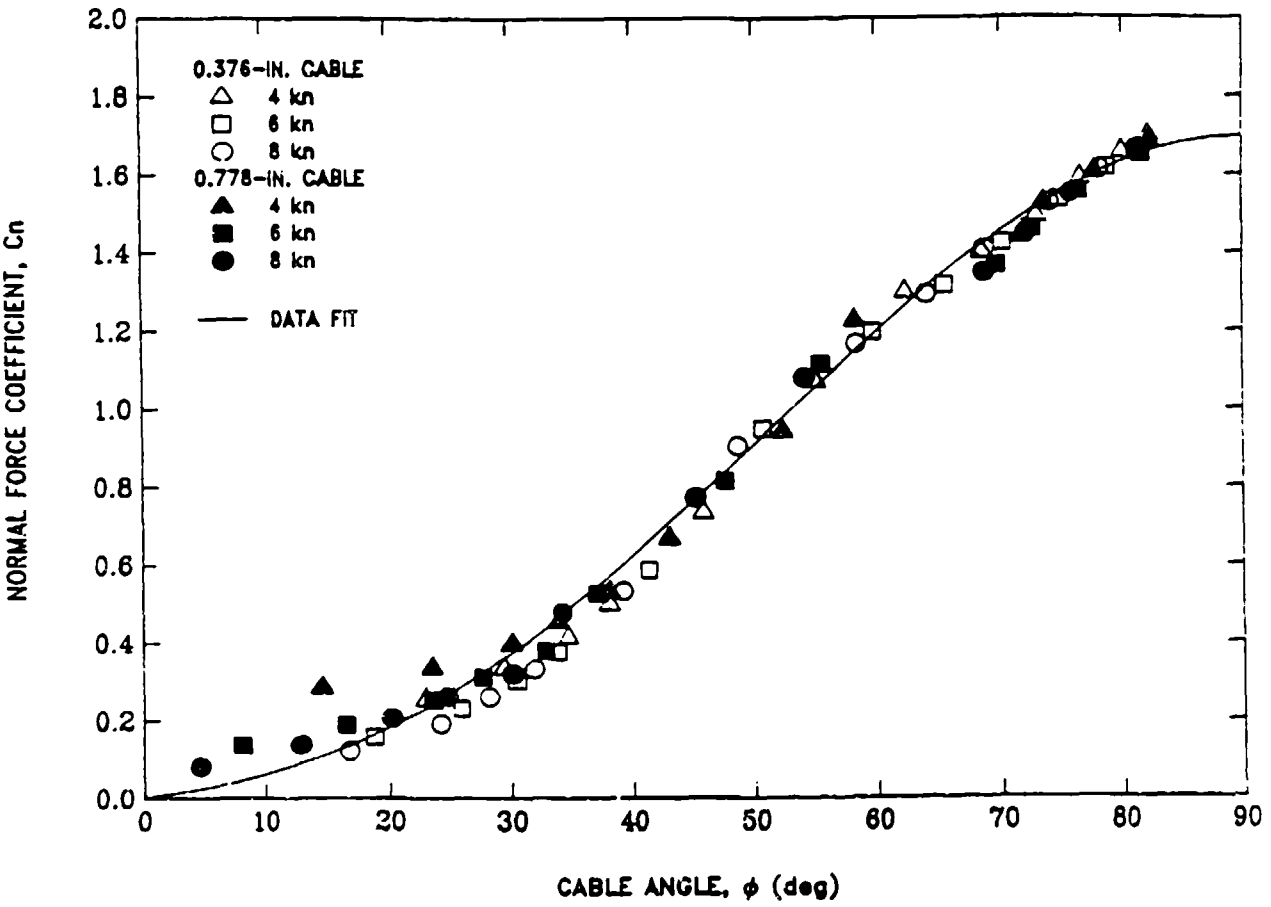

Fig. 23. Normal force coefficient as a function of cable angle.

fitted function using the first five terms of the trigonometric series given by Eq. 11. The value of the curve at ϕ = 90 deg is the average value of the normal drag coefficient C_r. End conditions were specified on the curve fit of C_n as follows:

$$C_n(\phi=0) = 0$$

$$C_n'(\phi=90) = 0$$

where $C_n(\phi=0)$ is the value of the curve at zero angle and $C_n'(\phi=90)$ is the slope of C_n at 90 deg.

A value of C_r is determined for each set of data by multiplying the fitted curve of C_n by a factor which provides the best overall fit for that set of data. The resulting C_r values for each set of data for both cables are plotted as a function of Reynolds number (based on cable diameter) in Fig. 24. The average value of C_r = 1.70 is also plotted in this figure for comparison. No Reynolds number dependency is apparent. Also, the C_r values for both cables are identical to within the scatter of the data.

The normal loading function f_n is determined by dividing the normal force coefficient C_n by the normal drag coefficient C_r. The normal loading function is shown in Fig. 25 as a function of cable angle ϕ. In this figure, the data points represent values calculated at each cable angle for which the angle was measured. The value plotted is the data value of C_n divided by the value of C_r determined for that set of data. The f_n curve plotted in Fig. 25 is the fitted C_n equation divided by the average C_r value. The resulting equation for the normal loading function f_n is

$$f_n = -0.424 + 0.869\cos\phi + 0.979\sin\phi - 0.445\cos(2\phi) - 0.434\sin(2\phi). \quad (19)$$

Normal loading function values calculated with Eq. 19 are compared to a sine squared normal loading function in Fig 26. The values from Eq. 19 are somewhat lower than sine squared at intermediate cable angles but are greater than sine squared at

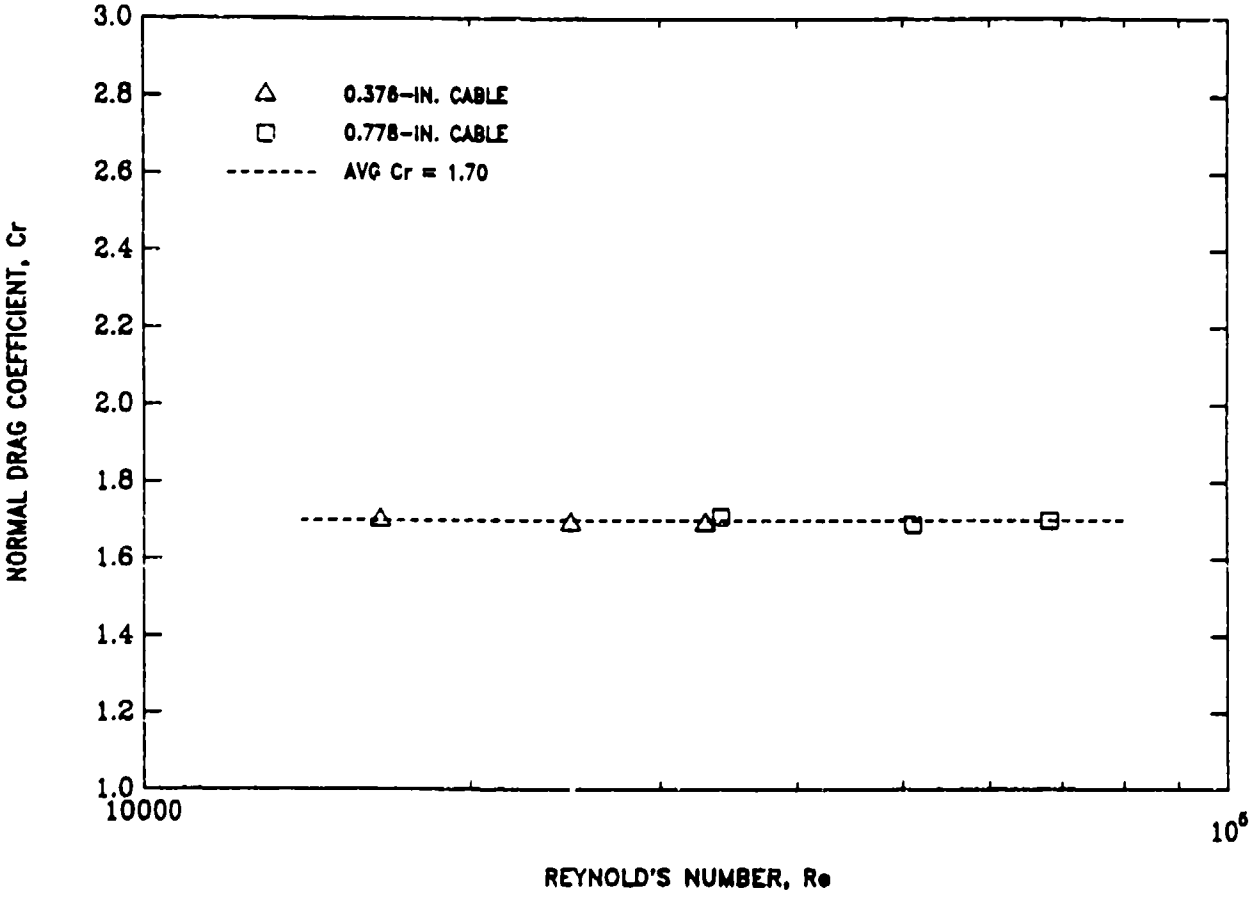

Fig. 24. Normal drag coefficient as a function of Reynolds number.

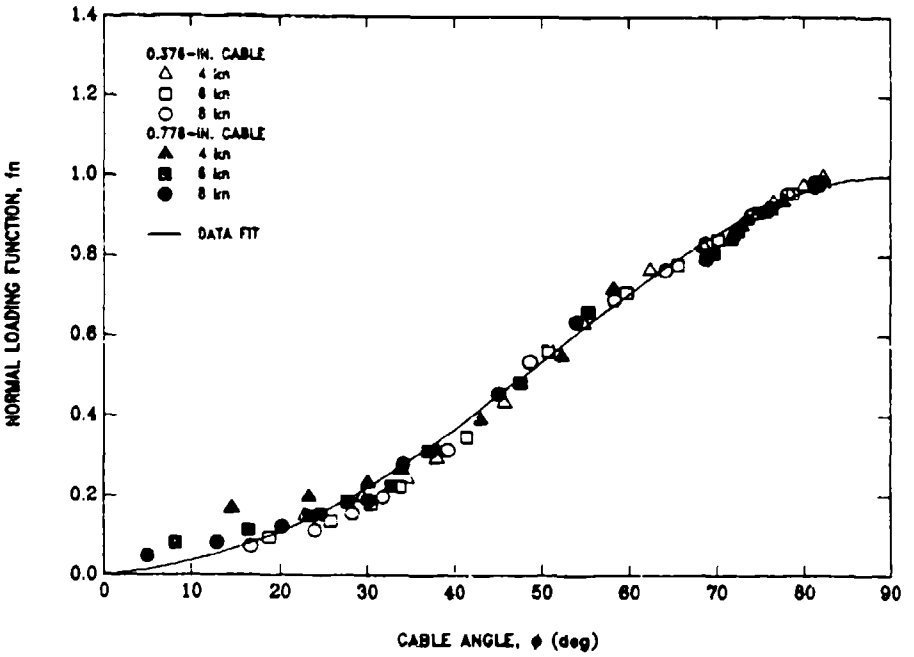

Fig. 25. Normal hydrodynamic loading function.

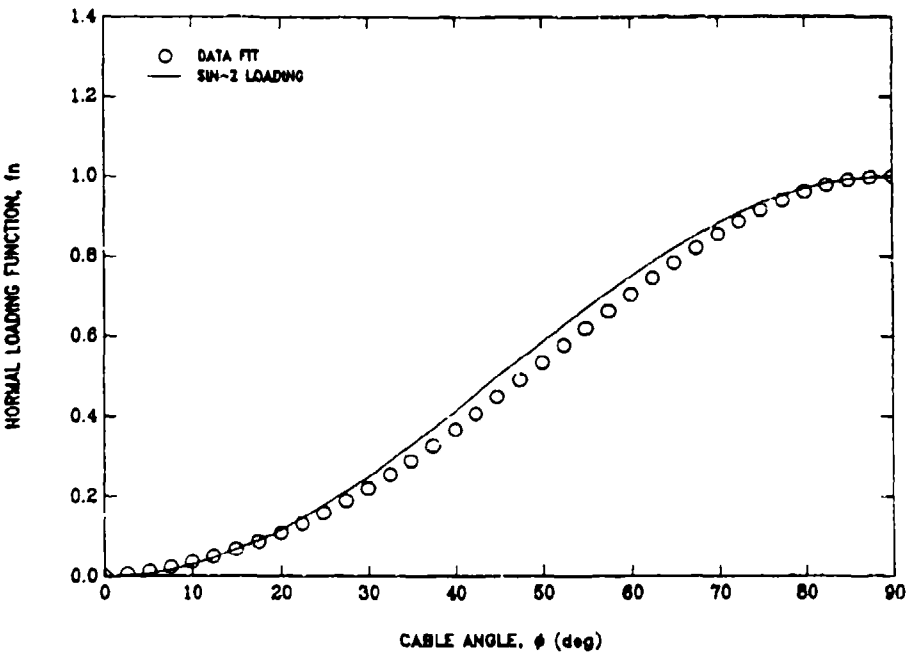

Fig. 26. Normal hydrodynamic loading function compared to $\sin^2 \phi$.

cable angles below 15 deg. Also of interest is a comparison of the normal force coefficient C_n determined by the present analysis to the normal force coefficient determined by Folb and Nelligan.[3] This comparison is shown in Fig 27. The two functions are nearly identical up to a cable angle of approximately 50 deg. Above 50 deg, the C_n values determined by the present analysis are considerably higher. This result may reflect the fact that cable angles near the depressor, where the angles are steep, have never been measured at sea prior to the evaluation reported here.

DRAG UNCERTAINTY

The measurement accuracies of the various sensors used during the at-sea evaluation are known both from manufacturer specifications and from laboratory calibrations that were performed prior to and after the evaluation. The major uncertainties result from environmental factors, the largest being ship motion and ocean currents.

Seas were relatively calm during the evaluation, never exceeding an estimated state 2, and ship motions were small. As discussed in the data results section of this report, ship motion had negligible effect on depressor motion and measurements of cable angle. Ship motion primarily affected speed and tension measurements as judged by standard deviations of the measurements during data runs. Springston[6] provides data related to the effect of heaving motion on knotmeter speed error. Heaving motions introduce a bias that increases indicated speed. For this at-sea evaluation, the speed error induced by ship motion is estimated to be no greater than 0.02 knot for the worst sea conditions encountered. This error magnitude corresponds to a knotmeter peak-to-peak heaving motion of 3 ft (0.9 m) at a towing speed of 4 knots and a frequency of 0.2 Hz. As speed increases, motion error is attenuated.

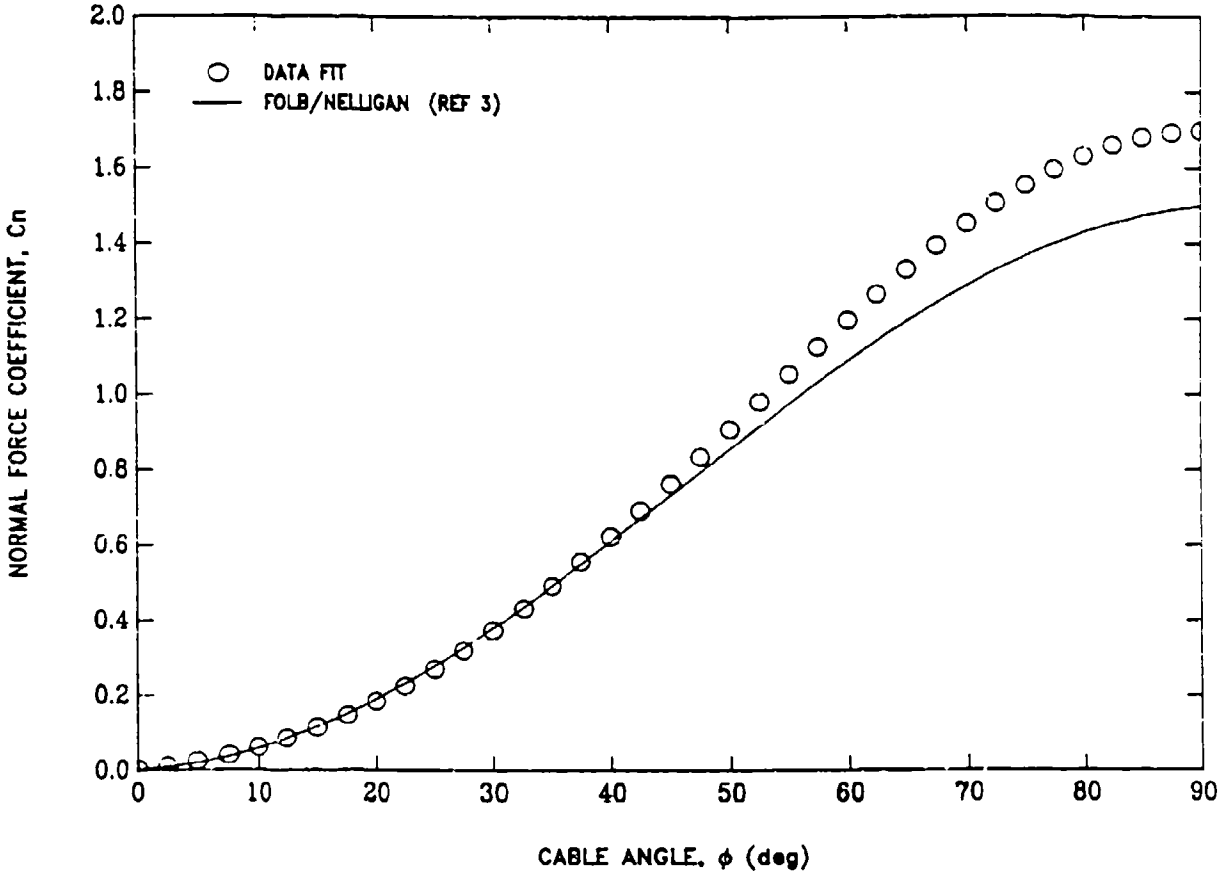

Fig. 27. Normal force coefficient comparison.

The effect of ship motion on tension measurement is less certain. If the motion is primarily heave and if tension varies linearly with heave, then over time, tension will average out to the correct value. Since ship motions were small during the evaluation and the cable catenaries were shallow as judged by the angles measured at the ship, the effect of ship motion on average tension is assumed to be negligible.

The other major environmental factor is ocean currents. If through-the-water speed is measured, as with a knotmeter, then constant currents that do not vary with depth will have no effect. Current depth gradients do affect speed measurement accuracy, however. Measurements made on reciprocal ship headings tend to negate speed errors induced by current gradients if the ship track is parallel to the ocean current direction (although this will increase apparent data scatter). If the ship track is not parallel to the current, however, the effect of current gradient is additive (or subtractive) by the vector sum of towing speed and current gradient in both towing directions. That is, the indicated through-the-water speed (as measured by the knotmeter) is less or greater than the true speed at depth in both tow directions in a cross-current gradient.

Current gradients also affect the measurement accuracies of all quantities that depend on speed. If the quantity varies linearly with speed, then the effect is negated with reciprocal tracks parallel to the current. However, if the quantity varies non-linearly with speed, the measurement error is not negated. Instead a bias error will be introduced. Bias errors induced by this effect cannot be accounted for without knowing the magnitude of the gradient, and therefore measurements on reciprocal headings are simply averaged together to minimize error.

The Tongue of the Ocean chosen to perform the evaluation is relatively free of ocean current gradients except near the surface where gradients are sometimes large. The data scatter indicated in the figures of this report that show various quantities

plotted as functions of speed is typically greater than the precision errors of the measurements, which suggest that current gradients were present and that the measurements were affected. Unfortunately, this effect is difficult to quantify without direct knowledge of actual gradients and directions.

Environmental data provided by the U.S. Naval Oceanographic Office[10] indicate mean current gradients between the estimated depth of the knotmeter and the depth of the depressor of up to 0.1 knot for the month of March and up to 0.2 knot for the month of August in the area of operation. Between the depth of the depressor and the surface, a mean gradient of up to 0.45 knot was observed during these two months. In all cases, the currents observed at the surface were greater than the currents at depth. Four sets of data are provided for March and August; no data are provided for May or June. However, on the bases of the four sets of data, the current gradient between the sea surface and the depressor can be expected to be no greater than 0.5 knot with a 95% confidence level.[11] If a 0.5-knot cross-current gradient at a towing speed of 4 knots is assumed, an additional 0.03 knot uncertainty is introduced into the speed measurement. If the speed errors due to knotmeter calibration, knotmeter motion, and ocean cross-current gradients are combined by the method of the root-sum-square uncertainty,[11] the total speed measurement uncertainty is 0.04 knot. This value is assumed in the uncertainty analysis.

The U.S. Naval Oceanographic Office data[10] also indicate that water salinity is greater than standard sea water and that water temperature is warmer than standard in the Tongue of the Ocean. Data for the months of May and June indicate temperatures as high as 75° F at towing depth. Therefore a water density uncertainty of 0.005 $lb\text{-}s^2/ft^4$ is applied to the uncertainty analysis to account for salinity and temperature effects.

The tension data at the ship, the angle data measured by the CAMD, and the depth data as functions of speed were all fitted with least squares equations to obtain values at common reference speeds that could be utilized to reduce the results to cable drag loading. Ordinarily, the data scatter about such curves is used to establish a confidence level in the data fit. However, towing on reciprocal headings with and against an ocean current gradient will, in itself, produce large scatter if significant gradients are present even though the average may still be correct. This type of scatter probably can be reduced if the complementary data on the two headings are averaged before the data is plotted. In practice, this kind of averaging procedure is not very practical since repeat conditions on opposite headings are rarely truly the same. Therefore for this analysis, the data on opposite headings are not averaged in the figures, and the scatter is not indicative of the confidence level of the fitted curve. Rather, the assumption is made that the value determined by the data fit has the same accuracy as the data.

The uncertainty analysis which follows is based on Coleman and Steel.[11] The uncertainty of a quantity r, which depends on a data reduction equation is approximated by a linear Taylor series expansion of the quantity about the uncertainty value. Assume an equation

$$r=r(x_1,x_2,\ldots,x_j) \tag{20}$$

where r is the quantity and x_1 through x_j are the functional variables. The uncertainty UN_r in the quantity r is

$$UN_r = \left(\sum (\partial\, UN_r/\partial\, x_i)^2\, UN_i^2 \right)^{\frac{1}{2}} \tag{21}$$

where UN_i is the uncertainty of the ith variable.

Quantitative uncertainties in the calculated tangential drag and normal drag coefficients are discussed separately below. The various uncertainty values needed for the analysis are summarized in Table 9. The rationale for the values used is discussed

at various locations of the report. The uncertainty in kite angle β is included in the analysis (see Eqs. 1 and 2) to examine its influence on the method used to obtain cable hydrodynamic drag.

Table 9. Uncertainty* values for the various quantities used to calculate cable hydrodynamic drag.

Sea-Water Density, $lb \cdot s^2/ft^4$ (kg/m^3)	0.005 (0.080)
Tow Speed, kn (mm/s)	0.04 (11.1)
Depressor Depth, ft (mm)	2.0 (609)
Depressor Tension Cal, lb (N)	10.0 (44.5)
Tension at Ship, lb (N)	10.0 (44.5)
Total Cable Length, ft (mm)	1.0 (305)
Cable Diameter, in. (mm)	0.001 (0.03)
Cable Weight in Water, lb/ft (N/m)	0.0005 (0.007)
Cable Length at CAMD, ft (mm)	0.08 (25.4)
CAMD Cable Angle	
Small Cable, deg (rad)	1.5 (0.026)
Large Cable, deg (rad)	1.7 (0.030)
CAMD $d\phi/ds$	
Small Cable, deg/ft (rad/m)	0.012 (0.0007)
Large Cable, deg/ft (rad/m)	0.024 (0.0014)
Kite Angle β, deg (rad)	15.0 (0.26)

TANGENTIAL DRAG UNCERTAINTY

Equations 12b and 13 are used to calculate the tangential drag coefficient C_{td}. Application of Eq. 21 to these reduction equations provides the uncertainty. Uncertainty results for both the small and the large experiment cables are listed in Table 10. The data scatter shown in Fig. 17 generally is within the calculated uncertainties. The primary contributor to the tangential drag coefficient uncertainty is the uncertainty in the rate of change of tension with respect to cable length.

*In this report the term "uncertainty" includes bias and random errors and refers to half the error band at a 95% confidence level.

Table 10. Tangential drag coefficient uncertainty UN_{Ctd} at 4, 6, and 8 knots.

	Small Cable		Large Cable	
Speed, kn	Uncertainty	%UN	Uncertainty	%UN
4.00	0.0118	35	0.0087	45
6.00	0.0052	17	0.0039	18
8.00	0.0030	16	0.0022	8

NORMAL DRAG UNCERTAINTY

Equations 16, 17, and 18 are used to determine the cable normal force coefficient C_n. Equation 21 must be applied to each of these equations to establish the uncertainty in the normal force coefficient as a function of speed and cable angle. Depressor tension To, which is required in Eq. 17, was determined in the basin and converted to standard sea conditions (see Appendix A) for the cable drag analysis but was not measured during the at-sea evaluation. Therefore, the effects of speed and water-density uncertainties need to be added to the depressor calibration uncertainty. The relationship between tension, water density, and towing speed for a depressor that achieves downforce primarily by hydrodynamic means is approximated by,

$$To=K\rho V^2 \tag{22}$$

where K is a proportionality constant, ρ is fluid density, and V is towing speed. Application of Eq. 21 to Eq. 22 will account for the effects of density and speed uncertainty. The total depressor tension uncertainty is then the root-sum-square of calibration uncertainty and the uncertainty related to density and speed.

The calculated normal force coefficient uncertainties for the small and large cables are plotted in Figs. 28 and 29, respectively, as functions of cable angle. The calculated uncertainties for the two cables are very similar. The normal drag uncertainty is dominated by the tension uncertainty for this evaluation. The neglect

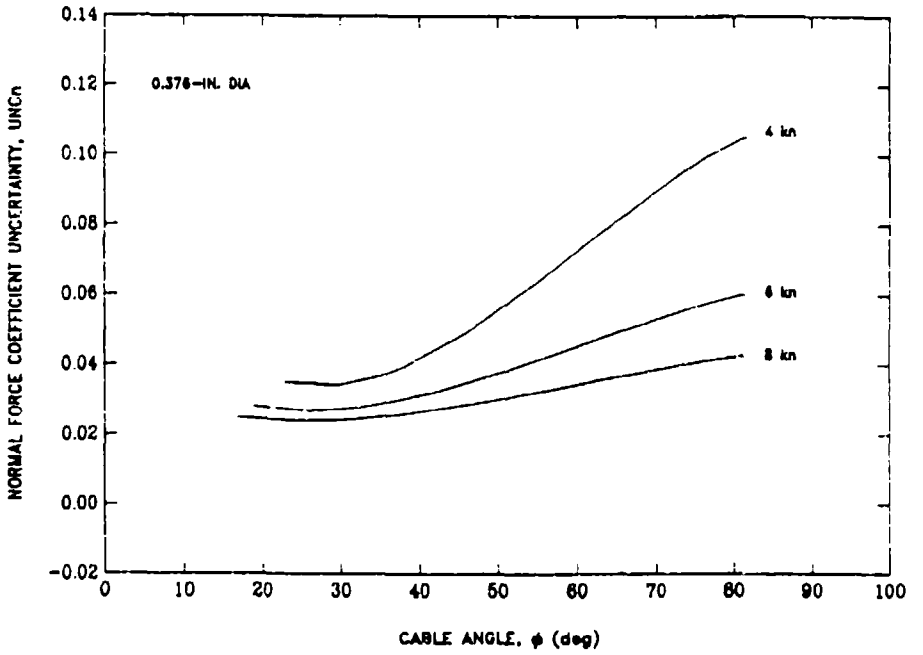

Fig. 28. Normal force coefficient uncertainty as a function of cable angle for the small cable at 4, 6, and 8 knots.

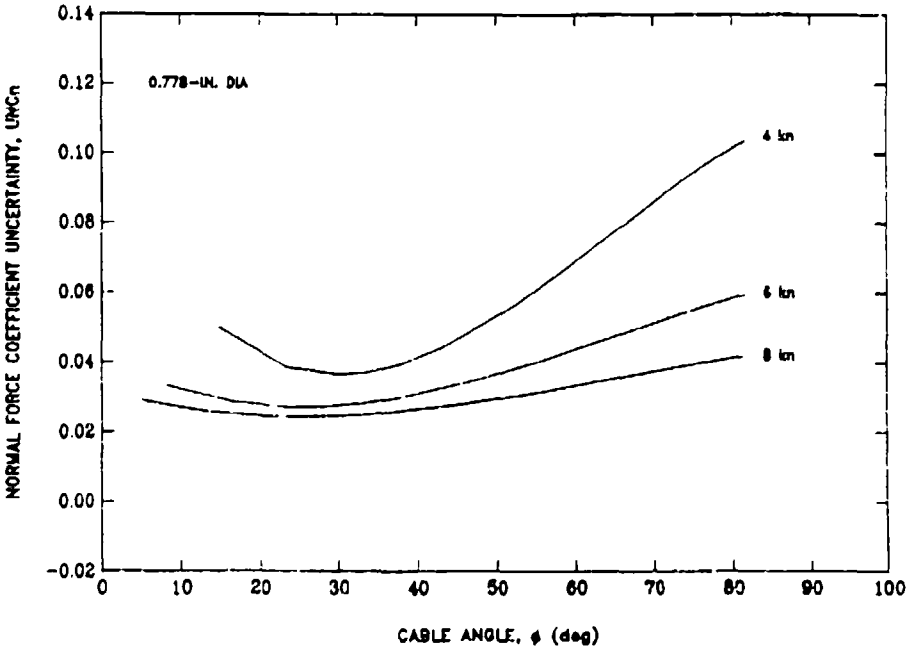

Fig. 29. Normal force coefficient uncertainty as a f[illegible] of cable angle for the large cable at 4, 6, and 8 knots.

of kite angle β in the drag analysis, within the assumed uncertainty range, has virtually no effect. The kite angle uncertainty affects the total drag uncertainty by 0.002%.

Generally, the fitted curve of C_n shown in Fig. 23 is within the calculated uncertainty of the data at the steeper cable angles. At cable angles between 25 and 45 deg, the data scatter is marginally outside the calculated uncertainties. At cable angles less than 25 deg, however, the data scatter is noticeably greater than the uncertainty, particularly for the large cable at 4 knots.

COMPARISON OF PREDICTED AND MEASURED VALUES

The validity of the new cable hydrodynamic drag loading can be examined by comparing predicted towing performance with the at-sea measured performance. To make this comparison, towing calculations were performed using the FORTRAN 77 version of the static cable program described by Knutson.[7] The average values of tangential drag coefficient C_{td} and normal drag coefficient C_r, shown in Figs. 17 and 24, respectively, are used for all calculations. The Eames[9] form of tangential loading is assumed. The results obtained for the small and the large diameter cables are described separately below.

SMALL CABLE COMPARISON

Calculated cable angles at various positions along the cable length are compared to values determined by at-sea measurement in Fig. 30. The predicted values compare to within ±1 deg at the steeper cable angles. At angles below about 40 deg, the predicted angles are less than the measured angles by as much as 2 deg for all speeds shown. The discrepancies are close to the calculated data accuracy of ±1.5 deg (see Appendix B).

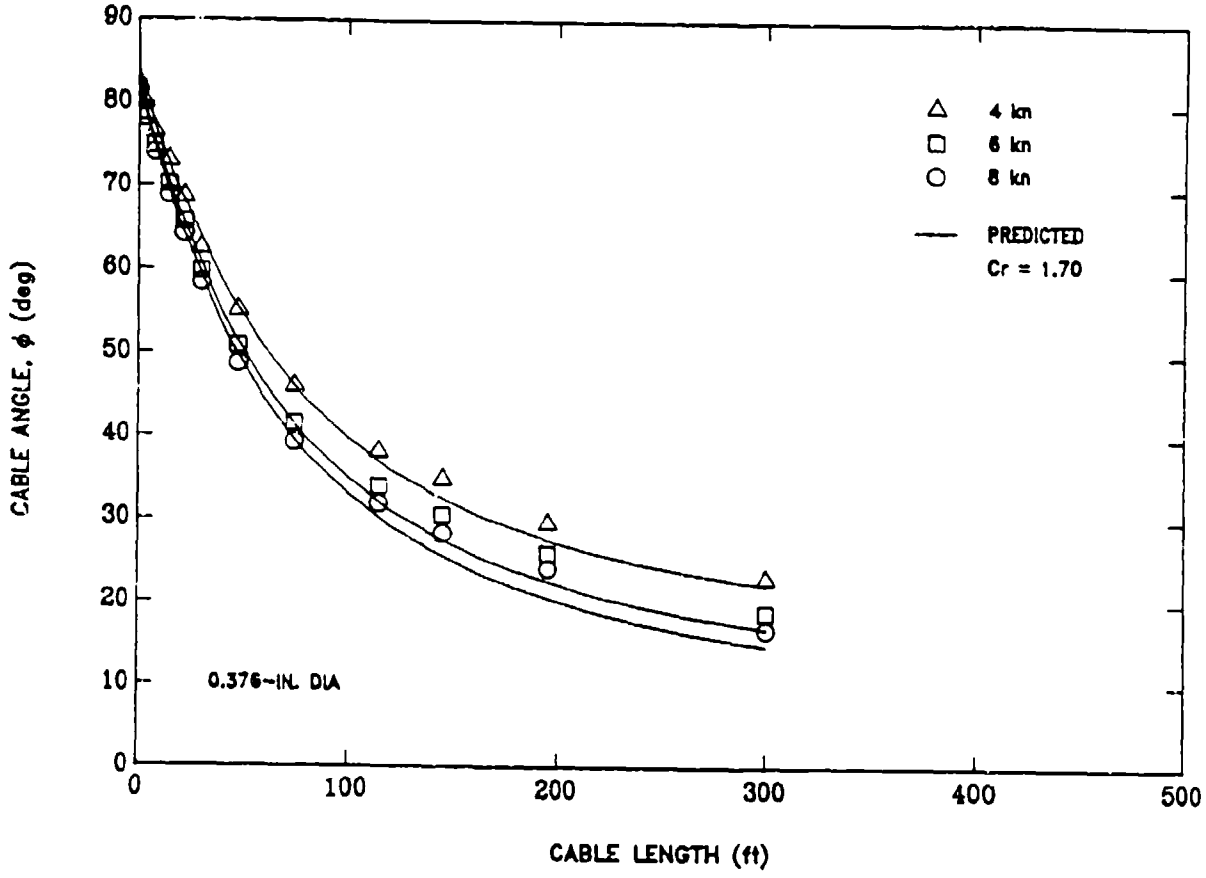

Fig. 30. Predicted cable angle near the depressor compared to measured angle for the small cable at 4, 6, and 8 knots.

Tension and cable angle measured at the ship are compared to the calculated values in Figs. 31 and 32, respectively. On average, the tension predictions are slightly higher than the measured values, particularly at the lower speeds. However, the tension predictions are typically within the data scatter for all speeds and cable lengths. Predicted cable angle also agrees well with the measured values and is within the data scatter.

Calculated depth is compared to measured depth for the small cable in Figs. 33 and 34. In Fig. 33, cable side loading is assumed to be zero. In Fig. 34, a side loading value is assumed for comparison. The actual side loading for the experiment cables is not known. Rather, for the calculations with side loading, a side loading coefficient value $C_s = 0.135$, obtained in a wind tunnel for a 1X19 wire rope, is used.[7] Although this side loading may not be correct, it serves the purpose of examining depth sensitivity to this effect.

The calculated depth in Fig. 33, without side loading, agrees with measured depth for the short cable length. As cable length increases, however, the calculations progressively over-predict depth. Depth is over-predicted by an average of 7% for the longest cable length of 800 ft (244 m). With a side loading coefficient $C_s = 0.135$ the depth over-prediction is reduced by about half.

Assuming the normal drag loading is correct, other effects, in addition to cable side loading, could contribute to the apparent discrepancies between calculated and measured depth. The combined accuracies of the speed and depth measurements are almost sufficient by themselves to explain the discrepancies even without cable side loading. However, the largest uncertainty is ocean current gradients. The indicated s, ed was measured at a nominal depth of 65 ft (20 m). Therefore, any current gradients would cause errors at deeper or shallower depths. This effect is discussed further in the uncertainty analysis contained in the previous section of this report.

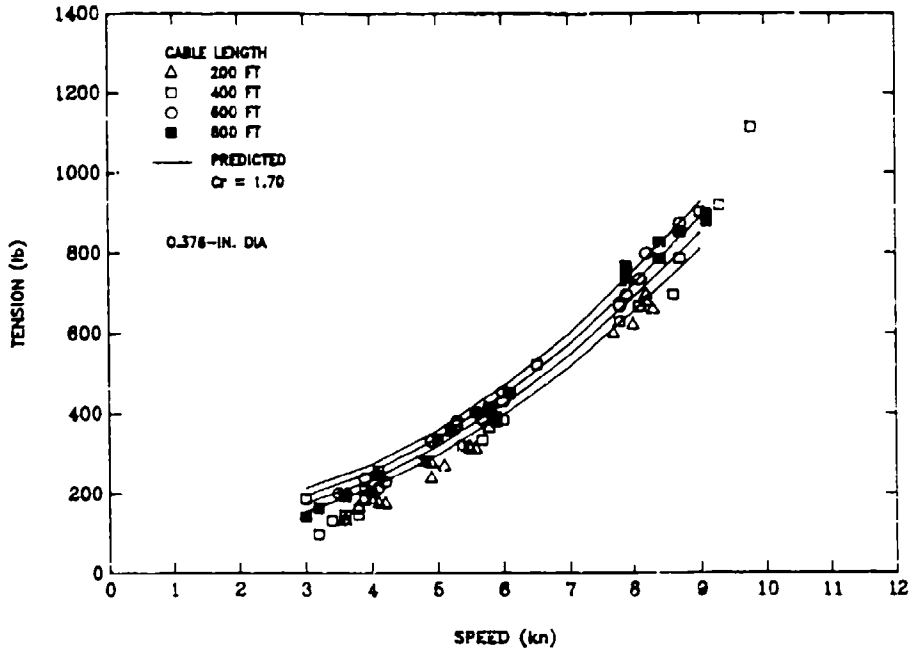

Fig. 31. Predicted tension at the ship compared tc measured tension for the small cable.

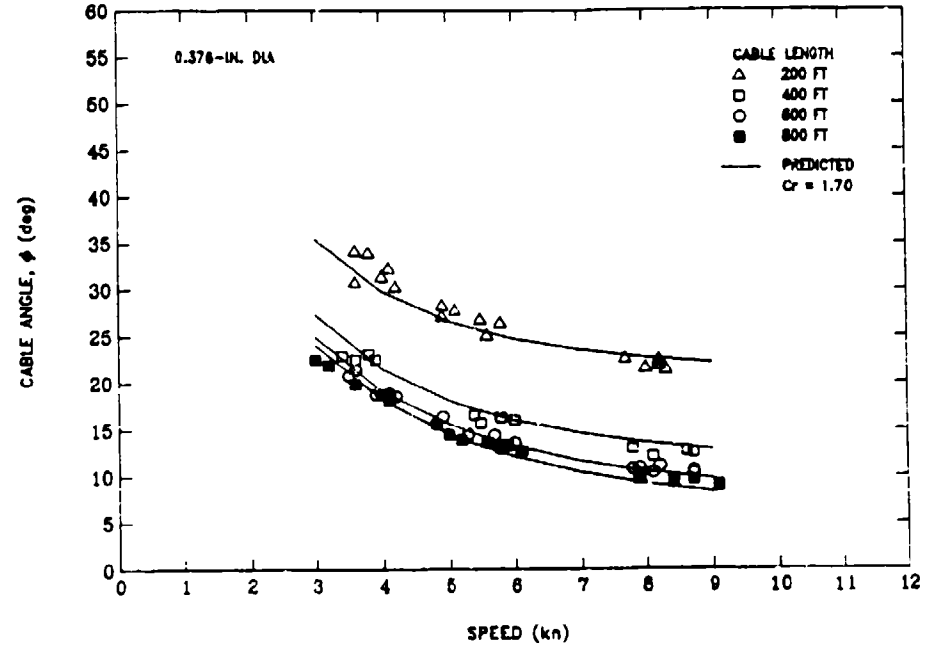

Fig. 32. Predicted cable angle at the ship compared to measured angle for the small cable.

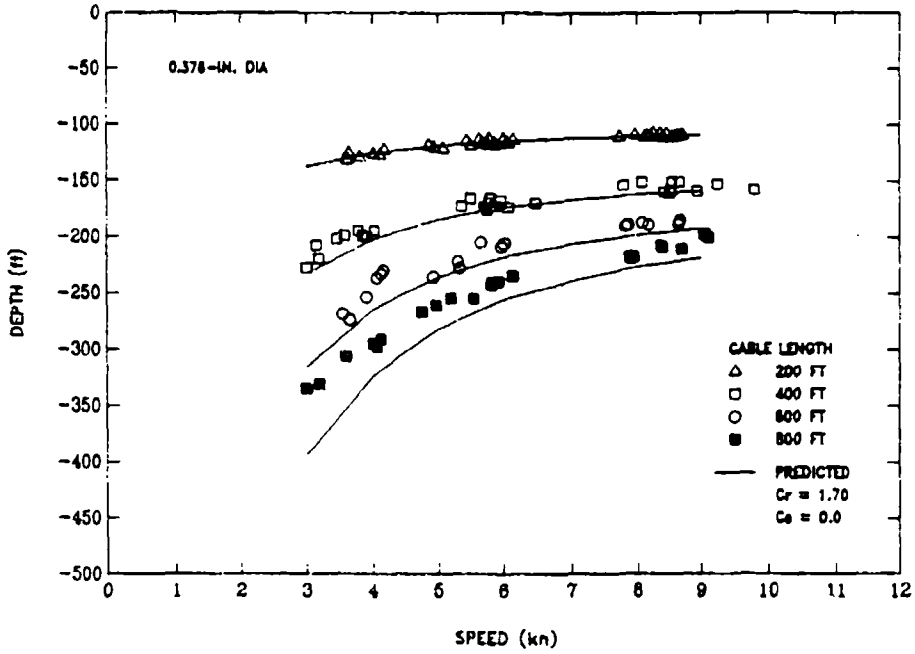

Fig. 33. Predicted depressor depth compared to measured depth for the small cable without cable side loading.

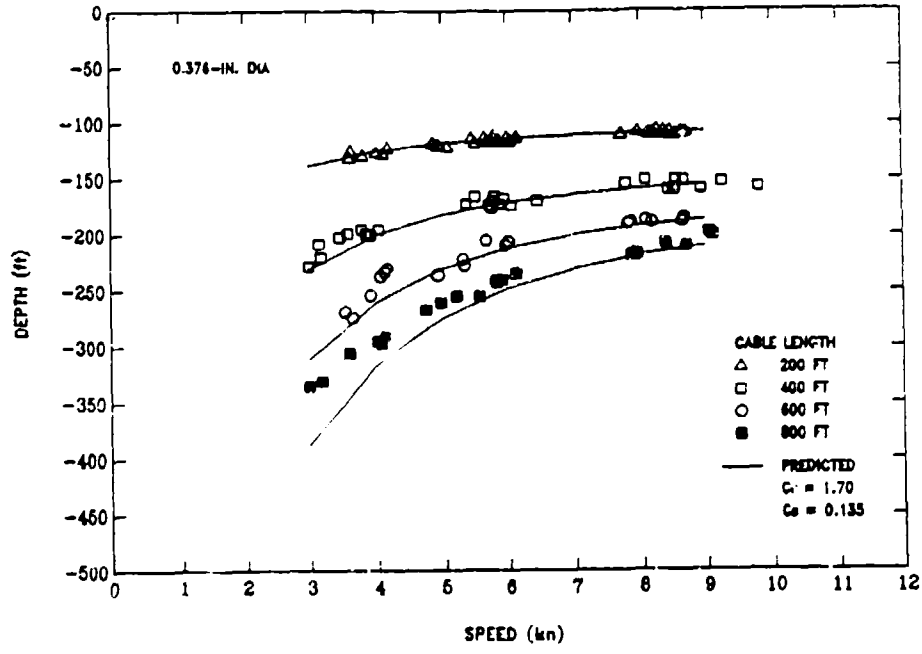

Fig. 34. Predicted depressor depth compared to measured depth for the small cable with an assumed cable side loading.

LARGE CABLE COMPARISON

Calculated cable angle is compared to measured angle at various positions along the cable in Fig. 35. The calculated values compare to within the accuracy of the measurement at all positions except at 400 ft (122 m) where the calculations over-predict the measured value by about 8 deg at 4 knots decreasing to about 6 deg at 8 knots. No explanation is apparent for the discrepancy at the 400-ft (122-m) position.

Measured tension and cable angle at the ship are compared to the calculated values in Figs. 36 and 37, respectively. The calculated tension at the ship agrees with the measured tension to within the data scatter except at the higher speeds where the calculations appear to under-predict average tension by approximately 50 lb (220 N) or 5% at the short cable length increasing to about 100 lb (440 N) or 10% at the long cable length.

The calculated cable angle at the ship, shown in Fig. 37, generally compares with the measured angle to within the data scatter and accuracy of the measurements. On average, however, the calculations appear to under-predict angle at the short cable length of 300 ft (91 m) by about one deg. This result contradicts the results shown in Fig. 35 where the calculations over-predict the measured cable angle at cable lengths greater than 180 ft (55 m).

Calculated depth with and without side loading is compared to measured depth in Figs. 38 and 39, respectively. The side loading coefficient C_s used in the calculations of Fig. 39 is the same as that used with the small cable (C_s = 0.135). The calculated depths in both Figs. 38 and 39 generally agree with the measured depths to within the accuracy of the measurements, although the calculations consistently under-predict measured depth at the higher speeds by about 6% without side loading and by about 10% with the assumed side loading.

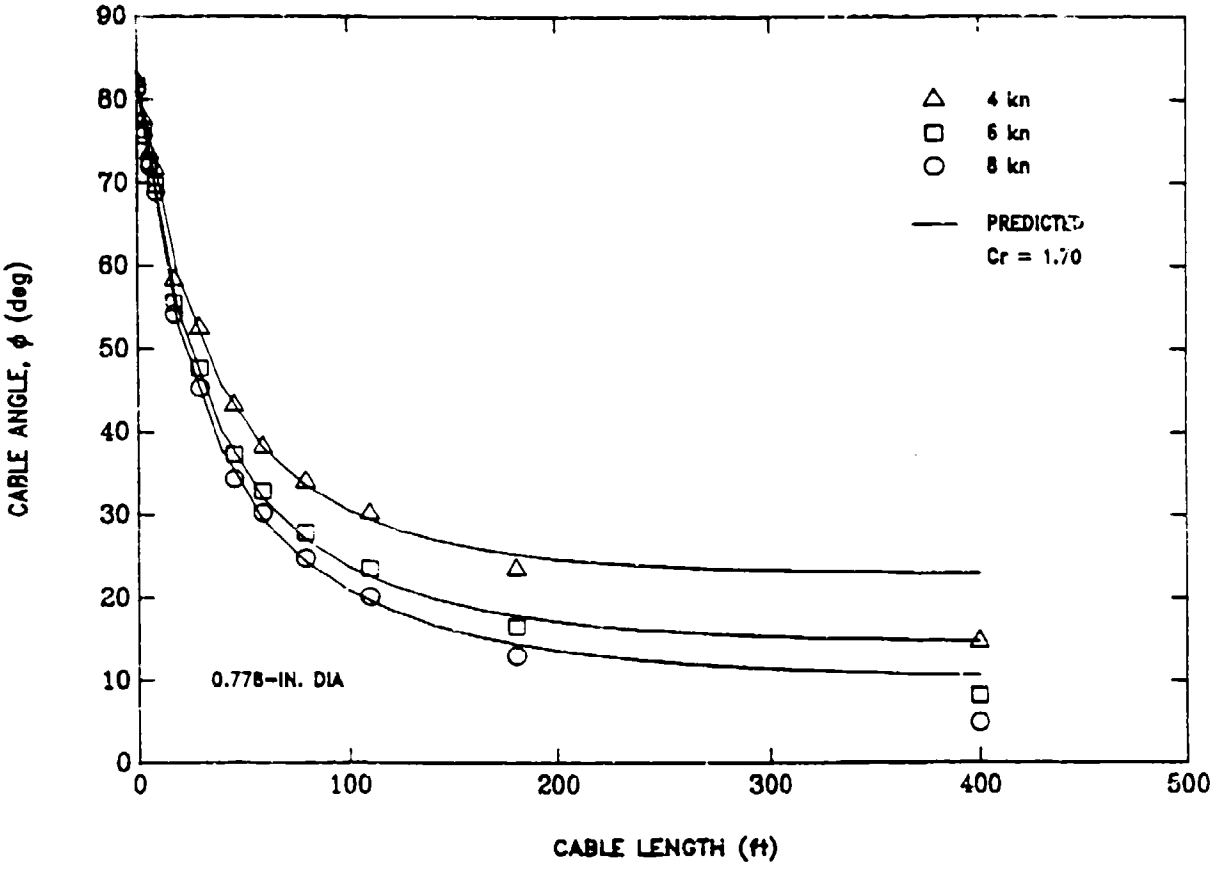

Fig. 35. Predicted cable angle near the depressor compared to measured angle for the large cable at 4, 6, and 8 knots.

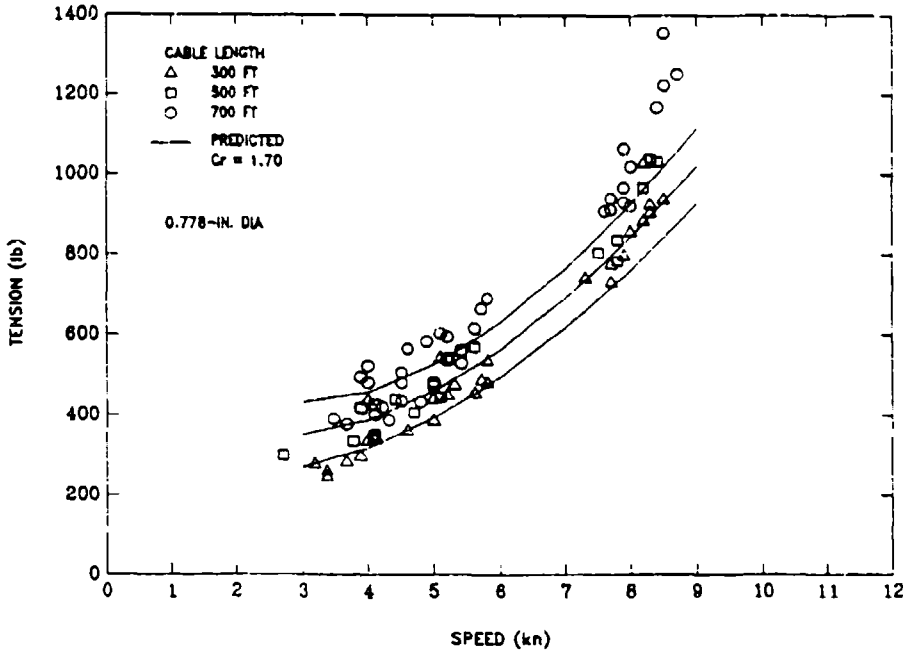

Fig. 36. Predicted tension at the ship compared to measured tension for the large cable.

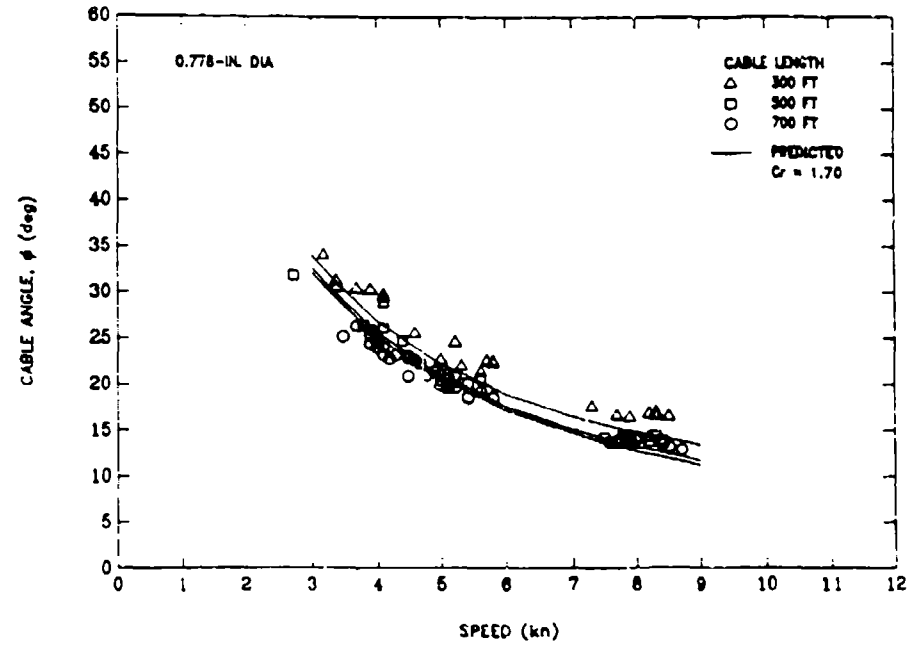

Fig. 37. Predicted cable angle at the ship compared to measured angle for the large cable.

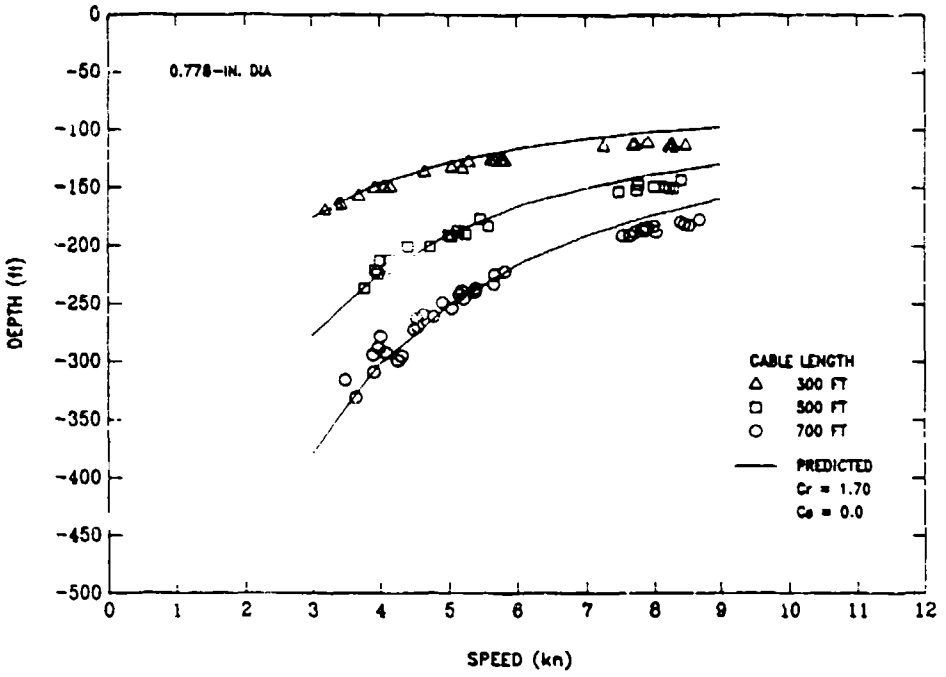

Fig. 38. Predicted depressor depth compared to measured depth for the large cable without cable side loading.

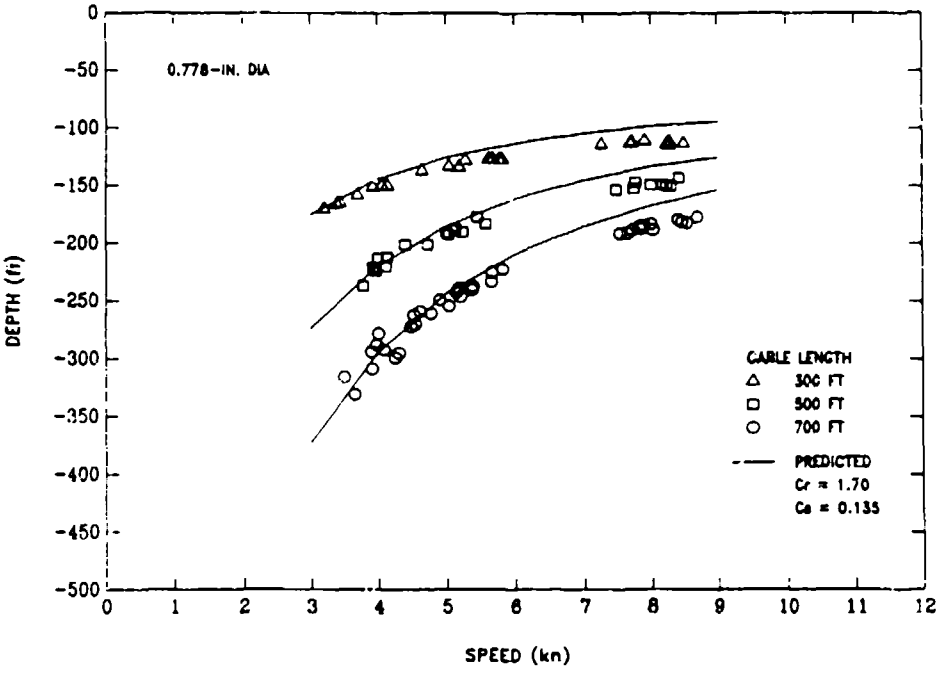

Fig. 39. Predicted depressor depth compared to measured depth for the large cable with an assumed cable side loading.

CONCLUSIONS

The results of the at-sea experiment to determine the hydrodynamic drag loading of two double-armored, bare cables lead to the following conclusions:

1. The use of a separate device attached to the cable to measure in-plane cable angle is a viable measurement technique.

2. The drag of the cable angle measurement device (CAMD) had negligible effect on the cable angle being measured (see Appendix B).

3. The influence of the cable on the CAMD measurement was negligible. The device measured the correct angle to a sufficiently high degree of certainty.

4. The use of a CAMD allows simultaneous determination of the cable normal drag coefficient and the normal loading function.

5. A single normal loading function and normal drag coefficient can be applied to a wide range of cable size and relative cable tension loading with good engineering accuracy. The newly determined drag coefficient values (based on cable frontal area) and the normal loading function for double-armored, bare cables are

$$C_{td} = 0.0249$$

$$C_r = 1.70$$

$$f_n = -0.424 + 0.869\cos\phi + 0.979\sin\phi - 0.445\cos(2\phi) - 0.434\sin(2\phi)$$

where C_{td} is the tangential drag coefficient, C_r is the normal drag coefficient, and f_n is the normal loading function. The value of C_{td} must be divided by C_r to obtain the Pode[8] tangential factor f.

6. The normal loading function for double-armored, bare cables differs significantly from the classically assumed sine squared relationship.

7. Over the range examined, the normal drag coefficient for double-armored, bare cables is independent of Reynolds number.

8. Within the scatter of the data, the two experiment cables have the same tangential drag coefficient. Other cable geometries, however, may have different tangential drag values.

9. Cable hydrodynamic side loading did not degrade the accuracy of the cable drag values determined by the new measurement technique. Cable side loading does, however, have a significant effect on towing depth.

RECOMMENDATIONS

If a similar at-sea experiment is attempted in the future, the following changes are recommended:

1. The angle recorder should be integrated into the cable angle measuring device (CAMD). The vibrational environment at the CAMD is sufficiently severe that electrical cables in the free-stream, as was necessary during the present evaluation, will not survive high-speed towing. The arrangement used was only marginally satisfactory even at relatively low towing speeds.

2. An attempt should be made to integrate measurement of kite angle into the CAMD to allow a determination of cable side loading.

ACKNOWLEDGMENTS

Bruce Webster, David Pickett, John Johnston, and Hung Vo of the Towed Systems Branch provided valuable planning and analysis support. John Johnston, Hung Vo, Bruce Hill, Stephen Hunt, Joseph Moeller, and Allan Muise of the Towed Systems Branch and Joseph Conte of EG&G, Inc. provided evaluation support in the laboratory and at sea. The contributions of these individuals are greatly appreciated.

THIS PAGE INTENTIONALLY LEFT BLANK

APPENDIX A

RESEARCH DEPRESSOR PERFORMANCE

The research depressor was evaluated in the TMB deep-water towing basin prior to the at-sea evaluation to check towing performance. A 20-ft (6-m) length of the 0.376-in (9.55-mm) diameter at-sea experiment cable was used to tow the depressor in the basin. Instrumentation located in the depressor as well as the top-side electronics were the same as those used during the sea evaluation. The instrumentation is described elsewhere in this report. In addition, a 10,000-lb (45-kN) load cell was located at the carriage for measurement of depressor tension. Although the specified accuracy of this load cell is ±50 lb (±200 N), a calibration performed prior to the basin evaluation indicated a laboratory accuracy[11] of ±10 lb (±45 N) with a 95% confidence level. The calibration was performed with the same processing electronics as were used during the basin evaluation.

The depressor was towed in the basin at a nominal depth between 10 and 12 ft (3 and 4 m). During all data runs, the pitch control flaps were deflected to the maximum lift setting in the manual mode to simulate the lift condition used at sea. The roll control was maintained in the automatic mode during the evaluation. The roll flap offset angle was changed at various times in an attempt to determine a setting that would provide near zero roll throughout the speed range. However, no attempt was made to adjust the flap offset during a run. Towing speed was varied between 4 and 14 knots in 2-knot increments during the evaluation.

The depressor towed in a steady and stable manner. Roll standard deviation during any run never exceeded 1.0 deg; pitch standard deviation stayed to within 0.5 deg. The final selected roll flap offset angle maintained the depressor roll to less than ±2.0 deg throughout the speed range. The pitch flap maintained an average angle of 19.9±0.5 deg.

The depressor strain-gaged towpoint designed to determine cable angle and tension at the depressor did not function with sufficient accuracy to be useful, and therefore, no direct method was available for measurement of these quantities at sea. Consequently, static hydrodynamic coefficients were calculated for the depressor to obtain at-sea tension and angle. The coefficients were determined by the methods described by Knutson.[12] The calculated, non-dimensional coefficients are listed in Table A.1. Static, vertical-plane performance is determined by solving the axial force, normal force, and pitching moment trim equations. These equations are given by Knutson.[12]

Table A.1. DTRC research depressor vertical-plane hydrodynamic coefficients relative to towpoint origin.

X_{uu}'	= - 0.0056	Z_{*}'	= + 0.0404	M_{*}'	= + 0.0029
X_{v}'	= + 0.0003	Z_{v}'	= - 0.3234	M_{v}'	= - 0.0325
$X_{\|v\|}'$	= - 0.0057	$Z_{\|v\|}'$	= + 0.0342	$M_{\|v\|}'$	= + 0.0223
$X_{v\|v\|}$	= - 0.0114	$Z_{v\|v\|}'$	= - 0.1577	$M_{v\|v\|}'$	= - 0.0928
$X_{\delta\delta}'$	= 0	Z_{δ}'	= - 0.0273	M_{δ}'	= - 0.0224

Tension, cable angle, and depressor pitch angle calculated for fresh water are shown in Fig. A.1 as functions of towing speed. The tension includes the weight of the cable clevis and clevis pin. Tension and pitch angle measured in the basin are also plotted in this figure for comparison. The predicted and measured values agree to within the accuracy of the measurements throughout the speed range. Measured tension at the carriage was corrected for towcable effects using a static cable program.[7] This effect, however, is less than 5 lb (22 N) through the speed range.

Predicted tension, cable angle, and pitch angle at the depressor calculated for standard sea water are shown in Fig. A.2. The tension predictions are used to reduce the at-sea data.

Depressor hydrostatic properties, which are required for the trim and force predictions, are listed in Table 3 of the main body of this report. The depressor exhibits a large difference in hydrostatic trim between fresh and sea water. In fresh water at zero speed the static pitch angle of the depressor is greater than 35 deg, tail down. In sea water the static pitch angle is nearly zero.

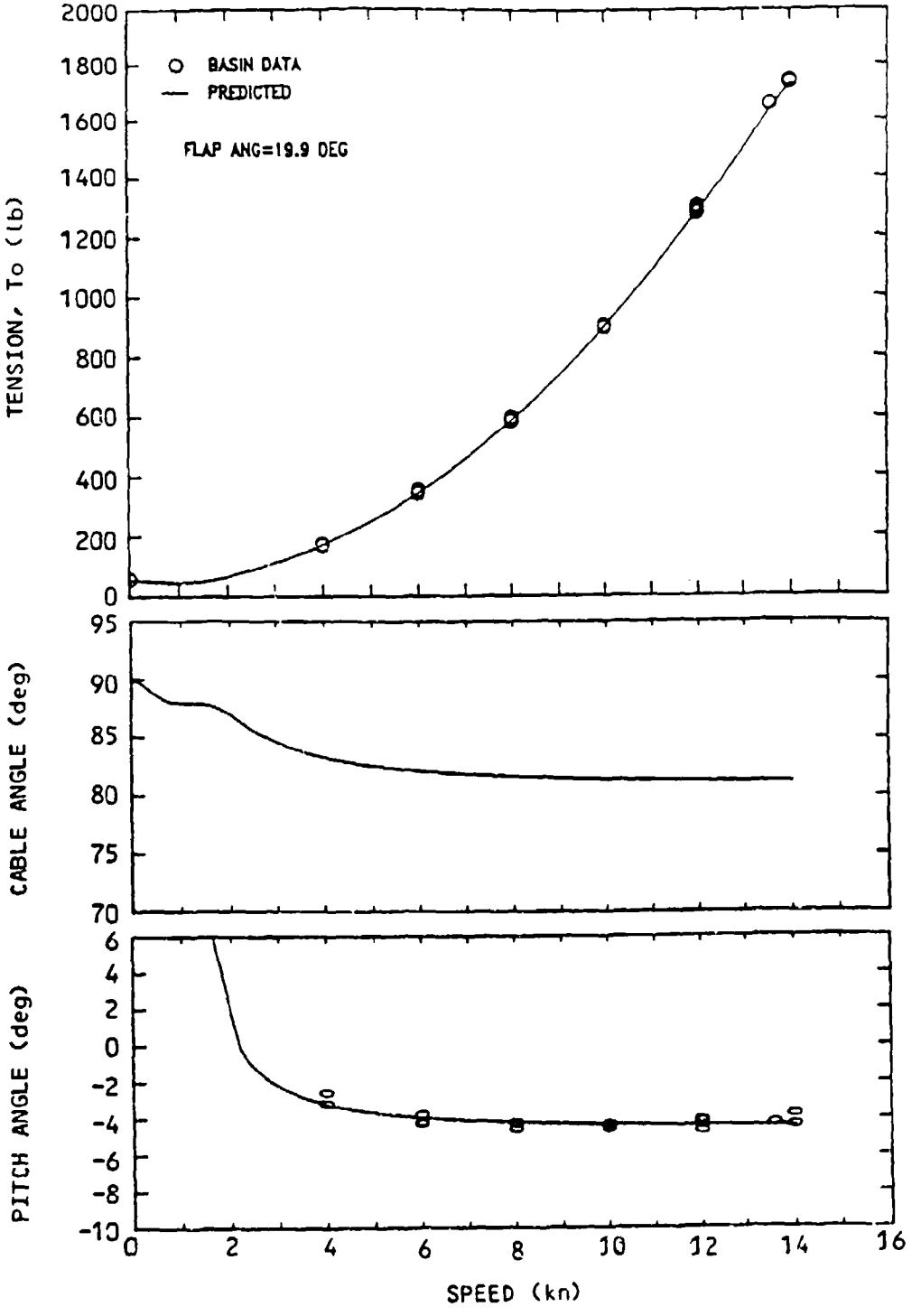

Fig. A.1. DTRC research depressor basin towing characteristics at high lift.

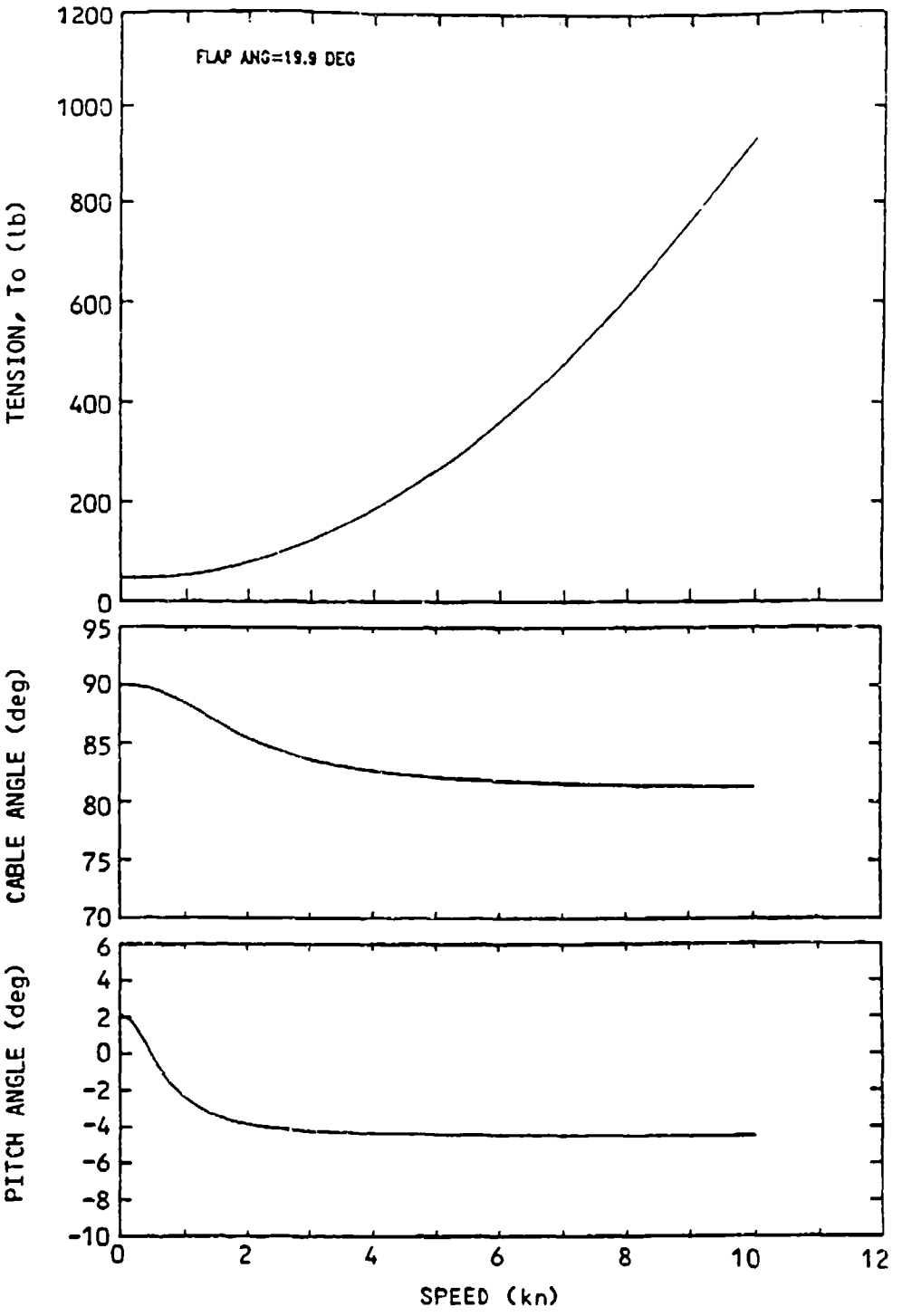

Fig. A.2. DTRC research depressor predicted at-sea towing characteristics at high lift.

THIS PAGE INTENTIONALLY LEFT BLANK

APPENDIX B

CABLE ANGLE MEASURING DEVICE CALIBRATION

Basin calibration experiments were performed to examine the effect of the experiment cables on the angle measured by the Cable Angle Measuring Device (CAMD). Since the alignment vane tows behind the cable, local flow around the cable could conceivably influence the angle measurement.

The experiment was performed in the TMB deep-water towing basin. A strut supported by the vertical rails on the carriage was used to provide a submerged attachment point for the bottom aft end of the cable. The above-surface towing girder of the carriage provided the attachment point for the upper forward end of the cable. A 1000-lb (4.5-kN) tension gage was inserted between the towing girder and the end of the cable to set a pre-tension in the cable before each run. The CAMD was located on the cable at a position that would provide a CAMD submergence of at least 3 ft (1 m). A pendulous potentiometer with an angle range of ±45 deg was mounted to the body of the CAMD for purposes of comparison with the CAMD measurement. As discussed in the main body of the report, the CAMD measurement accuracy is approximately ±0.5 deg. The accuracy of the ±45-deg pendulous potentiometer under static conditions is ±0.8 deg.

The electrical cables from both transducers were mated to the experiment cable above the CAMD and led to the carriage through the processing electronics to a PDP 11/73 computer which was used to collect the data.

Sample sections of both the small and the large at-sea cables were towed during the experiment. Cable angle was varied between 70 deg and 15 deg. The angle adjustment was accomplished by varying the submergence of the aft support strut and adjusting the longitudinal attachment point at the forward end of the cable. The cable was pre-tensioned to a nominal 400 lb (1.8 kN) prior to each run.

CAMD measured angle obtained during the experiment with the small and the large cables is plotted as a function of pendulum measured angle in Figs. B.1 and B.2, respectively. A line which represents a one-to-one correspondence between the measured angles is also shown for comparison. The data suggest some bias error which may indicate a flow-related effect on the CAMD measurement. However, the bias, if it exists, is not consistent with speed or cable size. Therefore, the discrepancies must be assumed to be random. If random error is assumed and the data for the various speeds are combined, the accuracy of the cable angle measurement using the CAMD is ±1.5 deg for the small cable and ±1.7 deg for the large cable with a 95% confidence level.[11]

Of related interest is the effect of the CAMD drag on the cable angle itself. No experiment was performed to examine this effect. However, cable configurations were calculated with the CAMD attached at various locations on the cables. The calculations assumed a CAMD drag coefficient of 0.3 based on frontal area. An allowance for the drag of the data cable loop leading from the CAMD to the data recorder also was included. The calculations were performed for speeds of 4, 6, and 8 knots. The results of the calculations indicate that, for both cables, the CAMD reduces cable angle by approximately 0.4 deg near the depressor. As the CAMD is moved away from the depressor, the effect becomes progressively smaller. At a position 300 ft from the depressor, a 0.1-deg decrease in angle is predicted. Thus, the CAMD drag introduces a small bias error into the measurements. However, the effect of this bias on the determination of cable drag is negligible since (1) The bias error lies well within the accuracy determined for the CAMD measurements, and (2) The method of data reduction depends primarily on the rate of change of cable angle with respect to length, and the bias, if it is slowly varying, will have negligible effect on the rate of change of angle.

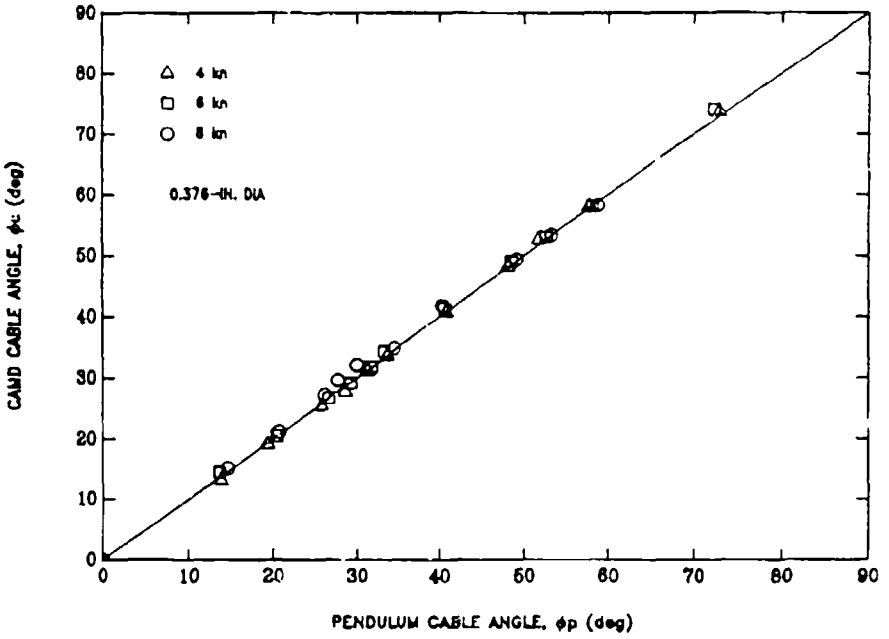

Fig. B.1. CAMD measured cable angle compared to pendulum measured cable angle with the small experiment cable.

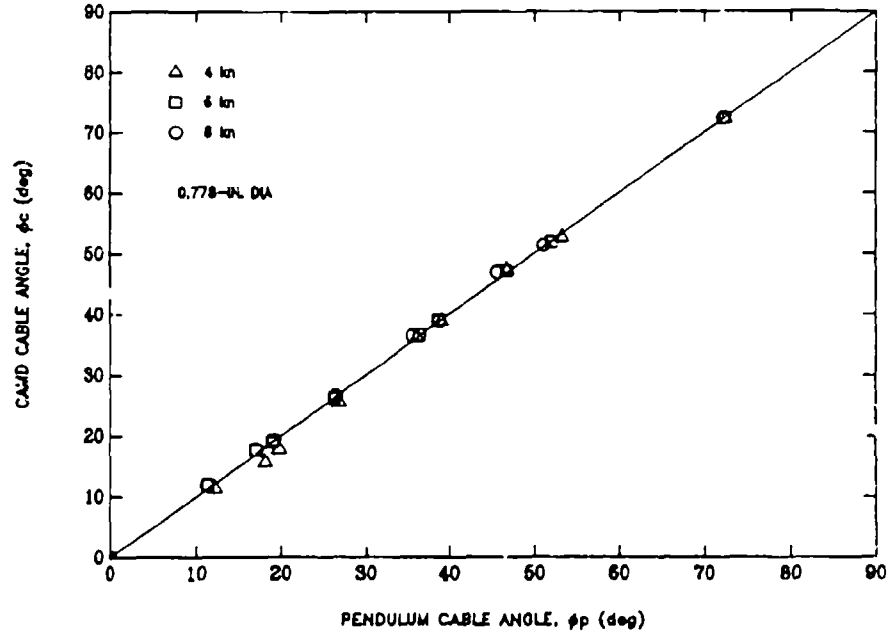

Fig. B.2. CAMD measured cable angle compared to pendulum measured cable angle with the large experiment cable.

THIS PAGE INTENTIONALLY LEFT BLANK

APPENDIX C

KNOTMETER SPEED CALIBRATION

The knotmeter was calibrated in the TMB high-speed towing basin prior to the at-sea evaluation. A 10-ft (3-m) length of standard knotmeter cable was used during the calibration. This length of cable provided a minimum estimated towing depth of 7 ft (2 m) through the calibration speed range to 15 knots. The top-side electronics, mainly a frequency-to-voltage converter, was the same as that used during the sea evaluation. The knotmeter electronics is described elsewhere in this report. The voltage output was read with a voltmeter.

The speed calibration data are presented in Fig. C.1 which shows carriage speed as a function of knotmeter voltage output. The calibration data are fitted using a linear, least-squares curve fit also shown in the figure. The coefficients of the equation shown were used as calibration coefficients in the data-collection computer used during the sea evaluation.

On the basis of the calibration data and the linear curve fit, the laboratory accuracy of the knotmeter is ±0.02 knot with a 95% confidence level up to a speed of 13 knots.[11]

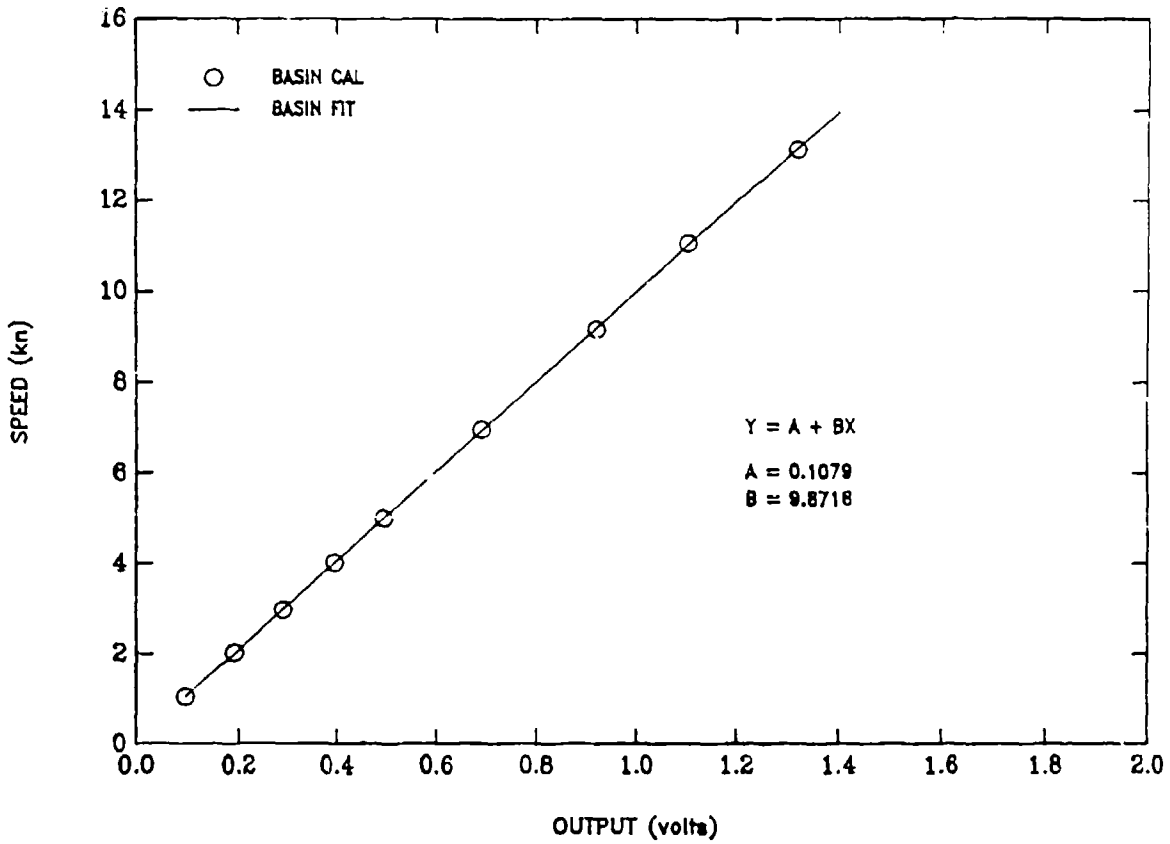

Fig. C.1. Knotmeter speed calibration.

APPENDIX D

TABULATED AT-SEA DATA

Data obtained during the bare-cable, at-sea evaluation of May 1989 are presented in Tables D.1 and D.2 for the small and the large cables, respectively. The data are organized by configuration and speed. The values shown are corrected for sensor calibrations.

Table D.1. Small cable at-sea data.

CAMD POSITION		CABLE LENGTH		SPEED	HDG	DEPTH		SHIP TENSION		CABLE ANGLE	
										gimbal	CAMD
(ft)	(m)	(ft)	(m)	(kn)		(ft)	(m)	(lb)	(N)	(deg)	(deg)
3	1	800	244	3.0	S	335	102	141	627	67.5	81.4
3	1	800	244	4.1	N	291	89	248	1103	71.7	79.6
3	1	800	244	4.8	N	267	81	282	1254	74.4	NO DATA
3	1	800	244	5.2	S	255	78	357	1588	76.1	79.2
3	1	800	244	5.8	N	243	74	413	1837	77.0	NO DATA
3	1	800	244	5.8	N	241	73	417	1855	76.7	78.9
3	1	200	61	5.9	N	118	36	356	1583	NO DATA	NO DATA
3	1	200	61	5.9	S	117	36	358	1592	NO DATA	NO DATA
3	1	200	61	6.1	N	114	35	380	1690	NO DATA	NO DATA
3	1	800	244	7.9	S	217	66	767	3412	80.3	78.2
3	1	800	244	8.4	S	207	63	785	3492	80.8	NO DATA
3	1	200	61	8.6	N	109	33	768	3416	NO DATA	NO DATA
3	1	200	61	8.7	S	110	34	793	3527	NO DATA	NO DATA
3	1	200	61	8.7	N	109	33	761	3385	NO DATA	NO DATA
3	1	800	244	9.1	N	197	60	878	3905	81.2	NO DATA
3	1	800	244	9.1	N	200	61	897	3990	80.9	78.0
3	1	200	61	12.5	N	106	32	1585	7050	NO DATA	NO DATA
3	1	200	61	12.6	N	105	32	1556	6921	NO DATA	NO DATA
3	1	200	61	12.7	S	106	32	1657	7370	NO DATA	NO DATA
8	2	200	61	3.6	S	126	38	131	583	59.3	77.0
8	2	200	61	4.2	N	123	37	174	774	59.8	76.2
8	2	200	61	4.9	S	119	36	238	1059	63.0	75.8
8	2	200	61	5.6	N	114	35	312	1388	65.0	75.2
8	2	200	61	8.0	S	109	33	620	2758	68.5	73.9
8	2	200	61	8.3	N	107	33	658	2927	68.7	73.9
15	5	200	61	3.6	S	132	40	134	596	55.9	73.3
15	5	200	61	4.1	N	128	39	176	783	57.8	72.8
15	5	200	61	5.1	S	122	37	268	1192	62.3	72.0
15	5	200	61	5.5	N	119	36	317	1410	63.3	71.0
15	5	200	61	5.8	N	118	36	347	1543	NO DATA	NO DATA
15	5	200	61	6.0	S	114	35	364	1619	NO DATA	NO DATA
15	5	200	61	7.7	S	111	34	599	2664	67.5	68.7
15	5	200	61	8.2	N	110	34	676	3007	67.8	68.3
15	5	200	61	8.4	S	108	33	720	3203	NO DATA	NO DATA
15	5	200	61	8.6	N	111	34	760	3380	NO DATA	NO DATA
15	5	200	61	12.0	N	106	32	1465	6516	NO DATA	NO DATA
15	5	200	61	12.0	S	105	32	1452	6458	NO DATA	NO DATA
22	7	400	122	3.6	S	199	61	146	649	67.6	68.9
22	7	200	61	3.8	N	130	40	165	734	66.1	69.4
22	7	400	122	3.9	N	200	61	189	841	67.5	68.7
22	7	200	61	4.0	S	127	39	182	810	68.7	68.9
22	7	200	61	4.5	N	113	34	386	1717	NO DATA	NO DATA
22	7	200	61	4.9	S	121	37	278	1228	61.8	67.2
22	7	400	122	5.4	S	173	53	320	1423	73.4	66.4
22	7	200	61	5.4	S	115	35	323	1437	NO DATA	NO DATA
22	7	200	61	5.7	S	117	36	319	1419	NO DATA	NO DATA
22	7	200	61	5.8	N	113	34	364	1619	63.7	66.6
22	7	400	122	6.0	N	168	51	384	1708	74.0	65.5
22	7	400	122	7.8	S	154	47	629	2798	77.0	64.2
22	7	200	61	8.1	S	111	34	681	3029	NO DATA	NO DATA
22	7	200	61	8.2	S	110	34	695	3091	68.2	64.3
22	7	200	61	8.2	N	111	34	695	3081	67.6	64.4

Table D.1. (Continued)

CAMD POSITION		CABLE LENGTH		SPEED	HDG	DEPTH		SHIP TENSION		CABLE ANGLE	
										gimbal	CAMD
(ft)	(m)	(ft)	(m)	(kn)		(ft)	(m)	(lb)	(N)	(deg)	(deg)
22	7	200	61	8.4	S	111	34	763	3394	NO DATA	NO DATA
22	7	200	61	8.5	N	108	33	740	3292	NO DATA	NO DATA
22	7	200	61	8.6	N	111	34	825	3670	NO DATA	NO DATA
22	7	400	122	8.7	N	151	46	786	3496	77.5	63.1
22	7	200	61	12.1	S	108	33	1522	6770	NO DATA	NO DATA
22	7	200	61	12.4	S	106	32	1590	7072	NO DATA	NO DATA
22	7	200	61	12.6	N	106	32	1640	7295	NO DATA	NO DATA
22	7	200	61	12.7	N	109	33	1709	7602	NO DATA	NO DATA
30	9	400	122	3.0	N	228	69	187	832	NO DATA	63.4
30	9	400	122	3.2	S	208	63	97	431	NO DATA	66.6
30	9	400	122	3.2	N	220	67	162	721	NO DATA	NO DATA
30	9	400	122	4.0	S	195	59	210	934	NO DATA	NO DATA
30	9	400	122	5.8	N	176	54	406	1806	NO DATA	NO DATA
30	9	400	122	5.8	S	170	52	377	1677	NO DATA	NO DATA
30	9	400	122	5.9	S	173	53	380	1690	NO DATA	59.9
30	9	400	122	6.1	N	174	53	451	2006	NO DATA	59.1
30	9	400	122	8.4	S	160	49	785	3492	NO DATA	58.5
30	9	400	122	8.5	N	160	49	860	3825	NO DATA	NO DATA
30	9	400	122	8.5	S	158	48	786	3496	NO DATA	NO DATA
30	9	400	122	9.0	N	159	48	902	4012	NO DATA	57.8
48	15	400	122	3.8	S	199	61	146	649	NO DATA	56.7
48	15	400	122	3.9	N	200	61	209	930	NO DATA	54.2
48	15	400	122	5.7	S	174	53	335	1490	NO DATA	51.7
48	15	400	122	6.5	N	170	52	522	2322	NO DATA	49.4
48	15	400	122	9.3	S	153	47	918	4083	NO DATA	47.8
48	15	400	122	9.8	N	158	48	1114	4955	NO DATA	47.8
75	23	400	122	3.4	S	202	62	131	583	67.1	48.1
75	23	600	183	3.6	S	274	84	199	885	68.6	48.0
75	23	400	122	3.8	N	195	59	161	716	66.9	46.7
75	23	600	183	4.1	N	233	71	214	952	71.1	43.8
75	23	600	183	4.9	S	236	72	332	1477	73.6	45.7
75	23	400	122	5.5	S	166	51	314	1397	74.3	41.6
75	23	600	183	5.7	N	205	62	387	1721	75.6	41.0
75	23	400	122	5.8	N	166	51	367	1632	73.7	41.4
75	23	600	183	7.9	S	189	58	696	3096	79.1	40.1
75	23	400	122	8.1	S	151	46	667	2967	77.9	38.7
75	23	600	183	8.2	N	189	58	798	3550	78.9	39.7
75	23	400	122	8.6	N	151	46	696	3096	77.3	38.5
115	35	600	183	3.9	S	254	77	238	1059	71.2	39.3
115	35	600	183	4.1	N	237	72	214	952	71.4	36.3
115	35	600	183	5.3	S	222	68	372	1655	75.6	36.1
115	35	600	183	6.0	N	209	64	431	1917	76.4	34.2
115	35	600	183	8.1	S	187	57	735	3269	79.6	31.2
115	35	600	183	8.7	N	185	56	852	3790	79.7	31.4
145	44	600	183	3.5	S	269	82	200	890	69.2	37.2
145	44	600	183	4.2	N	230	70	229	1019	71.4	32.2
145	44	600	183	5.3	S	228	69	383	1704	75.5	33.8
145	44	600	183	6.0	N	206	63	454	2019	76.4	30.1
145	44	600	183	7.8	S	190	58	668	2971	79.2	28.2
145	44	600	183	8.7	N	188	57	873	3883	79.4	27.5
195	59	800	244	3.6	S	306	93	192	854	70.1	30.1
195	59	800	244	4.1	N	298	91	256	1139	71.9	30.3

Table D.1. (Continued)

CAMD POSITION		CABLE LENGTH		SPEED	HDG	DEPTH		SHIP TENSION		CABLE ANGLE	
										gimbal	CAMD
(ft)	(m)	(ft)	(m)	(kn)		(ft)	(m)	(lb)	(N)	(deg)	(deg)
195	59	800	244	5.0	S	261	80	338	1503	75.5	27.3
195	59	800	244	6.1	N	235	72	453	2015	77.3	25.4
195	59	800	244	7.9	S	218	66	760	3380	80.2	24.2
195	59	800	244	8.4	N	209	64	827	3678	80.4	23.9
300	91	800	244	3.2	S	331	101	163	725	68.1	26.0
300	91	800	244	4.0	N	295	90	202	898	71.2	22.5
300	91	800	244	5.6	N	255	78	404	1797	76.4	20.7
300	91	800	244	5.9	N	240	73	393	1748	76.7	18.1
300	91	800	244	7.9	N	219	67	731	3251	79.8	16.8
300	91	800	244	8.7	N	210	64	852	3790	80.4	15.1

NOTES.

1. CAMD POSITION:DISTANCE ALONG TOWCABLE FROM DEPRESSSOR TO CABLE ANGLE MEASURING DEVICE
2. CABLE LENGTH: DISTANCE ALONG TOWCABLE FROM DEPRESSOR TO GIMBAL TOWPOINT ON SHIP
3. SPEED: SPEED MEASURED AT KNOTMETER.
4. HDG: HEADING OF SHIP.
5. DEPTH: DEPTH OF DEPRESSOR.
6. CAMD: ANGLE MEASURED USING CABLE ANGLE MEASURING DEVICE.

Table D.2. Large cable at-sea data.

CAMD POSITION		CABLE LENGTH		SPEED	HDG	DEPTH		SHIP TENSION		CABLE ANGLE	
										gimbal	CAMD
(ft)	(m)	(ft)	(m)	(kn)		(ft)	(m)	(lb)	(N)	(deg)	(deg)
3	1	300	91	3.2	S	170	52	276	1228	56.0	79.0
3	1	500	152	4.0	S	224	68	335	1490	64.7	NO DATA
3	1	500	152	4.0	N	213	65	436	1939	64.7	NO DATA
3	1	300	91	4.1	N	150	46	337	1499	60.3	77.3
3	1	300	91	4.6	S	137	42	360	1601	64.5	77.1
3	1	500	152	5.0	S	192	59	438	1948	68.8	NO DATA
3	1	500	152	5.1	N	188	57	541	2406	68.9	NO DATA
3	1	300	91	5.7	N	127	39	485	2157	67.5	76.1
3	1	300	91	7.9	S	111	34	797	3545	73.6	76.0
3	1	500	152	8.0	S	149	45	856	3807	75.9	NO DATA
3	1	500	152	8.2	N	150	46	1028	4573	75.8	NO DATA
3	1	300	91	8.3	N	112	34	903	4017	73.4	75.9
6	2	300	91	3.4	S	166	51	258	1148	58.8	NO DATA
6	2	300	91	3.9	N	151	46	296	1317	59.8	73.5
6	2	300	91	5.0	S	133	41	384	1708	67.4	NO DATA
6	2	300	91	5.8	N	127	39	478	2126	67.6	72.9
6	2	300	91	7.7	S	112	34	730	3247	73.4	72.0
6	2	300	91	8.2	N	114	35	883	3928	73.2	71.9
9	3	300	91	3.4	S	165	50	244	1085	59.5	72.9
9	3	300	91	3.7	S	158	48	282	1254	59.7	NO DATA
9	3	300	91	4.1	N	150	46	347	1543	60.6	71.3
9	3	300	91	4.1	N	150	46	340	1512	61.2	NO DATA
9	3	300	91	5.2	N	134	41	448	1993	65.5	NO DATA
9	3	300	91	5.3	S	128	39	473	2104	68.1	70.2
9	3	300	91	5.6	S	127	39	452	2010	68.7	NO DATA
9	3	300	91	5.8	N	127	39	533	2371	67.7	69.6
9	3	300	91	7.3	S	114	35	740	3292	72.5	69.1
9	3	300	91	7.7	S	113	34	776	3452	73.4	NO DATA
9	3	300	91	8.3	N	115	35	924	4110	73.1	69.0
9	3	300	91	8.5	N	113	34	936	4163	73.5	NO DATA
18	5	500	152	4.1	S	220	67	350	1557	66.0	59.1
18	5	500	152	4.4	N	201	61	438	1948	65.3	56.4
18	5	500	152	5.1	S	187	57	444	1975	70.4	56.8
18	5	500	152	5.4	N	177	54	558	2482	69.9	55.3
18	5	500	152	7.8	S	147	45	785	3492	75.9	54.6
18	5	500	152	8.4	N	143	44	1032	4590	76.1	54.0
30	9	500	152	2.7	S	275	84	298	1323	56.2	76.5
30	9	500	152	3.8	S	237	72	334	1486	63.6	54.8
30	9	500	152	3.9	N	221	67	417	1855	64.1	NO DATA
30	9	500	152	4.1	N	212	65	426	1895	63.9	50.2
30	9	500	152	4.7	S	201	61	405	1801	67.8	50.7
30	9	500	152	5.0	S	191	58	474	2108	69.6	71.0
30	9	500	152	5.2	N	190	58	536	2384	69.2	NO DATA
30	9	500	152	5.6	N	183	56	569	2531	69.4	47.6
30	9	500	152	7.5	S	153	47	805	3581	75.8	NO DATA
30	9	500	152	7.8	S	152	46	836	3719	75.5	45.5
30	9	500	152	8.2	N	149	45	966	4297	76.2	NO DATA
30	9	500	152	8.3	N	150	46	1039	4621	75.6	45.5
46	14	700	213	4.0	N	288	88	480	2135	65.5	42.7
46	14	700	213	4.1	S	292	89	400	1779	66.8	43.8
46	14	700	213	5.1	N	242	74	603	2682	70.1	38.5
46	14	700	213	5.4	S	240	73	528	2349	71.4	38.6

Table D.2. (Continued)

CAMD POSITION		CABLE LENGTH		SPEED	HDG	DEPTH		SHIP TENSION		CABLE ANGLE	
										gimbal	CAMD
(ft)	(m)	(ft)	(m)	(kn)		(ft)	(m)	(lb)	(N)	(deg)	(deg)
46	14	700	213	7.7	S	191	58	940	4181	76.3	35.2
46	14	700	213	7.9	N	185	56	1065	4737	76.0	34.3
60	18	700	213	3.9	N	294	90	493	2193	64.7	36.1
60	18	700	213	3.9	S	309	94	416	1850	65.6	41.5
60	18	700	213	4.9	N	249	76	583	2593	68.6	32.4
60	18	700	213	5.2	S	246	75	541	2406	70.4	36.4
60	18	700	213	7.7	S	188	57	913	4061	76.1	32.0
60	18	700	213	8.5	N	181	55	1355	6027	76.8	28.5
80	24	700	213	3.5	S	316	96	389	1730	64.8	37.1
80	24	700	213	4.5	N	270	82	480	2135	67.1	31.3
80	24	700	213	5.4	S	237	72	561	2495	71.5	28.5
80	24	700	213	5.6	N	233	71	615	2736	70.8	28.7
80	24	700	213	7.6	S	191	58	909	4043	76.3	25.4
80	24	700	213	8.0	N	188	57	1020	4537	76.0	25.2
110	34	700	213	4.2	S	299	91	418	1859	67.2	31.7
110	34	700	213	4.5	S	272	83	434	1930	69.1	29.2
110	34	700	213	4.5	N	262	80	505	2246	66.9	25.2
110	34	700	213	5.2	N	239	73	595	2647	69.0	23.4
110	34	700	213	7.9	S	184	56	967	4301	76.4	20.5
110	34	700	213	8.5	N	182	55	1223	5440	77	20.4
180	55	700	213	4.3	S	295	90	386	1717	66.8	23.2
180	55	700	213	4.6	N	259	79	565	2513	67.3	19.2
180	55	700	213	4.8	S	261	80	432	1922	69.0	21.0
180	55	700	213	5.7	N	225	69	665	2958	70.6	16.1
180	55	700	213	8.0	S	183	56	922	4101	76.0	13.1
180	55	700	213	8.7	N	177	54	1251	5564	77.1	12.8
400	122	700	213	3.7	S	331	101	376	1672	63.7	18.5
400	122	700	213	4.0	N	278	85	522	2322	66.0	12.6
400	122	700	213	5.0	S	254	77	481	2139	70.1	10.8
400	122	700	213	5.8	N	222	68	690	3069	71.5	7.6
400	122	700	213	7.9	S	187	57	931	4141	76.4	5.2
400	122	700	213	8.4	N	179	55	1168	5195	76.5	5.2

NOTES:

1. CAMD POSITION: DISTANCE ALONG TOWCABLE FROM DEPRESSOR TO CABLE ANGLE MEASURING DEVICE
2. CABLE LENGTH: DISTANCE ALONG TOWCABLE FROM DEPRESSOR TO GIMBAL TOWPOINT ON SHIP.
3. SPEED: SPEED MEASURED AT KNOTMETER.
4. HDG: HEADING OF SHIP.
5. DEPTH: DEPTH OF DEPRESSOR.
6. CAMD: ANGLE MEASURED USING CABLE ANGLE MEASURING DEVICE.

REFERENCES

1. Gibbons, T. and C. Walton, "Evaluation of Two Methods for Predicting Towline Tensions and Configurations of a Towed Body System Using Bare Cable," DTMB Report 2313 (Dec 1966).
2. Diggs, J., "Hydrodynamic Characterization of Various Towed Array Towcables," MAR Inc. Report 128 (Aug 1974).
3. Folb, Reece and John J. Nelligan, "Hydrodynamic Loading of Armored Towcables," DTNSRDC Report 82/116 (Feb 1983).
4. "Depth/Speed Recorder Operation and Maintenance Manual," EG&G Washington Analytical Services Center, Inc., DTRC Contract No. N00167-88-D-0018.
5. Fellman, M.S. and J.W. Johnston, "Evaluation of a Depth/Speed Recorder Hydrodynamic Prototype Body," DTRC Report SHD-1272-01 (May 1990).
6. Springston, George B. Jr., "The DTMB Mark 2 Knotmeter," DTMB Report 2042 (Sep 1965).
7. Knutson, Richard K., "BASIC Desk-Top Computer Program for the Three-Dimensional Static Configuration of an Extensible Flexible Cable in a Uniform Stream," DTNSRDC Report 87/029 (Aug 1987).
8. Pode, L., "Tables for Computing the Equilibrium Configuration of a Flexible Cable in a Uniform Stream," DTMB Report 687 (Mar 1951).
9. Eames, Michael C., "Steady-State Theory of Towing Cables," Defence Research Establishment Atlantic Report 67/5 (1967).
10. Waters, O.D., Jr (Commander), "Environmental Atlas of the Tongue of the Ocean, Bahamas," U.S. Naval Oceanographic Office Special Publication SP-94 (1967).
11. Coleman, Hugh W. and W. Glen Steele, Experimentation and Uncertainty Analysis for Engineers, John Wiley & Sons (1989).

12. Knutson, R., "An Estimate of Linear Hydrodynamic Coefficients for the Multi-line Towed Array (MLTA) Primary Vehicle," DTRC Report SHD-1292-01 (Dec 1988).

INITIAL DISTRIBUTION

Copies			
1	NOP/RADM H.W. Habermeyer		
2	ONCR		
	1	23	A.J. Faulstich
	1	235	W. Ching
4	NAVAIR		
	1	210	W. Emshwiller
	1	210C	H. Sheetz
	1	210C1	K. Haas
	1	210C3	J. Perry
3	NAVSEA		
	1	407	H. Dietz
	1	55W31	W. Louis
	1	55w32	J. Pattison
7	SPAWAR		
	1	153T	R. Allen
	1	1532	E. Benson
	1	1532A	P. Hixon
	1	1532C	C. McMillian
	1	1532G	L. Bundick
	1	183	C. Bohman
	1	SP-25	R. Yabic
7	NCSC		
	1	7112	Tech Lib
	1	2210	J. Crane
	1	2210	J. Kamman
	2	2220	C. Ferrer
	1	3220	C. Cotton
	1	4220	R. Gollwitzer
13	NUSC		
	1	0261	Tech Lib/NL
	1	0262	Tech Lib/NP
	1	3423	K. Lewis
	1	3492	P. Trask
	1	3493	T. Susi
	1	3496	F. Allard
	1	3321	P. Seaman
	1	3321	E. Kuo
	1	3321	A. Ruffa
	1	3321	N. Toplosky
	1	3323	S. Traggis
	1	2121	N. Owsley
	1	8333	J. Babb

Copies			
3	NRL		
	1		Tech Lib
	1	5841	O.M. Griffin
	1	5550	E. Kennedy
4	NSWC		
	1		Tech Lib
	1	U12	B. Park
	1	U13	M. Kumagai
	1	U13	G. Winkler
5	NCEL		
	1		Tech Lib
	1	L43	T. Kretchmer
	1	L44	D. Meggit
	1	L60	G. Wu
	1		P. Palo
2	NOSC		
	1		Tech Lib
	1	715	L. McKinley
2	NUWES		
	1		Tech Lib
	1	70D1	C. Martin
2	NEODTC		
	1		Tech Lib
	1	50B2	A. Pederson
1	USNA		
12	DTIC		
1	US COAST GUARD COMMANDANT/ CAPT D. Whitten		
2	US COAST GUARD R&D CENTER		
	1		P. Tebeau
	1		K. Bitting
1	EPA OFFICE OF R&D/R. Griffiths		
1	U Cal Berkeley/Naval Arch		
1	U Cal Scripps		
1	Catholic U/Mech Eng		

Copies

1 Florida Atlantic U/Ocean Eng

1 U Hawaii

2 Johns Hopkins U/APL
1 Tech Lib
1 C. Anderson

1 U Michigan/NAME

1 MIT/Ocean Eng

1 Oregon State U

1 Texas A&M

3 U Washington/APL
1 Lib
1 G. Welsh
1 J. Ward

1 Webb Institute

2 Woods Hole Oceanographic Inst
1 Lib
1 M. Grosenbaugh

1 SNAME

1 American Systems Eng Corp/
E. Corack
2121 Crystal Drive
Suite 607
Crystal Park Two
Arlington, VA 22202

1 Applied Measurements Systems,
Inc/J. Diggs
400 Bayonet Street
New London, CT 06320

1 AT&T Technologies, Inc/
W. Stewart
P.O. Box 20046
Greensboro, NC 27420

1 Bendix Oceanics/D. MacCulloch
15825 Roxford Street
Sylmar, CA 91342-3597

Copies

1 Cortland Cable Company/
E. Scala
P.O. Box 352
Cortland, NY 13045

1 EDO Corp/F. Otto
14-04 111th street
College Point, NY 11356

1 ENDECO, Inc/E. Brainard
13 Atlantic Drive
Marion, MA 02738-1448

2 Engineering & Services Assoc
1 J. Nelligan
1 S. Gay
6110 Executive Blvd.
Rockville, MD 20852

1 EG&G WASCI/C. Pease
1396 Piccard Drive
Rockville, MD 20850

1 International Investments
Organization/L. Siwecki
1000 Burnett Avenue
Suite 150
Concord, CA 94520

1 Interstate Electronics Corp/
R. Packard
604 E. Vermont Avenue
Anaheim, CA 92803

1 Kollmorgan Corp/L. Palecki
347 King Street
Northhampton, MA 01060

1 Mar, Inc/A. Brisbane
6110 Executive Blvd.
Suite 410
Rockville, MD 20852

1 Marine Spill Response Corp/
F. Engelhardt
1350 I Street NW
Suite 300
Washington, DC 20005

Copies

3 Martin Marietta Ocean Sys
1 J. Klein
1 C. Holberger
1 A. Pablac
6711 Baymeadow Drive
Glen Burnie, MD 21061

1 Neal Research Assoc/E. Neal
11809 Collins Drive
Germantown, MD 20874

1 ORI, Inc/A. Gilmore
1375 Piccard Drive
Rockville, MD 20850

1 Raytheon Company/M. Little
1847 West Main Road
Portsmouth, RI 02871-1087

1 Rochester Corp/A. Berian
P.O. Box 312
Culpeper, VA 22701

1 Sea Tech/W.N. Guild
11911 Pine Belt Drive
Cypress, TX 77429

1 South Bay Cable/W. Tell
P.O. Box 67
Idyllwild, CA 92349

1 Spears Associates, Inc/
S. Stabile
249 Vanderbilt Ave
Norwood, MA 02062

1 Tension Member Technology/
P. Gibson
15161 Golden West Cir
Westminster, CA 92683

1 TRW Systems Division/
D. Campbell
P.O. Box 10400
Fairfax, VA 22031

1 West Sound Assoc, Inc/
K.A. Tobin
P.O. Box 745
Bremerton, WA 98310

Copies

1 Westinghouse Electric Corp/
A. Jennings
P.O. Box 1488
Annapolis, MD 21404

1 Whitehill Manufacturing Corp/
A.S. Whitehill
P.O. Box 356
Lima, PA 19037

CENTER DISTRIBUTION

Copies	Code	Name
1	01	R. Metrey
1	15	W. Morgan
1	1504	V. Monacella
1	152	W. Lin
1	154	J. McCarthy
25	1541	R. Knutson
1	156	D. Cieslowski
1	1910.3	J. Schempp
1	3421	TIC (C)
1	3422	TIC (A)
10	3432	Reports Control